Towards Feedback Controlled Droplet Microfluidic Platforms

by

Tomasz Zablotny

A thesis
presented to the University of Waterloo
in fulfillment of the
thesis requirement for the degree of
Master of Applied Science
in
Mechanical and Mechatronics Engineering

Waterloo, Ontario, Canada, 2021

Author's Declaration

This thesis consists of material all of which I authored or co-authored: see Statement of Contributions included in the thesis. This is a true copy of the thesis, including any required final revisions, as accepted by my examiners. I understand that my thesis may be made electronically available to the public

I understand that my thesis may be made electronically available to the public.

Statement of Contributions

Tomasz Zablotny was the sole author for all Chapters except Chapter 3 which had sections taken from a submitted manuscript and reviewer comments. This manuscript was edited by Matthew Courtney who also aided in the microfluidic setup of experiments for this chapter.

- Tomasz Zablotny, Matthew Courtney, Jan P. Huissoon, and Carolyn L. Ren. "Lensless imaging for droplet identification towards visual feedback-based pressure controlled droplet microfluidic platforms" (2021)

All chapters were written under the supervision of Prof. Carolyn Ren and Prof Huissoon.

Abstract

Microfluidics, the manipulation of nanoliter to microliter volumes of fluids, can give important new capabilities to researchers in biology, chemistry, material science, and medicine. Broadly, current methods can be classified into passive and active approaches. Passive methods use physical properties and microfluidic geometry whereas active methods use external perturbations to drive desired behaviour. However, passive methods require expertise and skill, and active methods complicate fabrication, require large support systems, or are not congruent with many applications. These limitations make microfluidics practically inaccessible to many researchers. Unlike these approaches, the application of feedback control may provide users with a practical and simple way to use microfluidics. Through feedback, a controller manages the operation of a microfluidic chip without needing complicated fabrication, large support systems, and in a way that can be used in a wider set of applications.

State-of-the-art feedback-controlled microfluidic (FCM) devices have several shortcomings. First, typical microfluidic chips used in these devices are simple single or double T-Junctions. Such simple chips have few degrees of freedom thus limiting how many channels can be controlled concurrently. Secondly, feedback techniques, predominantly based on optical microscopes, are bulky and costly thus incongruent with FCM applications which require compact and low cost sensing. Third, a modeling approach based on an electrical analogy (Modeling channels through resistive, capacitive, and inductive elements) leads to untenable models. Fourth, Linear Quadratic Regulator (LQR) based control laws saturate unidirectional pumps. Finally, current FCM methods necessitate significant operator interaction, which is undesirable.

To improve FCM methods, this dissertation conceives a new type of chip topology with greater degrees of freedom. Secondly, a new feedback source based on lensless microscopy is developed and validated. Third, a simplified modeling approach is validated. The simplified model is used as the basis for a Model Predictive Controller (MPC). Finally, these subsystems are combined to develop a system that can generate and manipulate droplets autonomously. These developments work towards making FCM, and thus microfluidics, more accessible to the wider scientific community.

Acknowledgements

I would like to sincerely thank Prof. Carolyn Ren and Prof. Jan Huissoon for their supervision and support over the last two years. The provided guidance allowed me to grow and discover a vocation in research.

I would also like to thank the other member Waterloo Microfluidics lab. Especially, Matthew Courtney, whose initial support, mentorship, and friendship gave me a strong start. Additionally, Marie Hebert whose work and training on feedback control enabled my research. Finally, I want to thank other members of the Anna Nguyen, Weijia Cui, Jeff Farnese, Anson Lau, Kevin Chen, and Pei Zhao.

Dedication

To my parents, whose love and sacrifice allowed me to peruse possibilities they never had and to my sister, whose joy and dedication always inspires.

Table of Contents

List of Figures

List of Tables

Chapter 1

Introduction

Microfluidic systems allow manipulations of small (10^{-9} to 10^{-18} liters) fluid volumes [1] to be performed. The capacity to conduct manipulations on small fluid volumes has many advantages as it minimizes input consummation, lowers cost, and allows previously unavailable levels of control. With these many benefits and few limitations, it appeared microfluidics would spur rapid advancement and revolutionary changes in material science, biochemistry, among other fields [2].

Unfortunately, early development in single-phase microfluidic devices revealed fundamental and practical challenges. Singe-phase microfluidic devices have limited mixing performance, cross-contaminate samples [3], restrained throughput, and standard fabrication procedures are complex and often incongruent with applications [4].

In response to the problems of single-phase systems, the droplet microfluidic subfield emerged. Droplets are picolitre to nanolitre fluids (e.g. water) within another immiscible fluid (e.g. oil) [1]. Droplet microfluidics (DM) has the same advantages as single-phase as it can lower reagent consumption and reaction time. Unlike single-phase, droplet microfluidics has significant improvements in mixing, limits cross-contamination, increases throughput and gives previously unachievable control over reaction conditions [4].

1.1 Major Droplet Microfluidic Approaches

The potential of Droplet Microfluidics has led to the development several techniques to generate and manipulate droplets. The main approaches are Passive Microfluidics [5][6],

Microfluidic large-scale integration (MLSI) [7], Digital Microfluidics (DMF) [8], and Active Microfluidics [6]. However, each of these methods currently has severe limitations preventing widespread use.

Passive

Early droplet microfluidic devices were based on passive methods. Passive methods use the physical properties and channel design to bring about the desired behaviour [5]. Such passive approaches are well studied, and a substantial number of passive devices, techniques, and applications have been described in the literature [6].

Nevertheless, apart from specialist applications, passive microfluidics is not suitable for widespread universal application. The design and operation of passive systems requires significant interdisciplinary expertise. Advanced, and practically inaccessible, training is likely a prerequisite for successful use [4]. This need alone is prohibitive to widespread adoption of the passive approach. Secondly, microfluidic devices experience manufacturing variations, defects, coupled dynamics, and operational uncertainties that make use difficult even for experienced users [9].

Practically, the adoptions of any non-trivial passive microfluidic systems require significant microfluidic expertise. It is this skill requirement that prevents widespread adoption. Apart from specialist devices for specific applications, the grand promises of a revolutionary tool through passive microfluidics have not been met.

MLSI

Microfluidic large scale integrated (MLSI) is characterized as microfluidic chips integrated with hundreds to thousands of integrated micromechanical valves [7] [10]. The opening and closing of valves allows precise, parallelized, and automated manipulation of micro volumes of fluids without consideration of fluid properties [11]. MLSI complexity makes it a powerful technique, however, it also makes widespread use difficult.

Figure 1.1 shows a cross-section of an MLSI device and microvalves. The left channel is in the process of closing as an external force is applied. The right channel remains open. Through the open and closing of valves the device manipulates fluids [7] [11].

The significant amount of integrated micromechanical valves and the multilayer nature leads to very complicated chip designs both for development and fabrication [12]. This complexity has spurred the development of specialist software to aid design [11]. Although

perhaps standard mass-manufactured devices can remove fabrication details from the end-users, the design of such devices is too complex for most end-users.

Secondly, the pneumatic control system for hundreds to thousands of integrated micromechanical valves is unwieldy, bulky, and prohibitively costly. The cost of a valve control system has been identified as preventing widespread MLSI adoption [12]. In response to this, alternative control methods based on electrostatic [13], magnetic [14], thermal [15], and shape memory [16] actuators have been devised. However, these methods are not without issues as they have either insufficient performance or further complicate fabrication [12].

Although MLSI is a very powerful technique, the fundamental complexity required makes large-scale use of this method untenable. Although there exist promising attacks to these problems, they have thus far proved insufficient in managing the complexity.

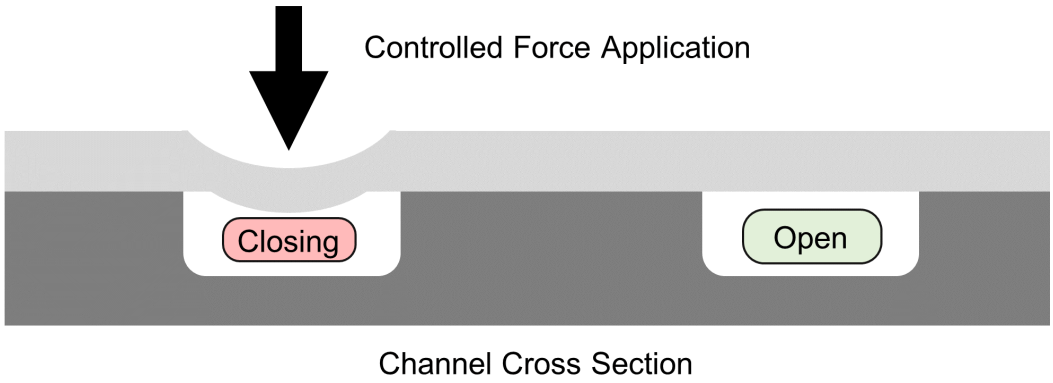

Figure 1.1: MLSI Operating Principle

Digtial Microfluidics

Choi defined Digital Microfluidics (DMF) as an integrated system composed of electrode arrays that are coated with a hydrophobic insulator [8]. This contrasts with conventional microfluidics which is based on enclosed channels. The DMF system manipulates picoliter to microliter-sized droplets by applying an electrical potential to the individual electrodes. Through this mechanism, the DMF system can carry out basic unit operations, such as

droplet merging, splitting, and movement from a reservoir [8]. However, the DMF approach faces fundamental and practical limitations that impede the widespread application of this technique.

Figure 1.2 shows the operating principle of DMF. A droplet (light blue) is on a grid of electrodes at time a. At time b, a potential between the red and dark grey electrodes appears. As a result, the droplet moves to a new electrode in frames c and d.

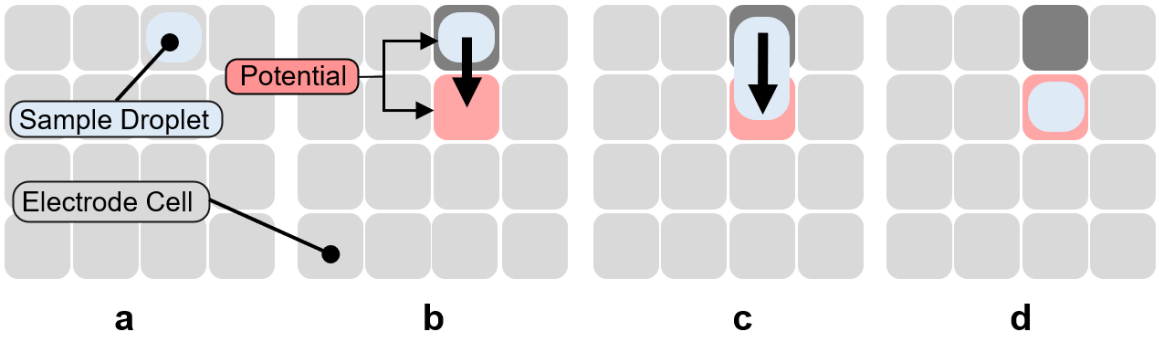

Figure 1.2: Digital Microfluidics Operating Principle

Fundamentally, DMF requires the application of (often large) voltages to manipulate droplets. In most implementations, the required potentials are prohibitive to the use of this technique. Such voltage can also damage cells, DNA, and proteins [17]. Thus, fundamentally, DMF cannot be applied to many applications as it renders the samples being studied unusable. Although there is a trend in DMF to decrease voltage levels, these methods are complex, costly, or have adverse effects on the droplets [17]. Another limitation of DMF is evaporation [17] [18][19]. The high voltages and open nature of DMF cause higher rates of droplet evaporation.

Practically DMF poses other limitations. Firstly, DMF requires a complicated manufacturing procedure that is infeasible as a widespread technique. Additionally, manufacturing restrictions on electrode area drive minimum droplet size [8]. The minimum droplet volume in DMF systems is much larger compared to conventional microfluidics. Secondly, DMF has significant issues with residue [20]. If multiple samples are used, residue will often remain despite experimental provisions. This can lead to contamination issues which are limiting.

Overall, although advantageous for some specific applications, DMF has many fundamental and practical limitations. These issues prevent the widespread adoption of this technique.

Other Active Methods

Apart from DMF and MLSI, other active microfluidics methods exist. Active methods rely on an external controlled input that affects the system physics. Common existing active systems use magnetic [21], electrical [22], acoustics [23], or physical perturbations [7] [6]. These active control systems often involve the integration of many additional components such as metal electrodes which tend to complicate the chip fabrication and operation [9]. None of these approaches are ideal and limit the widespread application of these systems.

1.1.1 Summary of Limitations for Major Approaches

Today, thirty years from the birth of the field, microfluidics is in 'Late Adolescence' [24]. Despite the apparent benefits of microfluidics, adoption has been left wanting. Even with achieved and anticipated advances neither MLSI, DMF, passive or active techniques appear capable of addressing the ultimate objective of microfluidics. That is, none can create a universal widely accessible, and applicable microfluidic tool. These approaches are either fundamentally incompatible with the application domain, are too complex, large, and costly, or lack adequate reliability, or require too great a domain knowledge to be used outside the field. In short, the limitations in applicability, accessibility, ease of use, and robustness are the main challenges of current approaches.

1.2 Feedback Control Microfluidics (FCM)

A novel and promising approach is the application of feedback control to microfluidics [25] [26] [27]. Feedback control allows easy manipulations of droplets while having the advantageous physical simplicity of passive microfluidic systems [27].

Figure 1.3 shows the conceptual FCM components. The FCM has a sensing system (a) to measure relevant system properties, a control law (b) that determines the necessary perturbations that actuators (c) apply to the microfluidic chip (d). The control law is a mathematical equation that uses feedback data to determine the inputs to the system to achieve the desired state, despite chip variations and disturbances [28] [26].

With feedback, one can abstract away device operation as only the desired state needs to be specified. Feedback may create a tool that is accessible for end-users as it operates the device for the user [27].

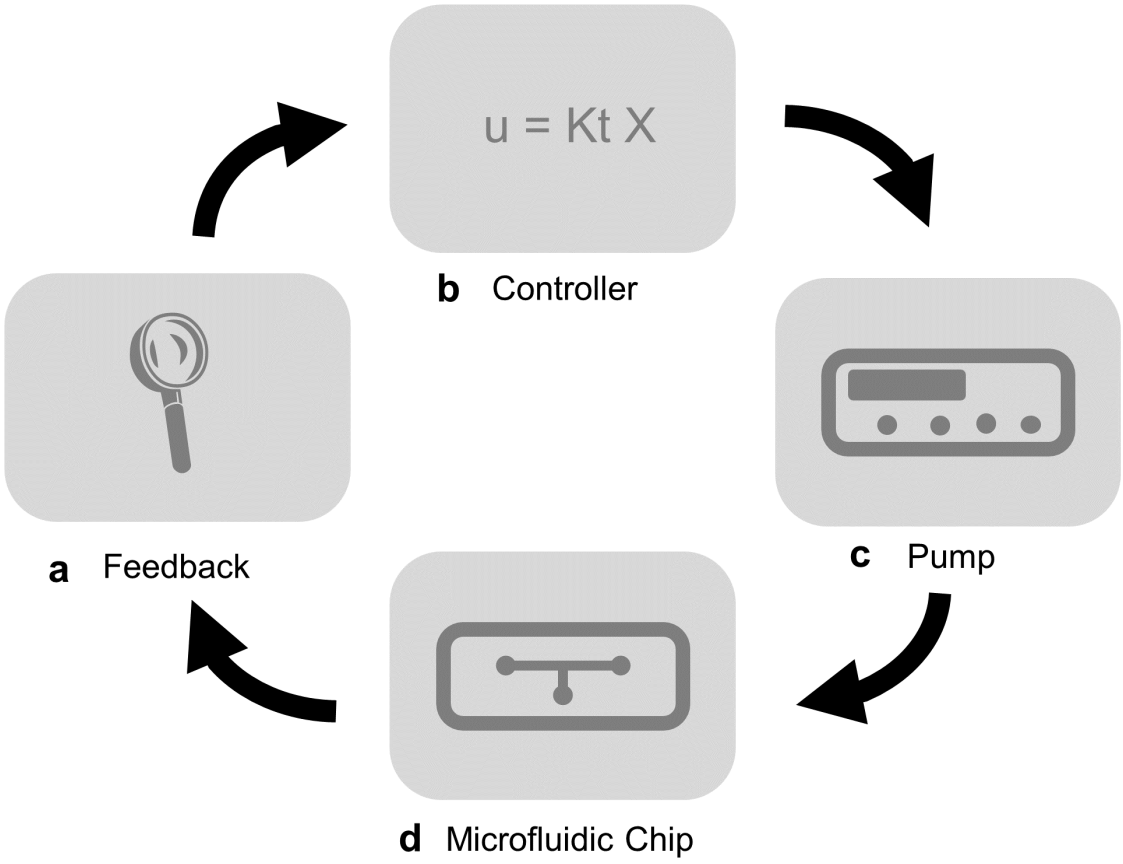

Figure 1.3: Typical Feedback Control Microfluidics System Architecture

1.2.1 Early Control Applications

Several researchers have applied feedback control in microfluidics [25]. However, early applications of feedback control were focused on specific applications. For example, in [29] [30] pressure feedback was used to control interface location, in [31] [32] droplet generation was regulated, and in [33] for control of particle manipulation. All of these devices were only applicable for specific applications or functions. Fundamentally, these early efforts differ from DMF or MLSI. DMF or MLSI are designed to be platforms. Rather than being only applicable for a specific application or function, DMF and MLSI are used universally.

1.2.2 Feedback Control For Droplet Manipulations

In contrast to early efforts, Wong developed a system that solves the microfluidic problem in a more general sense rather than for a specific application [34]. Wong's method builds towards a universal FCM platform. The system is based on a Linear Quadratic Regulator (LQR) Controller with Integral Action. For visual feedback, a digital camera (Andor Zyla 5.5), optical microscope (Eclipse Ti-E, Nikon), and custom image processing are used to track droplet interfaces. References are generated with a GUI where to user selects and moves the droplet interfaces. The LQR controller manipulates the microfluidic chip with a pressure pump (MFCS, Flugient). Generally, chips with single or double T-Junctions are used as the plant.

Modeling

LQR controllers require a model of the systems as they are model based [35]. Wong devised a modeling scheme, termed the electrical analogy, where channels are modeled as electrical circuits [26]. Figure 4.2 shows the electrical analog for a single microfluidic channel. The equivalent state space representation is shown in Equation 1.1. With this approach, each microfluidic channel model has a capacitive, C, inductive, I, and resistive, R element.

$$\begin{bmatrix} \dot{V}_o \\ \dot{I}_i \end{bmatrix} = \begin{bmatrix} 0 & \frac{1}{C} \\ -\frac{1}{L} & -\frac{R}{L} \end{bmatrix} \begin{bmatrix} V_o \\ I_i \end{bmatrix} + \begin{bmatrix} 0 \\ \frac{1}{L} \end{bmatrix} V_i \tag{1.1}$$

The values of these elements are found analytically with equations 1.2,1.3, and 1.4 respectively [25] [26].

$$C = \frac{A}{k} + \frac{l}{\beta} \tag{1.2}$$

$$L = \rho l \tag{1.3}$$

$$R = \frac{32\mu l}{d_h^2} \tag{1.4}$$

The effective inductance (fluid inertia term) depends on channel length l and fluid density rho. The effective capacitance is determined by the channel cross-sectional area,

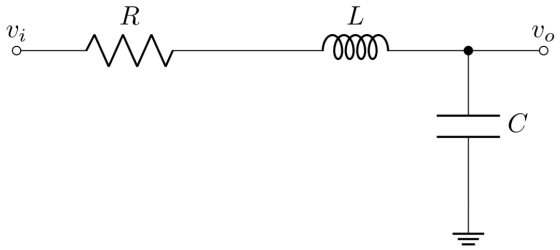

Figure 1.4: RLC Channel Model

A, effective stiffness, K, and fluid adiabatic bulk modulus, β. The effective resistance (that causes pressure drop due to flow), is the Hagen-Poiseuille law [25], and is driven by the fluid viscosity, μ and d_h the hydraulic diameter. Tubing elements are modeled similarly.

Given individual models, the full channel network can be modeled by spatially arranging and interconnecting individual channel models to match the underlying channel network topology. The channel network is converted into a discretized state-space model. Additional states, corresponding to charge, are appended to the state space. Pump dynamics, obtained through system identification, are also integrated into the state space model [25].

Control Law

Two main parts, a state feedback term and a state observer compose the control law. The state observer estimates the full system state as only certain states, droplet position, are measurable with visual feedback. The state feedback term uses the observer's state estimates to generate a stabilizing command signal. The integral action allows the controller to track non-zero steady-state values.

Through the separation principle, the observer and state feedback law can be designed separately. The state feedback law for the augmented model is in the form of 1.5, where the control signal, u, is based on static gain K and the system state x.

$$u = Kx \tag{1.5}$$

The value of K is found by finding the minimization of a cost function, Equation 1.6. Q and R are symmetric matrices, used for controller tuning, that penalize large state variation and control input [35].

$$J = \int_0^\infty (x^T Q x + u^T R u) dt \tag{1.6}$$

Given the cost function, the value of the state feedback gain, K, is given by Equation 1.7, where the value of P satisfies the Algebraic Riccati equation, Equation 1.8 [35].

$$K = R^{-1} B^T P \tag{1.7}$$

$$A^T P + PA - PBR^{-1} B^T P + Q = 0 \tag{1.8}$$

However, state feedback only ensures states are regulated, not that they track references. To track a reference, tracked system outputs are added to an augmented state space system. The augmented plant is used to find new feedback gains [35] [25]. The state gain K_{aug}, is split proportionally between the augmented and non-augmented states.

As state feedback requires full feedback, an state observer needs to be devised to estimate the immeasurable states. Wong's system uses a Lundberg observer for this purpose [25], Equation 1.9 [35], where A is the state matrix, B is the input matrix, C is the observation matrix, and measurements are y. The value of the observer gain, L, is the dual of state feedback gain and is found similarly [35].

$$\dot{\hat{x}} = A\hat{x} + Bu + L(y - C\hat{x}) \tag{1.9}$$

Semi-Automatic Control

Despite the success of Wong's system, the method required manual interaction with droplets through a GUI application. This is undesirable as it necessitates a trained human operator. Consequently, the system's precision, repeatability, and performance are operator limited [9].

Hebert introduced a set of higher-level algorithms that can carry out droplet unit operations when integrated with Wong's system. The algorithms can generate, split, merge, and mix individual droplets. The higher level algorithm allows semi-automated control of certain unit operations with far less manual interaction [27].

1.3 Critical Review of FCM Components

Current FCM components have several limitations. First, the chip topologies limit what control actions can take place. Second, existing sensing systems are incongruent with practical use. Third, currently used modeling and control law methods break down when applied to complex chip topologies. Finally, the use of FCM requires operator interaction which is undesirable compared to autonomous operation.

1.3.1 Microfluidic Chip Design

Existing FCM systems as demonstrated by Wong and Hebert are based on simple microfluidic chip topologies, typically, single or double T-Junctions. The problem with such simple topologies is they have limited Degrees of Freedom (DOF). The principle of conversation of mass, absent significant compression, means only two of three channels in a T junction can be controlled independently [25]. The third channel in a T junction acts as a source or sink to satisfy the flows in the other channels. This creates fundamental limitations in what can be achieved with FCM.

Wong found the DOF for a specific chip using equations 1.10, 1.11 and 1.12 [25]. The DOF, N, is a function of the channel count, c, and the number of inlets, i.

$$N_{i-1} = \binom{c}{i-1} \tag{1.10}$$

$$N_{i-2} = \binom{c}{i-2} \tag{1.11}$$

$$\vdots$$

$$N_1 = \binom{c}{i} \tag{1.12}$$

To better understand why insufficient DOFs are limiting, consider the following system. Figure 1.5 shows three microfluidic T-junctions that are feedback controlled. Working cooperatively, T-Junction 3 should merge droplets generated by T-junctions 1 and 2.

When the T-junctions are independent, the controller can set the flow in two of the three channels, the flow in the third channel is the sum of the other flows, but cannot be

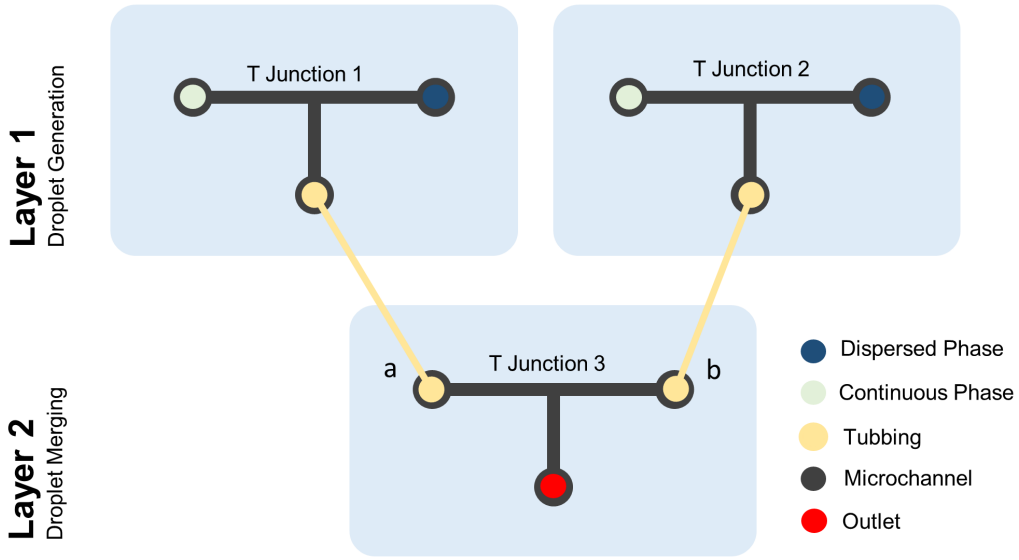

Figure 1.5: Example of DOF Limitations in a Modular T-Junction System

independently controlled. T-Junctions thus must have sufficient DOF to generate or merge droplets.

However, when T-junctions 1 and 2 are connected to T-Junction 3, the merging T junction (in layer two) no longer has enough DOF. The flows in the input channels (labeled a and b) are dependent on the uncontrolled flows of the T-Junctions in layer one. Without these controlled flows, the position of droplets in the T-Junction in layer two can not be controlled. If the positions can not be controlled the droplets can not be made to merge.

Given these constraints, single or double T-junctions can not carry out multiple concurrent droplet operations that a realistic system use would entail. Consequently, a method to increase chip DOF is needed. Although hardware modifications, through microvalves [36] for example, may increase DOF, it undesirably complicates fabrication. Instead, a more promising approach may introduce a new chip topology with additional DOF, which will be shown in Chapter 2.

1.3.2 FCM Measurement

FCM requires a method to measure relevant properties of the system. Existing methods are based predominantly on visual feedback using conventional microscopes, but have significant practical limitations in terms of physical size and field-of-view. Microwave and capacitive sensing schemes have also been proposed, but these also have limitations. Lensless imaging has comparable performance to conventional microscopes in terms of resolution, while also being compact. These methods are further described below.

Conventional Optics for FCM

Several studies have successfully used microscopes as a source of feedback in the FCM context [25] [9] [34] [31] [33]. Typically in FCM applications microscopes measure the position of droplet interfaces in relevant channels. Microscopes are advantageous in that they allow microscale features of a microfluidic device to be observed readily [37]. Expertise and equipment are widely and commercially available [38] [39]. Microscope techniques for biological and chemical studies are extensive and well developed [40].

However, conventional microscopes are not well suited as a feedback source for FCM. Firstly, conventional microscopes are physically large in comparison to the chip, and are costly. The cost and size lead to practical restrictions on the total field of view (FOV) and the number of concurrently observable channels. Secondly, microscopes fundamentally have large footprints relative to the available FOV [38] [39] [41]. This prevents multiple conventional microscopes from observing a single chip. The physical design limits the chip regions for which feedback, and thus control can be provided.

In addition to conventional microscopes, other more specialized microscopes, emphasizing low cost, microfluidic integration or compactness, have been developed (see [42] [43] [44] [45] [46] [47] [48] [49] [50] [51]). Other approaches such as [52] [53] [54] [55] integrate optical elements with microfluidic chips, or leverage smartphone cameras [56] [57], [58] [59]; some commercial options are also available [60]. These methods may surpass conventional microscopes in terms of cost, size, or both. However, for FCM, in addition to compactness and low cost, a large FOV is needed, which many such systems have trouble providing. In the literature, systems with suitable FOV are generally oversized, while compact systems have inadequate FOV (typically < 1 mm^2). These limitations result from practical and fundamental challenges of optical elements. Moreover, the complexity and specialist nature of optical design inhibits custom optical designs [39] [38].

Microwave and Capacitance sensing for FCM

Alternate approaches based on microwave or capacitance sensing have been used [61] but are today unsuitable for FCM. Current microwave methods only provide limited point measurements, require bulky and expensive instrumentation, and complicate fabrication [27] [62] [63], although the ability of microwave sensing to directly measure fluid velocity is promising. Capacitive elements complicate fabrication, have nosier measurements and have relatively large resolutions limited by element size [64] [27].

Lensless Techniques for FCM

Lensless imaging techniques do not have the same limitations in the FCM context. For FCM, lensless imaging techniques allow comparable performance to a conventional microscope while having smaller footprints and lower cost.

Generally, lensless imaging techniques are categorized into two approaches: Holographic, and Contact or Shadow microscopy [65] [66]. Holographic methods use an interference pattern to reconstruct a high-quality image from a captured lower quality image [67]. However, the complexity and required computational resources limit application for the FCM problem.

In contact or shadow imaging, a microchannel network is placed close to an image sensor and is illuminated [67]. The shadow cast by a droplet interface is recorded directly by the sensor. In contrast to holographic techniques, shadow imaging methods are simpler with minimal post-processing, although shadow methods have lower image quality [67].

Shadow imaging has been applied to microfluidics extensively, although applications have been focused on the analysis of biological samples. Lange et al. studied C. Elegans with a shadow imaging system [68]. Ozcan created a cell counting apparatus with lensless imaging [69][70]. Many other lensless systems have been applied in studying biological samples [71][72][73][74]. However, transparent droplets differ from the studied biological samples. Moreover, the control system dictates different performance requirements than biological studies.

Despite this uncertainty, lensless techniques appear very promising for FCM. The small footprint and low cost allow previously impractical possibilities.

1.3.3 Model Development

Plant Modeling Method

The electrical analogy modeling scheme becomes challenging when applied to more complex chip designs. Models resulting from this approach can be high order ($n > 50$), numerically ill-conditioned, and require tuning values, making them challenging and unsuitable for complex chips.

System Identification

The RLC model approach determines the system model analytically. Alternatively, system models may also be found experimentally, a process known as system identification. During system identification, known signals are applied to the system of interest. Using the measured response the system model is then found. In practice, system identification generates more accurate models compared to analytical models [75].

1.3.4 Controller Design

LQR controllers

FCM control laws have been based predominantly on LQR controllers. The approach is attractive as it is simple to design, analyze and implement, directly accounts for the high coupling between inputs and outputs in microfluidic systems, has satisfactory performance and has robustness.

However, LQR methods do not account for actuator saturation [27][35]. Actuator saturation is significant in pressure-driven FCM as most common microfluidic pumps can not create negative pressures. In simpler chip topologies, LQR controllers can function adequately despite actuator saturation. In more complex topologies actuator saturation may contribute to controller failure through windup.

Model Predictive Control

Within the control literature, there exist several methods to compensate for actuator saturation [76]. Modified LQR controllers or compensation schemes are examples of such methods [77].

However, a more direct and thus preferable approach may be a different type of control, Model Predictive Control (MPC). Unlike LQR, MPC can explicitly account for actuator bounds thus avoid saturation [78]. Figure 1.6a shows the application of an MPC controller. Given the desired state, droplet position in [μm], and a state measurement, the MPC uses its internal model to predict what set of inputs to apply to the system

Internally, at a high level, MPC is composed of a model, optimizer, and cost function as shown in Figure 1.6b [78][79]. A standard quadratic cost function found in many MPC texts is given by Equation 1.13. The cost is weighted by tuning factors, w, and is based on sum of square difference between set position, r, and actual position, y, and total control input, u. Additionally, constraints can be placed on the cost functions. Equations 1.14, 1.15, and 1.16 are examples of commonly applied constraints on actuation input, actuation slew rate and system outputs, respectively. These constraints can be used to explicitly accommodate actuator limits [78][80][79][81].

$$J = \sum_{i=1}^{n} w_{cv}^2 (r - y)^2 + \sum_{i=1}^{n} w_{\Delta u}^2 (\Delta u)^2 \tag{1.13}$$

$$u_{min} \leq u \leq u_{max} \tag{1.14}$$

$$\dot{u}_{min} \leq \dot{u} \leq \dot{u}_{max} \tag{1.15}$$

$$y_{min} \leq y \leq y_{max} \tag{1.16}$$

The MPC uses an optimizer to find the inputs that minimize the cost function given model predictions over some finite time horizon. The design of an optimizer is an active research area as issues of solving time, accuracy, required computer hardware, and numerical robustness present challenges [82]. However, MPC with linear models and quadratic cost function can be formulated as a Quadratic Programming (QP) problem. Many methods of solving QP problems exist in the literature [83] [82] [84]. The MPC then applies the inputs and measures the new state of the system. The process repeats for the next cycle [78] [85].

Unlike LQR methods, MPC can explicitly consider actuator saturation. An MPC will not exceed given limits on actuator levels. A controller with such a property is advantageous.

Like LQR methods MPC can account for the high coupling between inputs and outputs in microfluidic systems. Commercial software can simplify controller design and creation. MPC controllers can have comparable performance to LQR-based systems [86].

However, MPC requires significantly more computing power than LQR-based controllers [82]. Additionally, the design and analysis of MPC controllers is more complex and difficult than for LQR controllers [78].

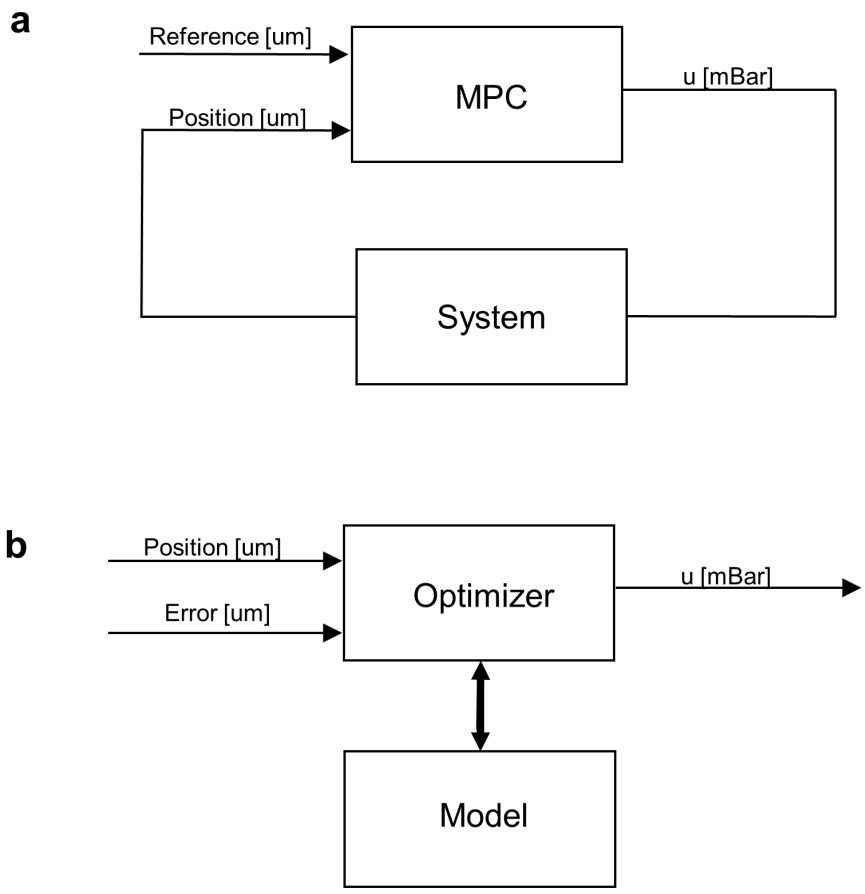

Figure 1.6: Typical MPC Structure

1.3.5 Automatic Control

Existing FCM techniques require operator interaction to realize functions. In Wong's work, the user directly controls all device actions. Hebert added semi-automated functionality through a set of algorithms. Although an improvement over fully manual methods, the semi-automated approach has some limitations. First, the algorithms need a human to identify the relevant droplet interfaces. An example is during the droplet generation process. Secondly, the algorithms require a manual setup to standard initial conditions. In droplet splitting, for example, the droplet must be manually positioned to have droplet interfaces in both channels [27].

For the widespread adoption of FCM methods, the required operator interaction is inappropriate. Necessitating an operator means performance is operator dependent, investment in training is required, and autonomous operation is not possible. In a more theoretical sense, an operator limits the level of abstraction in which FCM can operate.

1.4 Thesis Overview

Given the limitations of current FCM devices, the development of a new FCM system that addresses these limitations is described in the following chapters. This includes the development of a new chip topology, novel lensless feedback sensing, an MPC based on a simplified modeling approach, and the development of an automatic controller.

These developments will improve the viability of FCM as a microfluidic platform. It is hoped that these improvements will lead to FCM becoming an attractive yet extremely accessible alternative to DMF and MLSI. Such accessibility can spur the widespread adoption of microfluidics. Widespread adoption of microfluidics will contribute powerful and transformative capabilities to material science, biochemistry, among other fields.

Chapter 2 provides an overall methodology and description of the FCM system. Validation of the lensless sensing subsystem is provided in Chapter 3. Chapter 4 validates the simplified modeling approach. An MPC controller is designed and tested in Chapter 5. Chapter 6 describes and demonstrates autonomous operation. Chapter 7 summarizes the results and provides recommendations for future work.

Chapter 2

Methodology

2.1 Introduction

In this chapter, an overview of the complete feedback control based microfluidic system is provided. High level descriptions of critical subsystems and descriptions of standard methods used in all projects are provided. Additionally, the design and important features of the standard microfluidic chip used in subsequent chapters are given. Subsystem specific details are provided in later chapters.

2.2 System Overview

Figures 2.1 and 2.2 show the complete FCM system, which consists of five major subsystems:

- A standardized microfluidic chip with sufficient degrees of freedom for control. Within this chip, all droplet manipulations will occur. It is shown in Region 1 in Figure 2.1 and Region 4 in Figure 2.2.
- A visual feedback source, based on lensless microscopy techniques, observes the behaviour of the system. It is shown in Region 2 in Figure 2.1 and Section 4 in Figure 2.2. Power is provided from the benchtop power supply in Region 5 in Figure 2.2.
- A pressure system provides actuation for the microfluidic chip. The pumps are shown in Region 2 and the fluid reservoirs in Region 3 in Figure 2.2.

- A visual feedback pressure driving controller, termed low level controller, sets appropriate pressures based on measurements from the lensless system to track references. This controller is implemented as software and runs on the computer shown in Region 1 in Figure 2.2.
- A supervisor controller that sets references for the low level controllers based on standard descriptions of arbitrary droplet motion. This controller is implemented as software and runs on the computer shown in Region 1 in Figure 2.2.

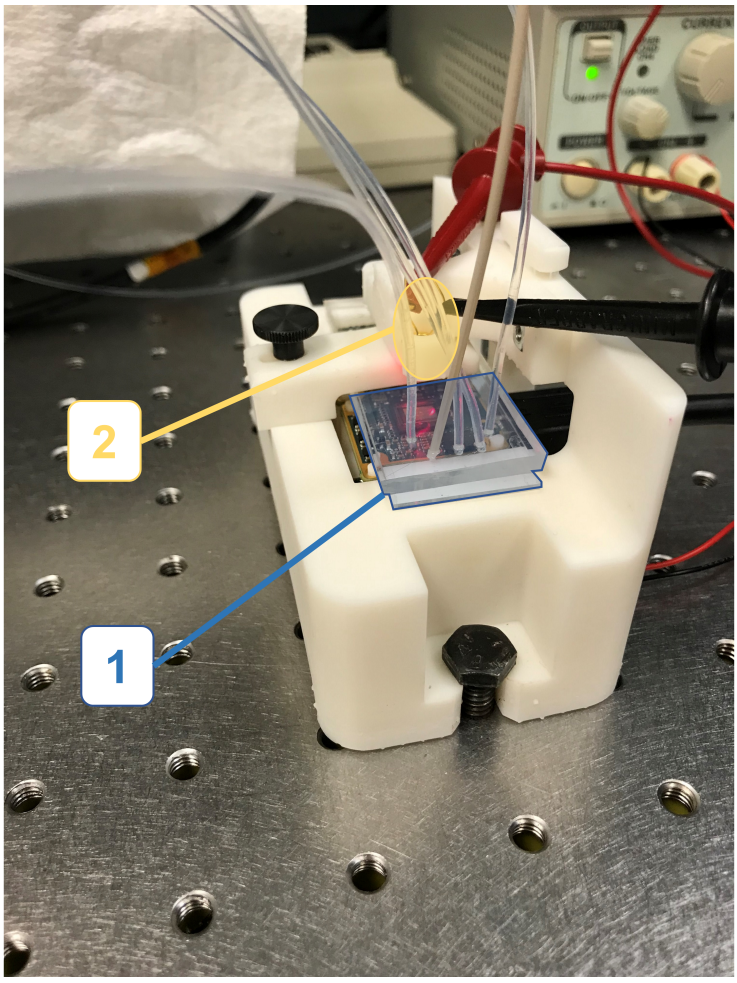

Figure 2.1: System: Microfluidic Chip (1) and Lensless Microscope LED (2)

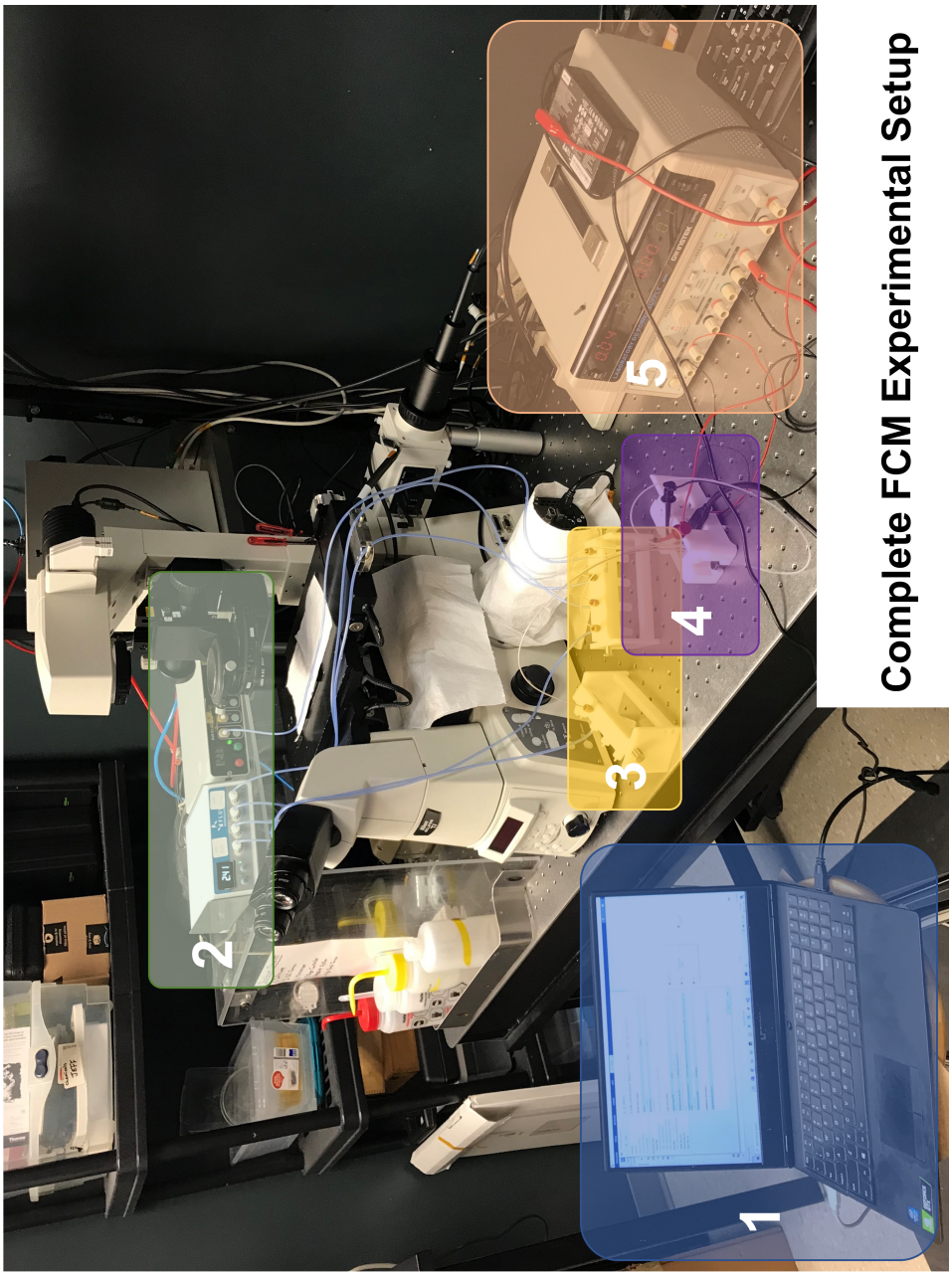

Figure 2.2: Experimental Setup (1) Computer (2) Pumps (3) Reservoir Holders (4) System (5) Power Supply

2.3 Major Subystems

2.3.1 Microfluidic Chip

Microfluidic Chip Design

Figure 2.3 shows the standard microfluidic chip. Lensless microscope FOV limitations and degree of freedom issues drive chip topology.

Within the chip, the carrier fluid (continuous phase) is 50 [cSt] silicon oil (Sigma-Aldrich). Deionized (DI) water composes the dispersed phase (droplet fluid). Surfactants are not used.

All channels are 50 [μm] in height and 120 [μm] wide. The choice of channel width is somewhat arbitrary as the lensless microscope can adequately measure droplets for channel widths of 60 [μm] and above. Chapter 3 details the lensless system.

The chip has ten total inlets and outlets ports. Ports can function as either an inlet or outlet as demanded by the use case. The channel network has 17 channels. To maximize plant stability, for example during droplet generation, vertical inlet and outlet channels have increased length [87].

There are two chip regions with visual feedback. The red outlines in Figure 2.3 show chip areas with feedback. The placement of feedback areas results from the minimum inter-sensor distance of the current sensor PCB. As the PCB extends a few millimeters beyond the CMOS sensor there is a physical limit on how close together the CMOS sensors can be placed. However, in principle, it is possible to reduce this distance with a custom PCB design. Within each sensing region, a 500 [μm] long cross can be used to calibrate the imaging system.

Microfluidic Channel Naming Convention

Figure 2.4 shows the channel numbering convention; odd numbers are assigned to horizontal channels, even numbers to vertical channels. Channel numbers are assigned from left to right, shown in light blue in Figure 2.4. Channel intersections are labelled with lowercase letters (shown in light orange) from left to right. Inlet and outlet ports are numbered left to right, shown in black in Figure 2.4.

For additional clarity, Figure 2.5, using the same convention, shows the channel, port and intersection naming on the microfluidic chip photomask.

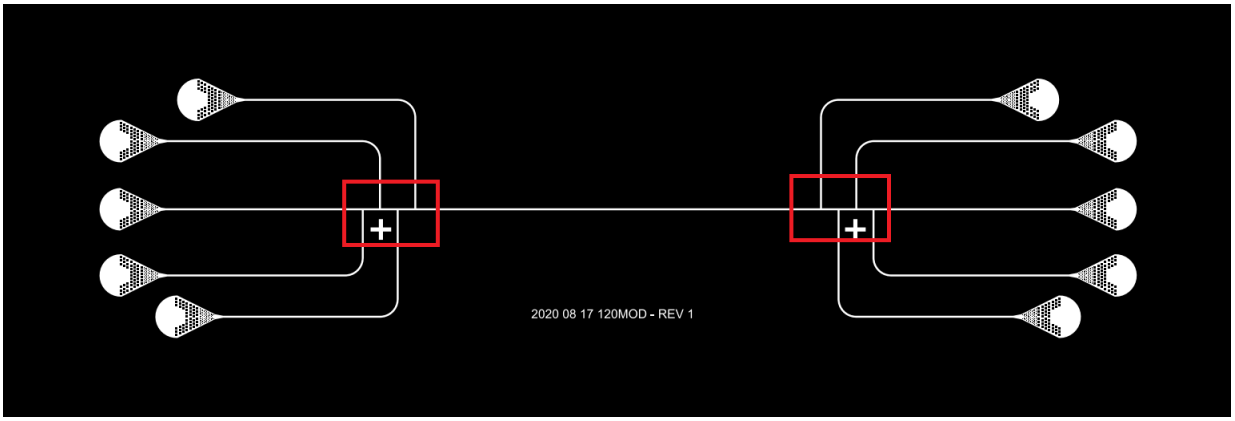

Figure 2.3: Chip Design

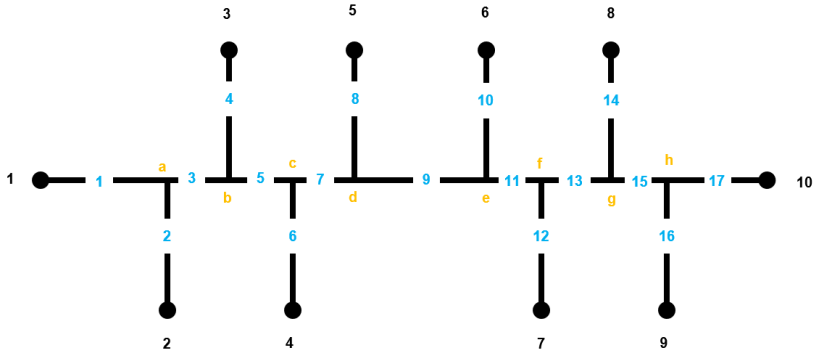

Figure 2.4: Channel Nomenclature

Floating Channel Concept and Degrees of Freedom

For a chip design to provide controllable functions it must have a sufficient DOF [26], as previously described in Section 1.3.1. Typical single or double T-junctions lack the needed DOF to carry out complicated or sequential unit operations. Thus, the standard chip design has additional channels to add extra DOF. These extra channels are called floating channels.

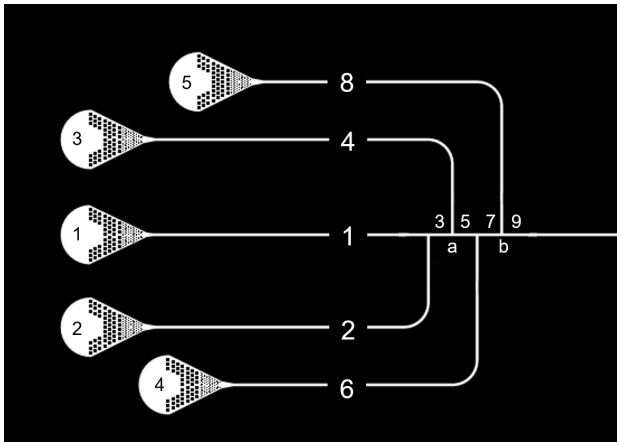

Figure 2.5: Channel Nomenclature Overlaid on Photomask

Floating channels have three properties that make their operation different from regular channels. First, a continuous phase reservoir directly feeds the floating channel.

Second, the fluid position in the channel is not regulated. No regulation allows the floating channels to act as a source or sink of the continuous phase. Floating channels can switch from source or sink modes during operation.

Third, floating channels are positioned adjacent to controlled or working channels. The adjacent positioning allows floating channels to isolate or decouple controlled channels from other controlled channels.

A schematic view of the floating channel concept is shown in Figure 2.6. Every second channel, shown in red, becomes a floating channel. The floating channels isolate the controlled channels, shown in grey.

Which channels are floating can vary during the operation of the system. It can be easily adjusted via software. This allows the system to have different functions that are configured virtually.

Dust Control

Dust is a considerable challenge to feedback control in microfluidics. Observations suggest dust produces significant (Order of Magnitude changes in gain) and fast (< 1 [s]) changes to the system dynamics. Fundamentally, feedback controllers are unable to effectively compensate for such disturbances [88]. Thus, controllers may not be able to ensure stability

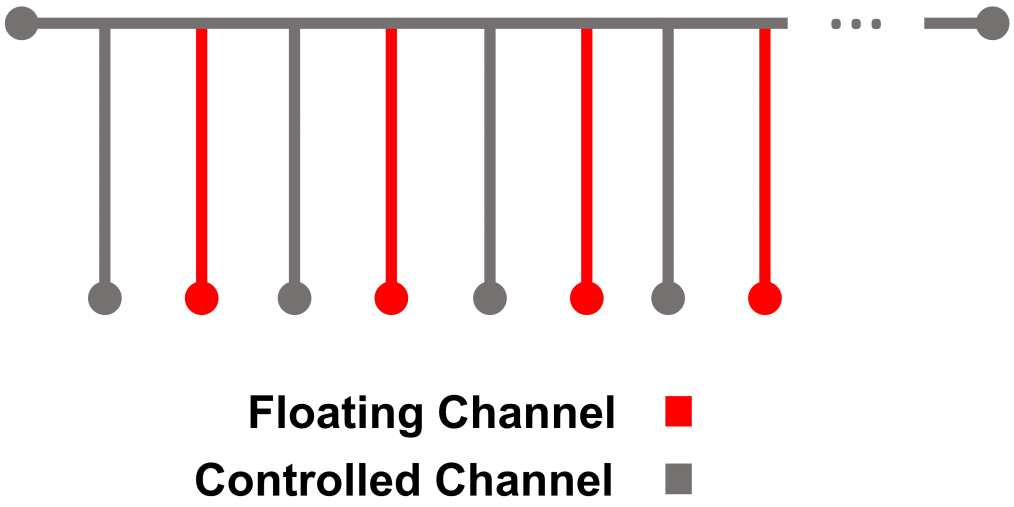

Figure 2.6: Floating Channel Concept

and performance with dust in the chip. Chapters 3 and 4 further discuss the impact of dust on the system.

A dust control surface, shown in Figure 2.7, is added to the chip inlets and outlet ports. The dust control surface moderates the effects of large dust particles. Ideally, large dust particles, which cause the most damaging changes in system dynamics, are caught by this structure, thus minimizing variations in the system dynamics.

Additionally, any fluid entering the chip is filtered by a 0.2 [μm] filter (28145-487, VWR). Any tubing that connects to the microfluidic chip is flushed with pure water and wiped with a damp cloth. The work surface is also wiped with a damp cloth.

Microfabrication

The microfluidic chips are made of polydimethylsiloxane (PDMS) (Dow Corning Sylgard 184) using replica molding. The molds are fabricated from a silicon wafer using standard soft lithography procedures [89].

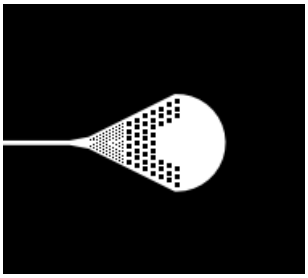

Figure 2.7: Dust Control Surface at Channel Inlets and Outlets

Briefly, the photoresist SU8-2025 (Microchem) is spin coated onto a silicon wafer resulting in a 50 [μm] thick layer, which is then exposed to UV light via a photomask. The unexposed regions are removed with a SU8 developer. The channels are thus 50 [μm] high and typically 120 [μm] wide, although a range of channel widths is possible.

2.3.2 Lensless sensing system

The purpose of the lensless system is to provide the control system feedback. Unlike other approaches, the lensless system is small and low cost while having comparable performance, from a control perceptive, to optical microscopes.

The lensless system is composed of a LED point source, CMOS sensor, and image tracking algorithm. The light source illuminates the sample chip which has its shadow captured by the CMOS sensor. The image tracking system detects and tracks droplet interfaces. Full details of the lensless system are provided in Chapter 3.

2.3.3 Controller

The purpose of the controller is to manage droplet position by manipulating pressure at chip inlets. An MPC based strategy is used for this system. Chapter 5 details the development of an MPC controller. The controller is run on a laptop computer (Legion Y530, Lenovo) with GPU (GTX 1060 6, Nvidia) for image processing acceleration under Windows 10 (Microsoft). The lensless and pump systems connect to the laptop through USB connections.

2.3.4 Supervisor

The purpose of the supervisor is to manage all other subsystems for the user allowing autonomous operation of the system. The supervisor takes a user's specification, or program, which in this implementation is in the JSON file format. The program can describe any useful operation, such as droplet generation, merging, or splitting, as a sequence of step references, and controllers. Based on the state of the system, the supervisor interacts with the low-level controllers to follow the specified step references. The supervisor is run on the same computer as the low-level controller described in Chapter 5. Chapter 6 provides details of the supervisor subsystem. The supervisor carries out autonomous system operation, defined by the user provided program.

2.3.5 Minor Subsystems

Tubing

The selection of tubing plays an important role in the control system. The positioning resolution of the system is dependent on the gain of the system. A large gain means low positioning resolution. Thus, a large tubing resistance and thus length is preferred. For silicon oil this is a 500 [mm] length of 381 [μm] diameter perfluoroalkoxy (PFA) tubing (Idex). For water, a 500 [mm] length of 127 [μm] diameter PFA tubing is used.

Pump

Throughput this project, two Fluigent MFCS series pressure pumps are used: a four outlet MFCS-EZ and an eight outlet MFCS pump. The Fluigent pumps are shown in Region 2 in Figure 2.2. The four channel pump is shown on the left in the image.

The pumps communicate to the control PC via a USB 2.0 connection at 10 [Hz] [90]. Although the design is proprietary, previous work suggests that electro-pneumatic (E/P) transducers comprise the internals of the pump [26]. The pumps receive 2.4 [Bar] and 1.3 [Bar] respectively from an external source. The pressure at each outlet is within the range of 0 to 2100 and 0 to 1100 [mBar] with 0.3 [mBar] resolution.

Pump outlets are connected through perfluoroalkoxy (PFA) tubing to the reservoirs (Flugient). Reservoirs, shown in Region 3 in Figure 2.2, hold fluids. When pressure is applied, the fluids flow from the reservoirs into the chip.

2.4 System Operation

Figure 2.8 describes how the components of the complete system interact. A user provides a program (a) that describes desired droplet actions to the supervisor (b) (Chapter 6). The supervisor breaks down complex actions into simple commands the controller (c) (Chapter 5) can follow. The controller then interacts with pumps (d), which manipulate the chip (e) (Chapter 2), based on lensless system (f) (Chapter 3) measurements. The supervisor and controller run on the same computer.

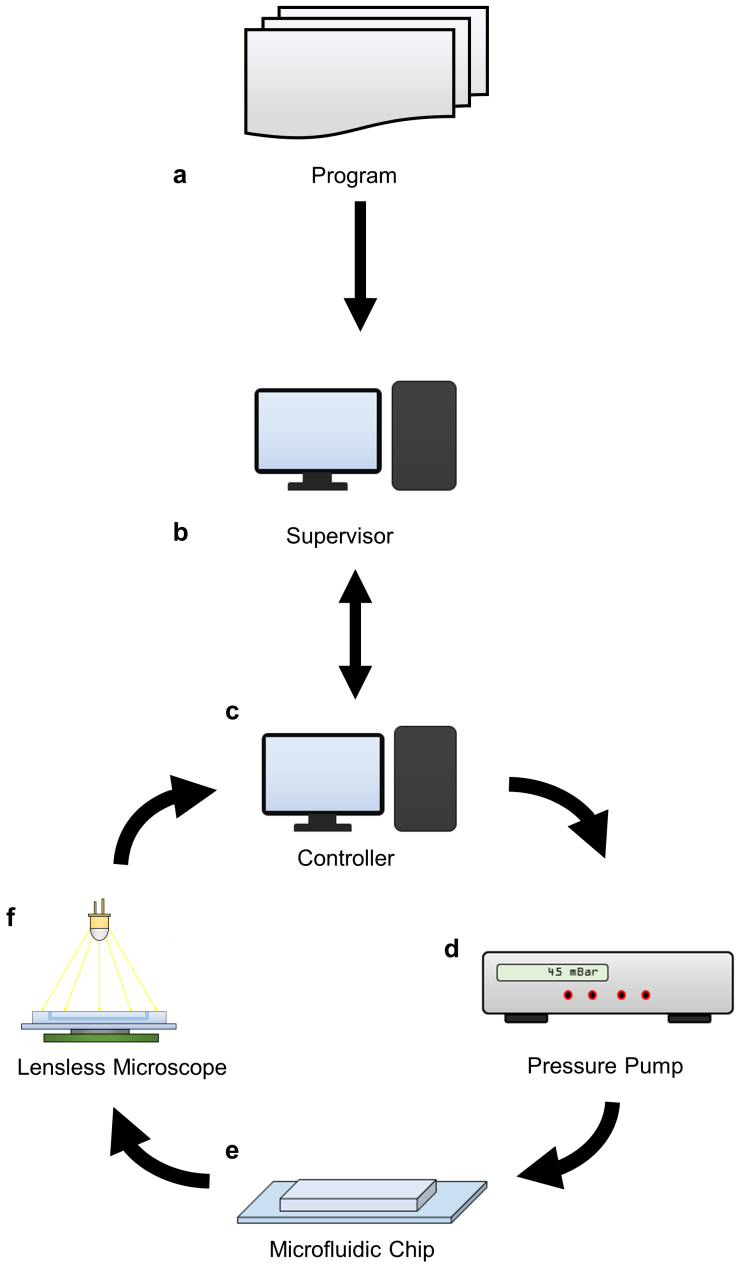

Figure 2.8: Subsystem Interaction

Chapter 3

Lensless Feedback

3.1 Introduction

Droplet microfluidics offers great potential and new capabilities in many application areas[1]. Yet microfluidic's adoption has been limited as the operation of such systems is challenging. Unlike previous methods, feedback control microfluidics can address usability challenges without performance or hardware challenges [4].

Despite the potential, in practice, FCM is limited by current feedback methods. Many studies use an optical microscope to provide visual feedback [34] [27] [26]. Conventional microscopy-based feedback systems impose restrictions on the physical size and system cost [39] [38]. The requirement of a microscope makes the application of the control technique incongruent with practical concerns. Alternative methods based on capacitive or microwave sensing lack required performance, complicate microfluidic device fabrication or require bulky instrumentation [64]. Therefore, a new feedback method for droplet tracking is needed.

Here we show a new method of droplet tracking based on existing lensless imaging techniques. The method is based on a simple device that consists of a single LED and a CMOS sensor. Results show that this system has the potential to provide a low-cost alternative to conventional microscopic droplet imaging in visual feedback-based active control platforms.

[1]Sections of this chapter are taken from submitted manuscript and reviewer comments: Tomasz Zablotny, Matthew Courtney, Jan P. Huissoon, and Carolyn L. Ren. "Lensless imaging for droplet identification towards visual feedback-based pressure controlled droplet microfluidic platforms" (2021).

3.2 Working Principle

The physical mechanism by which droplet interfaces are recorded by a shadow imaging method is based on Snell's law. Snell's law [39], Equation 3.1, describes the behaviour of a light ray during refraction, where n is a dimensionless number describing the speed of light in the medium and θ is the incident angle, as depicted in Figure 3.1.

$$n_1 sin\theta_1 = n_2 sin\theta_2 \tag{3.1}$$

Figure 3.2 shows the idealized paths of light rays through a microfluidic chip cross section. Pixels P1 to P8 record incident light intensity. According to Snell's Law, light rays that do not cross the curved droplet interface continue with their path unchanged across different material boundaries because their incident angle is near zero. On the other hand, a light ray that crosses the droplet interface will have a nonzero incident angle. Therefore, as shown in Figure 3.1, Snell's Law indicates that the light ray will change its direction at the droplet interface. The resulting difference in illumination at Pixel P4 is used as the basis of droplet interface detection.

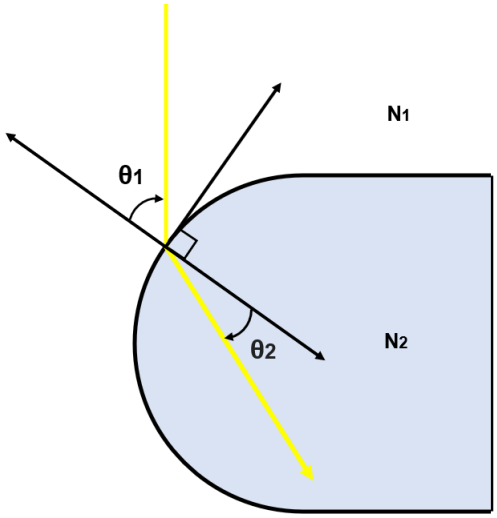

Figure 3.1: Snell's Law for a Droplet Interface

3.3 Limitations

Figure 3.1 describes the ideal case. Practically, non-ideal behaviours like diffraction, the degree of collimation, illumination uniformity, pixel saturation, pixel density and pixel noise place limits on the achievable performance.

3.3.1 Diffraction

Diffraction is a fundamental limiting factor for shadow imaging [67]. Diffraction, the bending and spreading of waves around an obstacle's edges contributes to the blurring of the image [39] [38]. The effect of this phenomenon causes gradients rather than step changes in the light intensity. While this effect cannot be eliminated, it can be limited by minimizing the distance between the sample and the imaging sensor and selecting sources of small wavelengths [67] [39].

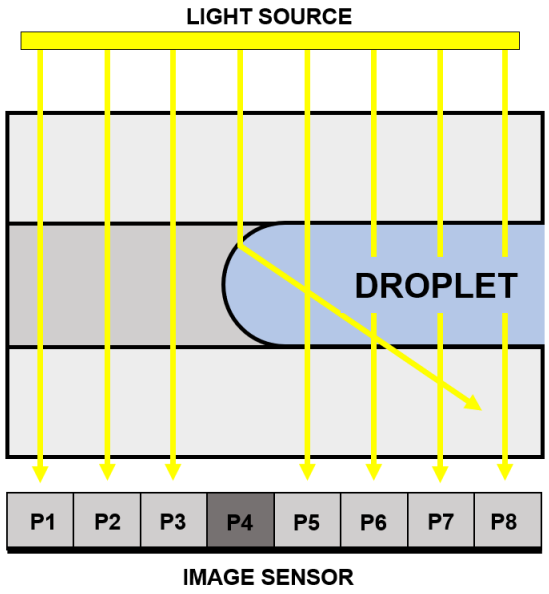

Figure 3.2: Ideal Shadow Imaging Cross-Section

3.3.2 Collimated

The ideal shadow imaging case assumes parallel, or collimated, light rays perpendicular to the chip surface. This is not the case in practice even with specialized sources. If the light enters at a significant angle it will distort the resulting image. This non-ideal behaviour contributes to blurring in the image. This can be minimized by selecting source LEDs with smaller beam angles [68] and positioning the light source, sensor and samples to optimize the perpendicularity.

3.3.3 Illumination Uniformity

Poor illumination uniformity will make image processing more difficult, thus affecting system performance. Selecting an appropriate LED, and tuning the LED to sensor distance and the LED intensity minimizes spatial illumination variation. The acceptable spatial illumination variation is dependent on the microfluidic chip design.

3.3.4 Pixel Saturation

Pixel saturation limits performance as differences in intensity are not registered beyond hardware limits. With a high source intensity, saturated pixels will output a white image from which droplets will not be detected. Pixel size places limits on system performance as one pixel will only quantize the light intensity over its area. Thus smaller pixels will provide a more detailed image. This is important for droplet detection as the channel width can be less than 100 [μm]. Pixel noise, random noise from the sensor, causes the appearance of high frequency noise in the image. This noise is especially significant at smaller field-of-view (FOV) where this noise is more predominant.

3.4 Method

3.4.1 Chip Fabrication

The microfluidic chips are made of polydimethylsiloxane (PDMS) using the standard method described in Chapter 2. The T-junction channels are 50 [μm] high and 30, 60, 90, 120 and 150 [μm] wide. All chips included a repeating saw-tooth pattern of 200 [μm] period parallel to the main channel. The pattern was used for calibration. Silicon oil 50

[cSt] (Sigma-Aldrich) and Deionized water are used as the carrier fluid (continuous phase) and droplet fluid (dispersed phase) respectively. No surfactants were used. A pressure system (MFCS-EZ, Fluigent) is used to pump both phases.

3.4.2 Lensless Imaging System

Figure 3.3 shows a schematic (a), cross-section view (b), and photo (c), of the lensless imaging system respectively. The microfluidic chip is secured directly to the top of the image sensor (MT9P031, ON Semiconductor) with a 3D printed polycarbonate enclosure and a 30 [mm] optical cage system (ThorLabs). A 650 [nm] point source LED (MTPS9067P-C, Marktech Optoelectronics) is attached perpendicularly to the enclosure 20 [mm] away from the CMOS sensor. The 20 [mm] distance was optimized through experimental testing. The LED is connected to a DC power supply (GPS-4303, GW Instek) with a 140 [Ohm] series resistor (Vishay). The x-y position of the chip and LED voltage (1.7 to 1.9 [V]) are tuned to minimize the illumination gradient in the region of interest.

3.4.3 Microscope

A conventional microscope with a 2X Objective (TI-E Eclipse, Nikon) is used to generate images that are defined to be the ground truth in this testing. Given the superior optical quality and high resolution ($\approx 1.75\ [\frac{um}{pixel}]$) of the microscope, it has sufficient accuracy needed to provide ground truth.

3.4.4 Image Processing

Peak Detection

The characterization of the lensless method uses a peak detection approach. The distance between intensity peaks, that correspond to droplet interfaces, define droplet lengths. Defining droplet position by intensity peaks gives a consistent and unbiased method of determining droplet length.

Figure 3.4 illustrates the peak detection method. Prior to processing, raw images are manually straightened/aligned (Image A). The images are then inverted (Image B) thus converting interface location to local brightness peaks, and blurred with a Gaussian filter to remove noise (σ 5) (Image C). Following this, background features are removed by

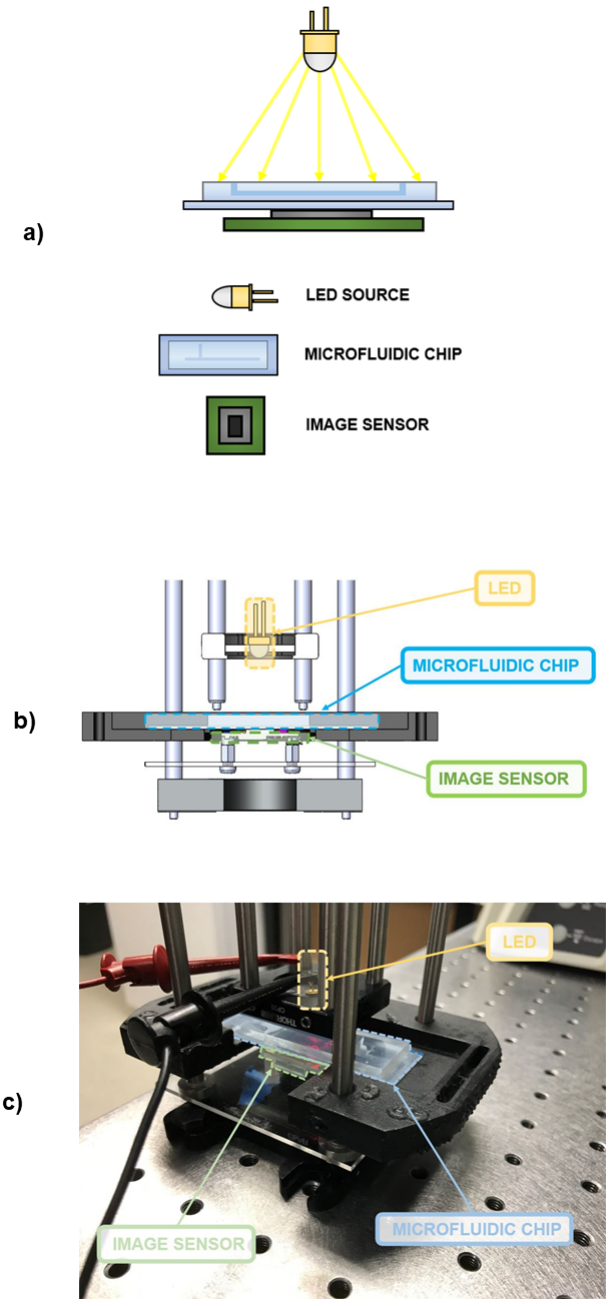

Figure 3.3: Schematic (a) Cross-Section View (b) and Image (c) of Lens-less Imaging Apparatus

subtracting the local mean, found via a box filter (Image D). The size of the box filter is tuned based on the image's illumination gradient. Finally, the droplet length is defined as the difference in the x-position of the peaks of the mean intensity plot (Image E) along the centerline of the channel. Figure 3.5 shows a plot of the mean intensity plot.

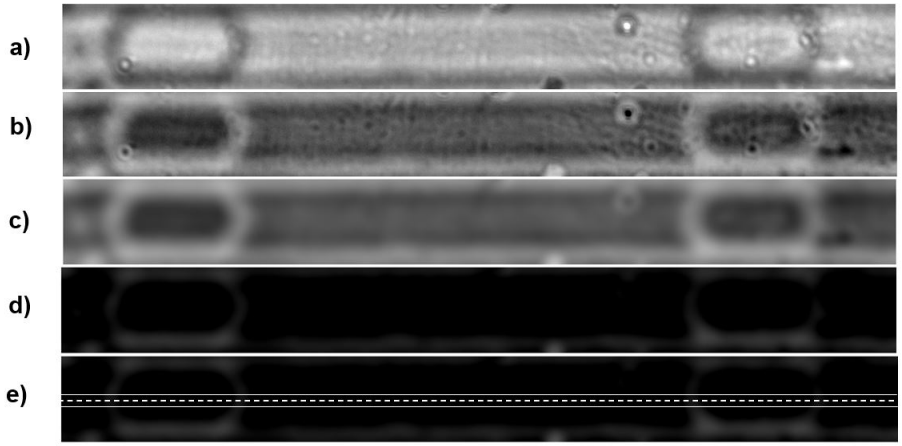

Figure 3.4: Droplet Peak Detection [μm] Channel

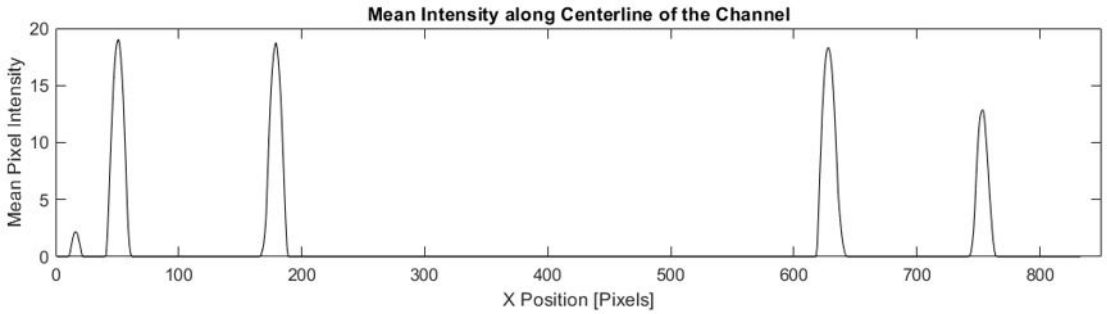

Figure 3.5: Lensless Intensity Plot

Template Matching

Peak detection provides a consistent and unbiased framework for droplet measurement useful for calibration studies. A major problem is that peak detection is susceptible to local

noise or dust causing false detections. Template matching may be used to identify interfaces more reliably. For template matching, droplet interface templates are generated for a specific channel geometry. Figure 3.6 shows leading and lagging interfaces for a 120 [μm] wide channel. Before commencing the study, channel boundaries are manually defined. These boundaries define where template matching will occur. Within each channel boundary, normalized cross-correlation is applied (OpenCV) [91]. Following this, thresholding is applied to remove obvious nonmatches. Points of maximum intensity, corresponding to the area of a high likelihood of a match, are found. Local non-maximum suppression is applied to prevent a single interface from creating multiple detections.

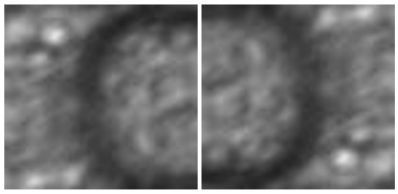

Figure 3.6: Lensless Template

3.5 Results

3.5.1 Raw Image Result

Figure 3.7 shows a comparison between the microscope and lensless system images of nominally 200 [μm] long droplets in various channel widths. In channels wider than 30 [μm] the image quality is fairly consistent.

It is theorized that for channels smaller than 30 [μm], the relative size of the channel height (50 [μm]) results in a greater proportion of light being refracted. This causes the droplet interface to have lower contrast as the background channel image is darker. Additionally, being a smaller channel, the sensor has fewer pixels to detect the droplet interface (the pixel size is 2.2[μm] square).

The blurred appearance of the lensless images is due to diffraction and non-perpendicular light rays. Diffraction causes the shadow edges to appear less sharp, and as the light source

is not collimated, the shadow is projected onto the sensor plane at an angle making the edges of channels and droplets appear thicker.

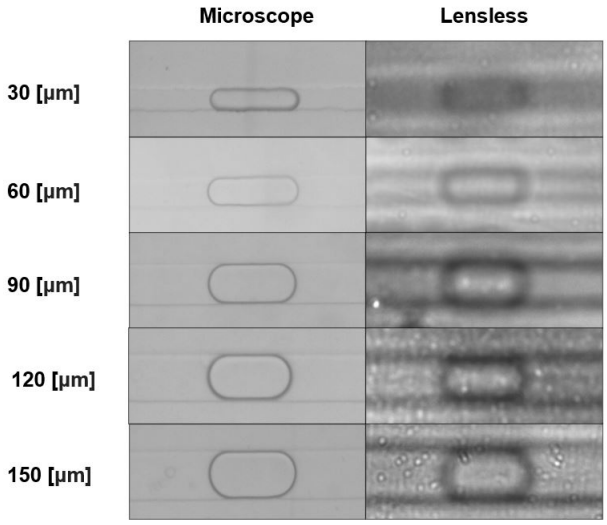

Figure 3.7: Raw Lensless Result Compared to 2X Microscope Image

It should be noted that the appearance of the droplets in Figure 3.7 depends on the magnification, as shown in Figure 3.8. On the left of Figure 3.8 is a lensless image of a 120 [μm] channel with four droplets. On the right of this Figure are the scaled images of the circled droplet at roughly 1.25, 2.5 and 5 times magnification. Note that the channel width is about 55 pixels.

Although the images shown in Figure 3.8 are all of the same scaled image, it appears that the less scaled images are qualitatively better. This is a well known consequence of the human visual system as higher frequency spatial components are less dominant at lower magnifications [92]. Thus the image characteristics which make the scaled images appear worse are less detectable at lower scales. This effect causes the perceived quality discrepancy at different scales.

3.5.2 Detection Rate

In order for the automated control systems to function, the system needs to be able to automatically identify droplet interfaces. The performance of the system with respect to

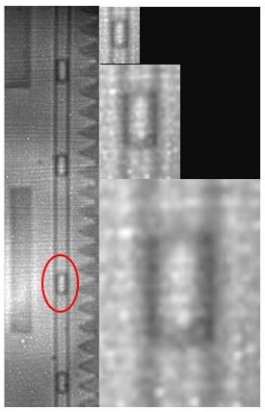

Figure 3.8: Consequences of High Frequency Spatial Components

this is quantified by two metrics: the miss rate (MR) and the positive predictive value (PPV). The system's performance is compared to a human labeled ground truth.

The miss rate indicates the failure of the system to detect a droplet interface when the interface exists. Equation 3.2 defines the miss rate as the number of misses over the total number of droplets [93]. In this equation, Tp is true positive, or the number of interfaces correctly identified, and Fn is false negative, or the number of interfaces not identified correctly. For each channel width 50 droplet interfaces were used.

$$MR = \frac{Fn}{Fn + Tp} \tag{3.2}$$

The PPV measures the ability of the system to distinguish between true interfaces and false detections. It is defined by Equation 3.3 as the true positives over the total number of detections. Fp represents the number of detections that do not belong to a true interface [94]. The true positives are taken from the human labeled ground truth.

For this test, we define an interface detection as all peaks of mean pixel intensity along the centerline of the microchannel which exceed a threshold. This threshold value is tuned based on illumination levels.

$$PPV = \frac{Tp}{Tp + Fp} \tag{3.3}$$

Table 1 summarizes the detection rate performance of the system. For channels above 30 [μm] the performance is satisfactory as almost all droplet interfaces are detected and very

few misdetections occur. It should be noted that when using the microscope, misdetections due to dust also occur.

Table 3.1: Droplet Detection at Different Channel Widths [μm] (N=50)

Width	PPV	Miss Rate
30	0.929	0.02
60	0.961	0.00
90	0.980	0.04
120	0.980	0.02
150	0.961	0.00

Cases where droplet interfaces are not detected often occur in regions with noticeable intensity gradients. Thus by maximizing the uniformity of illumination in the region of interest one can minimize errors in interface detection.

Cases in which a droplet interface is erroneously detected occur when an artifact is found in the image. Ensuring the sensor and chip are free of dust and residues will improve performance in this respect. Droplets in the 30 [μm] channel are more likely to be miss-identified due to poorer contrast and higher noise leading to a lower PPV value.

3.5.3 Accuracy and Precision

To give a quantitative measure of accuracy and precision, the lensless imaging measurement was compared to ground truth data, generated by a conventional optical microscope described in Section 3.4.3. The droplets were generated in channels of width 30, 60, 90, 120 and 150 [μm]. The images of the droplets were then taken on both the lensless imaging system and the conventional microscope. The droplet interfaces were used as the measured quantity as they remain ideally constant despite the movement of the chip between the two measurement systems. The location of the interfaces was defined by the peak of the intensity along the centerline of the channel.

Although the droplet length was assumed to be constant, this is not entirely true in practice. Transitioning between the two measurement systems, a period of 2-3 minutes elapsed. In that time, droplet evaporation could occur, and therefore the error presented is likely higher than the true error. For smaller width channels the contribution of this error source is larger.

It should be noted that having the microfluidic chip in contact with the sensor caused the chip to heat up and accelerated droplet evaporation. However, this heating can be lowered significantly by implementing a cooling system in the future [95].

Figure 3.9 shows the parity plots ($n = 10$) comparing the lensless imaging and the microscope measurements. Note that the data show that the mean absolute error for all the channels except 30 [μm] wide is less than 10 [μm]. The mean absolute error for the 30 [μm] wide channel is 15 [μm]. This performance is sufficient for the control application [26]. For 30 [μm] width channels the error appears higher as the noise is more dominant, the contrast is lower and droplet shrinkage is larger.

3.5.4 Resolution

The resolution, the smallest detectable change in droplet position, is limited by pixel size, which for this sensor is 2.2 [μm] [95]. 2.2 [μm/pixel] is the calibration value that was consistently achieved, based on the micro-patterned 200 [μm] period saw-tooth pattern adjacent to the channel. To determine the resolution, droplets were generated within a 150 [μm] wide channel and tubing connections were removed. After the chip reached steady state, the position of the droplet interface was tracked. Evaporation caused uncontrolled but very slight movement in the interface position.

Figure 3.10 shows the droplet interface position (in pixels) over successive images at 25 [Hz]. Note that the step in the graph represents the minimum detectable change in position. This figure shows that at very small movements the system was able to detect one-pixel changes, which is the system resolution.

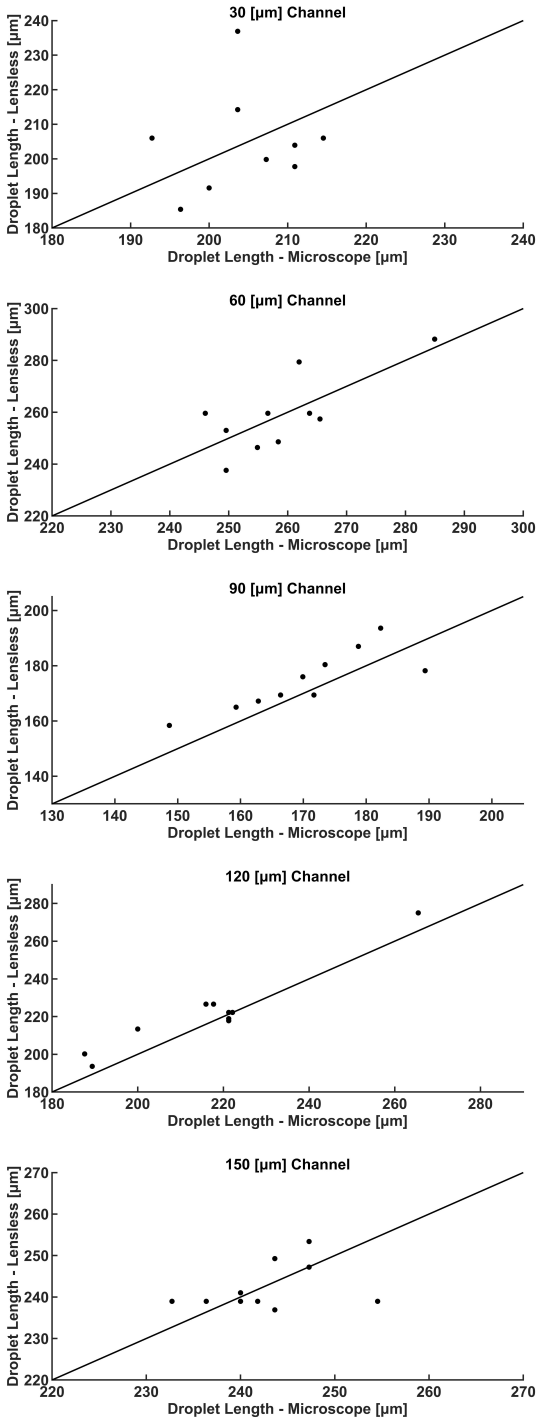

Figure 3.9: Lensless Accuracy at different channel widths

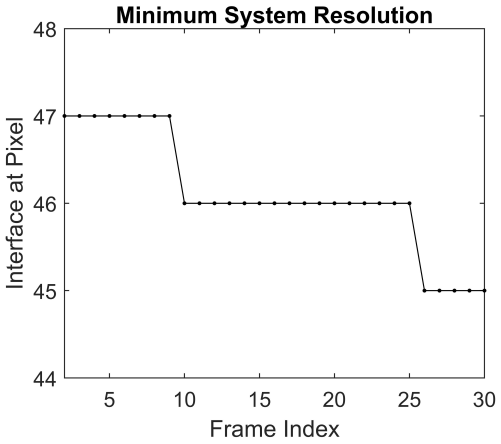

Figure 3.10: Droplet Interface Location under slight movement

3.5.5 Frame Rate

For full frame 2592 by 1944 pixels (5.70 by 4.27 [mm] area), the specified frame rate of 14.1 [Hz] was consistently achieved [95]. However, in practice, the full frame image is not required as only a portion of the image will contain microchannels. Typically, images sensors are configurable and allow a reduction in FOV to enhance frame rate. For example, at a reduced frame size of 2000 by 815 pixels (4.40 by 1.79 [mm] area), the system has a frame rate of 40.2 [Hz] which is comparable to the 40 [Hz] camera (5.5 sCMOS, Andor Zyla) used by [26]. Moreover, for current implementations of control systems, such a high frame rate is not needed as the typical microfluidic pumps limit system update frequency to 10 [Hz] [26] [9].

3.5.6 Cost

The cost of the system is substantially lower than conventional microscopes. The Bill of Materials (BOM) cost for the image sensor, LED and 3D printed enclosure is slightly less than 200 [USD]. This excludes the cost of a laboratory DC power supply, which can be replaced with off-the-shelf modules quite cheaply and easily. Assembly is quite simple with no high tolerances or specialist assembly techniques required. Compared to conventional microscopes this is a significant cost reduction.

3.5.7 Footprint

The footprint of the lensless system is significantly smaller than conventional optical microscopes. Disregarding the holder, which can be designed to meet arbitrary needs, the absolute minimum required footprint is around 27 (L)x27(W)x32(H) [mm]. This leads to an interesting outcome not possible with a conventional microscope. Two lensless systems can image a single standard size microfluidic chip because of the reduced footprint. This gives the capability to provide feedback control at multiple regions. Another consequence of the small size and low cost is that multiple lensless systems can be used for feedback, and also provides the potential for creating feedback controlled interchangeable modules which is not possible with optical microscopes.

3.5.8 Droplet Tracking

Finally, the validated lensless system was applied to track droplets, one of the key functions in typical droplet microfluidic applications. Using the 150 [μm] width channels described in Section 3.4.1, droplets of 300 [μm] nominal length were generated. The motion of the droplet was recorded at 25 [Hz] using the lensless system. Figure 3.11 and 3.12 show the droplet movement over time. The algorithm, described in Section 3.4.4, was applied and the location of the droplet interfaces was recorded. The interface detections occur automatically so only interfaces belonging to the tracked interfaces are shown in Figure 3.12.

The results demonstrate that the droplet interfaces were tracked consistently. It should be noted that the presence of dust or residue which occurs often in regular labs (not cleanroom) can cause false detections and thus should be avoided as much as possible. However, given the results, the position of the droplets can be fed back for use in a control algorithm. Appendix A shows an video of this action.

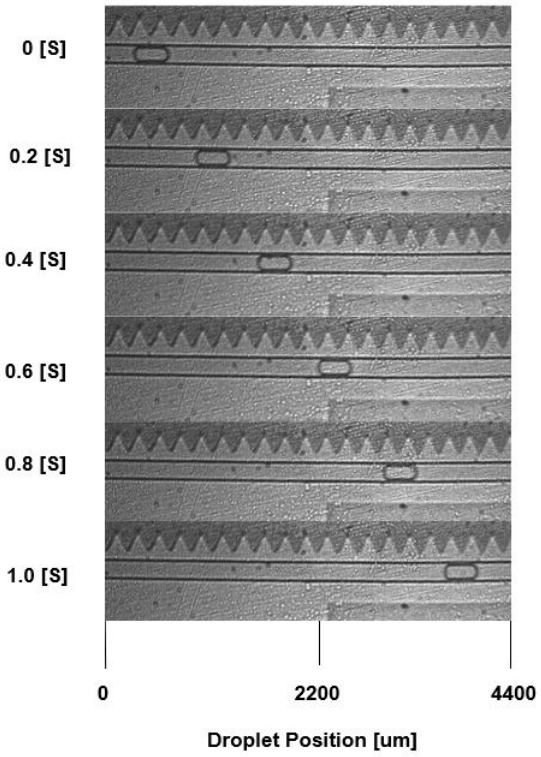

Figure 3.11: Movement of Tracked Droplet in 150 [μm] Channel

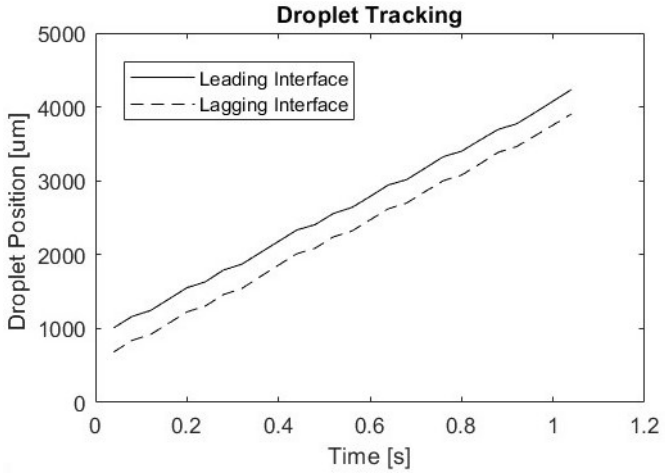

Figure 3.12: Tracked Droplet Movement in 150 [μm] Channel

3.6 Discussion

For the lensless system to be sufficient to replace a conventional microscope, it should be comparable with the microscope for the following properties:

- Droplet interfaces should be correctly detected by the system. This means that droplet interfaces should be identified as such, and non-interfaces should not be misidentified as interfaces.
- The measured value should be accurate and precise. The droplet measurement should reflect the true value of the measured property.
- The frame rate of the imaging system should be fast enough so that it is sufficient for active control. Previous studies have successfully used a 10 [Hz] sample rate [34] [9].
- The FOV should be large enough to observe a reasonable chip area.
- The system cost should be suitable for widespread use and be significantly lower than that of a conventional microscope.
- The footprint of the system should be sufficiently small so that bench-top use is possible.

Based on the presented results, the lensless system can be used in place of a conventional microscope for visual feedback-based pressure controllers for droplet manipulation. It has shown comparable performance as well as having successfully tracked a droplet. Thus, one can conclude the lensless system can detect droplets accurately over a reasonable FOV at an adequate frame rate and resolution. It can do this while being smaller and lower cost.

Compared to the previous system devised by Wong, the lensless system has a reduction of both cost and footprint by an order of magnitude. Yet, in terms of performance, from the control system perspective, it is comparable for a wide range of channels widths.

The success of this technique has multiple implications for Visual Feedback Controlled Microfluidics. Firstly, as a result of the low cost and small footprint, multiple lensless units can feasibly be used for one experiment. This provides fundamentally new capabilities that could not be done with a single conventional microscope. Secondly, because of the small print, multiple lensless units can observe a single microfluidic chip. This provides new freedom in the design and use of Visual Feedback Controlled Microfluidics methods.

However, some limitations exist with this technique. The close contact between the sensor and chip can lead to channel heating (unless a cooling system is implemented). The current system does not allow for more sophisticated microscopy techniques, such as fluorescent imaging [96][97]. However, there exist in the literature modifications to the lensless techniques that would permit some of these approaches. Fundamentally, smaller channels are difficult to observe with this method.

Despite these challenges, the lensless system overcomes practical challenges that limit the application of FCM. By overcoming these challenges, it provides new capabilities and greater accessibility of FCM methods.

3.7 Summary

The capabilities of feedback control in microfluidics are tempered by constraints on feedback systems. This chapter presents a novel application of lensless microscopy techniques acting as a feedback system. While having adequate measurement performance the presented system has significantly lower cost and size compared to existing feedbacks techniques. The modest cost and small size widen the accessibility of feedback control microfluidics.

Chapter 4

Modeling

4.1 Introduction

The application of feedback control in droplet microfluidics has shown promise as it can increase the usability and consistency of droplet microfluidic devices [27]. However, in microfluidics successfully applied feedback control techniques are model based and require the development of mathematical system models [34].

In the literature, for control purposes, droplet microfluidic dynamics relating the droplet velocity (or flow rate) along a channel to the input pressure have been modeled as an equivalent electrical circuit with a resistance, capacitance, and inductance (Voltage-Pressure analogy) [26]. This approach will be referred to as the RCL methodology. Channels are arranged to match the microfluidic chip topology. The values of each channel's fluidic resistance, capacitance, and inductance are assigned to the model. Tuning values are used to adjust the model parameters [26].

However, the RCL methodology presents several limitations. The models produced are high order, poorly numerically conditioned, and require non-obvious tuning values. High-order models complicate the control design process as they are harder to understand and manipulate. The poor numerical conditioning necessitates the use of non-standard analysis techniques [26]. Furthermore, poor conditioning can lead to situations where stable systems yield unstable models, complicating the design process. Additionally, finding valid tuning values is non-obvious, especially for non-specialist users. The limitations of the RLC modeling approach increase the difficulty of control design and successful use. Such complexity leads to poorer controller designs or inhibits the use of potentially powerful feedback control techniques in microfluidics.

In initial experiments investigating the droplet dynamics, an integral-like droplet displacement response to a step input in pressure was observed. This observation led to the hypothesis that the system could be more simply modeled as a first order system. Based on this insight, this chapter presents an alternative method that models each microfluidic channel as an integrator with a resistive gain. Individual channels are arranged to match the microfluidic chip topology as before. However, the values of the resistive gain are found with a simple experimental procedure, rather than from first principles. This modeling method approach yields a lower order system and numerically well-conditioned model that requires no tuning values, and can be used as the basis for a successful controller design.

4.2 Modeling Methodology

The simplified modeling approach is based on the insight that the capacitive and inductive elements of the RCL model are only significant at higher frequencies. For most microfluidic control applications, the high frequency effects can be disregarded with minimal impact on model accuracy. From this insight, a simplified model of single microfluidic channels, including offset compensation, is developed. This single-channel model is extended to the Multi-Input Multi-Output (MIMO) channel network model and a generalized state-space representation is presented. Finally, the assumptions of system linearity, stabilizability, and detectability are justified.

4.2.1 Single Channel Nominal Model

The simplified approach models microfluidic channels as integrator and resistive gain. A block diagram representation of this approach for a single input single output (SISO) channel is shown in Figure 4.1. Alternatively, the differential equation 4.1 describes an equivalent single channel mathematically. The model input, u or Pressure Input Block, is the pressure differential between the start and end of the channel. The model output, Droplet Displacement Block, is fluid displacement in the channel, x. The R term is equivalent to the fluidic resistance of the channel.

$$\frac{\mathrm{d}x}{\mathrm{d}u} = R \tag{4.1}$$

In contrast to the simplified approach, Figure 4.2 demonstrates the previous modeling methodology. The channel is modeled using the full RCL electrical analogy. In the model,

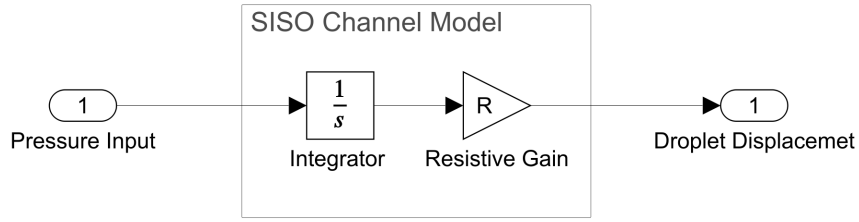

Figure 4.1: Single Channel Block Diagram for Oil Channel

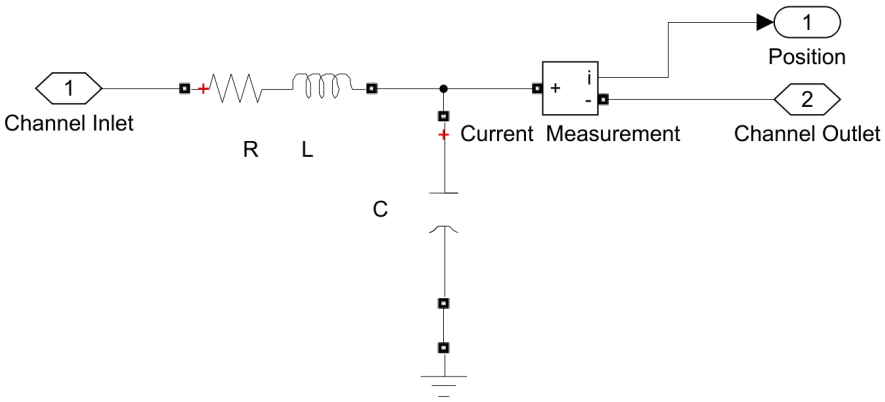

Figure 4.2: RCL Channel Simulink Model

Diamond Box 1, is input voltage or in the microfluidics context applied pressure. The output of the model is current, or fluid flow, through the channel. The current output block outputs this value. R, C, and L are the fluidic resistance, capacitance, and inductance respectively.

Offset

The simplified approach is valid for channels mainly filled with oil. However, models for water filled channels must be adjusted to account for a previously negligible effect. Typically, water filled channels have a backward (towards the source inlet) flow in an unpressurized chip. Previous work suggests Laplace pressure is, in part, the cause of this

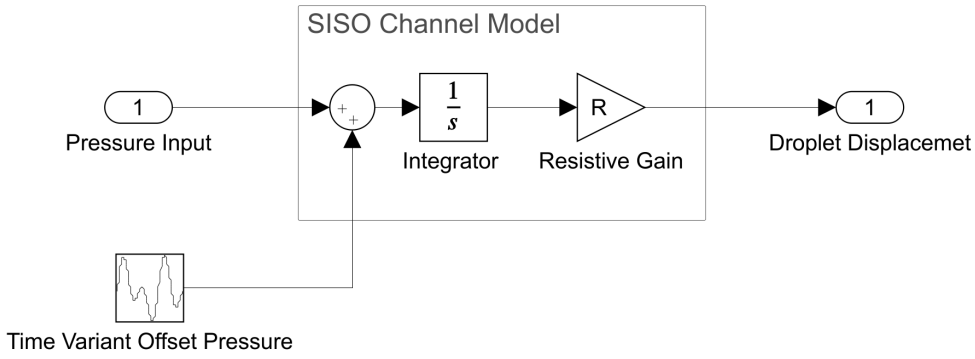

Figure 4.3: Single Channel Block Diagram for Water Filled Channel

flow [26]. A new offset term at the input can account for this phenomenon.

Figure 4.3 shows the block diagram of the modified water channel model. An additional block, Time Variant Offset Pressure, is added to water channel models to account for this flow. The offset magnitude is variable with a typical value of -35 [mBar] ± 35. Seldomly, a forward flow (away from the source inlet) can occur. Alternatively, Equation 4.2, describes the offset's, γ, affect on the true input pressure, u_{adj}.

$$u_{adj} = u - \gamma \tag{4.2}$$

The offset term magnitude exhibits time variant behaviour. It has been observed that significant magnitude variances appear to be correlated with large dust particles and large surface wetting changes. These observations suggest that dust and surface wetting change channel resistance and cause time variance.

4.2.2 Channel Network Model

Thus far, the simplified approach only models single oil or water channels. For practical use, the methodology must model complete channel networks. A channel network model can be created by modeling each channel individually. Tubing resistance can be included in the resistive gain of channels directly connected to the tubing.

Individual channel models are then interconnected to match the spatial orientation of the chip network. Figure 4.4 shows the resulting simplified model when applied to the standard chip. The chip schematic can be seen in Figure 2.3 in Chapter 2.

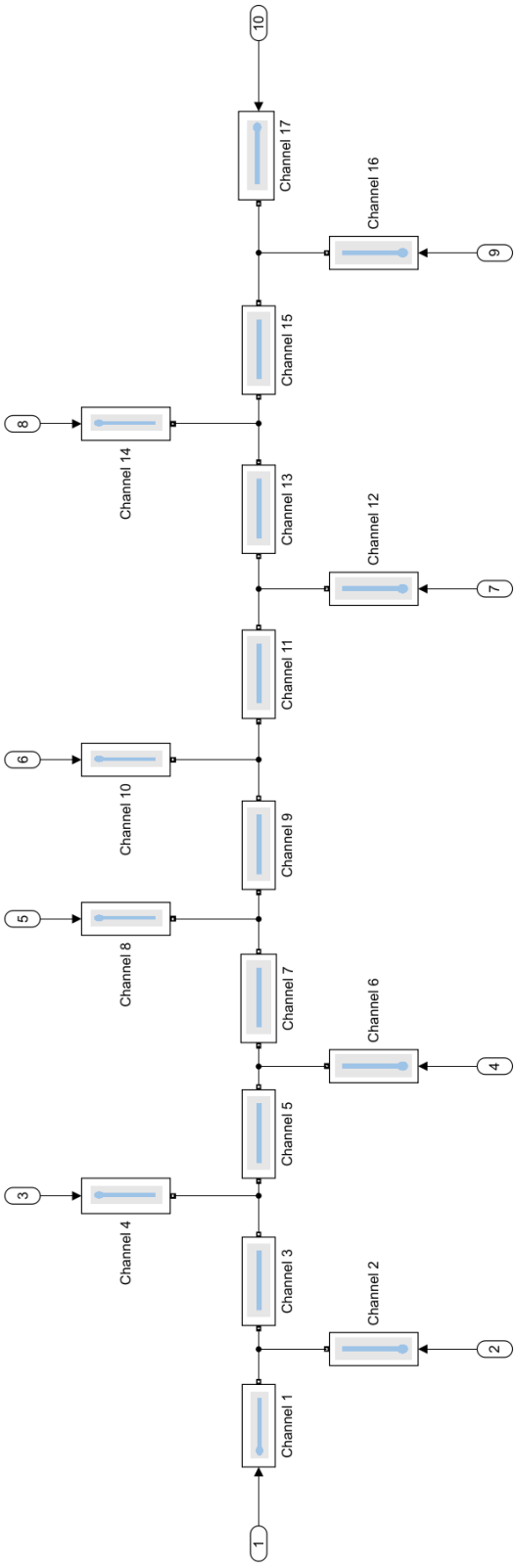

Figure 4.4: Complete Block Diagram for Complete Chip

One should note that unlike the RCL method each channel is treated separately in the simplified approach. At channel interconnections, with RCL, flows at each junction must sum to zero. However, for the simplified approach, the system's state, position, is not subject to these physical constraints. Thus requiring each channel to be treated separately.

Simplified Model Structure

More formally, a generic state-space representation of channel networks is described by Equations 4.3 to 4.7. The general state-space form is shown by Equations 4.3. Equations 4.4 to 4.7 show the structure of the state space matrices.

$$\begin{aligned} \dot{x} &= A \cdot x + B \cdot u \\ y &= C \cdot x + D \cdot u \end{aligned} \tag{4.3}$$

In this description, u is the input vector in the form of applied pressures. x is the state vector representing the position of fluid in the channels. A, B, C, and D are the state, input, output, and feedthrough matrices respectively.

$$\mathrm{A} = \boldsymbol{0_{n,n}} \tag{4.4}$$

$$\mathrm{B} = \begin{pmatrix} R_{1,1} & R_{1,2} & \dots & R_{1,u} \\ R_{2,1} & R_{2,2} & \dots & \vdots \\ \vdots & \vdots & \ddots & \vdots \\ R_{n,1} & \dots & \dots & R_{n,u} \end{pmatrix} \tag{4.5}$$

$$\mathrm{C} = \boldsymbol{I_{n,n}} \tag{4.6}$$

$$\mathrm{D} = \boldsymbol{0_{n,u}} \tag{4.7}$$

n is the number of controlled channels. A controlled channel is any channel with an interface that can be used for position feedback and thus controlled. Since each channel is modeled as a pure integrator the state matrix is a null matrix of size n. The input matrix is of size n by u. Where u is the number of inputs. The output matrix is simply the a square identity matrix of dimension n. No feedthrough means that the feedthrough matrix is null. Each channel and inlet pair have a channel resistance which makes up the input matrix. $R_{n,u}$ is the resistive gain at channel n from input u.

4.2.3 Model Assumptions

Linearity

Like the RCL method, the simplified modeling methodology assumes the plant is linear for a particular channel configuration [26]. A single model for all channel configurations would be highly non-linear and is not considered.

Looking forward, in Figure 4.8 observe the plant response's (droplet interface position) to steps inputs (Pressures of 20, 50, and 80 [mBar]). It is quite clear that the assumption is valid.

Importantly, linearity means superposition can be applied [98]. Superposition is essential for modeling the relationship between system inputs (pressures applied at the channel inlets) and system outputs (channel displacement). With superposition, the net stimuli on the channel is simply the sum of individual pressure inputs. This allows the structure of the input matrix B to be as described in Equation 4.5.

The assumption of linearity is not valid for all regions and operating modes. Droplet motion through microchannels intersections is highly non-linear. However, this non-linearity is negligible as droplets will only be in this region briefly. Therefore, the importance of this region is minimal.

Assumption of Stabilizability and Detectability

The RCL method models single channels as second-order equations. In contrast, the simplified channel model is only first order. This modeling has important implications for control design. First, the model clearly shows that it is not possible to concurrently control all channels. Section 1.3.1 provides full details on the DOF limitations. In other words, the entire plant, that is, all channels are not concurrently controllable [35][98]. Second, since the plant in its full form is not controllable, one must assume that the underlying plant is stabilizable and detectable [98]. Briefly, the assumption of stabilizability (and it's dual detectability) is important as despite the system being uncontrollable, it may be possible to formulate a control law if the system is at least stabilizable (and detectable). Kailath gives the definition stabilizability as [98],

Definition 1 *A realization is stable if and only if the uncontrollable modes are stable*

In the following section, we shall show that these assumptions are valid.

The implications can be understood by examining a generic system model, Equation 4.8 and 4.9. Consider a generic system with n_t total channels and n_u pressure inputs. n_o is the number of channels with trackable and thus controllable droplet interfaces. To illustrate, consider the chip in Figure 2.3 using the nomenclature of Figure 2.5. If channel 4 has a droplet interface, n_t would be 17 whereas n_o would be 1.

$$\dot{x} = A_{n_t,n_t} \cdot x + B_{n_t,n_u} \cdot u \tag{4.8}$$

$$y = C_{n_t,n_t} \cdot x \tag{4.9}$$

Firstly, the principle of conservation of mass indicates that for the system to be controllable n_o to be less than n_t. Again, Section 1.3.1 provides full details on the DOF limitations, however, a brief examination of a T-Junction will demonstrate why the number of controllable channels must be less than the total channels. It is not possible to have all channels concurrently flow towards or away from the intersection. Yet, for all channels to have arbitrarily position control, that impossible condition must be met. But one can not control all three channels concurrently. At least one channel must be free to act as a fluid source or sink. Thus, the number of controlled channels, n_o, will always be much smaller than total number of channels, n_t.

Secondly, in a practical device, as not all channels are controllable concurrently (as $n_o < n_t$) the system will be uncontrollable [99]. Some channels must act as a sink or source.

Thus, to design a controller one must allow all source and sink channels to be uncontrolled. Thus, the position states of all source and sink channels must be removed from the state space used for control design [26]. In other words, the state matrix will be of order n_o. All other states, $n_t - n_o$, are ignored.

However, one must ensure that one can remove these states. Understand that what has occurred is that the state space has been split into two parts. The two parts are a (1) controllable and observable portion and an (2) uncontrollable and unobservable portion [98]. The controllable and observable parts of the system will be for control design. It will have n_o states in terms of this generic system.

For this system decomposition to be valid, the uncontrollable and unobservable parts must be at least stable. This stability requirement comes from the definition [98][35]. But as A is a null matrix this is not the case [28]. It has pole(s) at $s = 0$.

But consider the true system rather than the idealized system. The true state matrix is not a null matrix. The ideal state matrix being a null matrix is just an approximation, and the physical state matrix is more like Equation 4.10, where in A_r the pole locations,

$e_{n,n}$, are some small negative value close but not equal to $s = 0$. If this is the case the A_r is stable and thus the system is stabilizable and detectable.

Consider also the physical meaning of state – the position of fluid in the channel. Any uncontrolled channel contains silicon oil or another continuous phase by definition. The associated state is the position of some arbitrary volume of the continuous phase. However, there is nothing significant about some volume of the continuous phase. This volume is interchangeable with any other continuous phase. Thus, even if the continuous phase has some large movement it is of no practical consequence. It is replaced with an equivalent continuous phase. Thus these states, as long as they are stable, can be ignored safely.

$$A_r = \begin{pmatrix} e_{1,1} & 0 & \dots & 0 \\ 0 & e_{2,2} & \dots & \vdots \\ \vdots & \vdots & \ddots & \vdots \\ 0 & \dots & \dots & e_{n,n} \end{pmatrix} \tag{4.10}$$

4.2.4 System Identification

Although the model structure has been defined, for the model to be useful the resistive gains of the input matrix must be found. An analytic approach was often unsuccessful due to plant variations. An experimental system identification was chosen as it better represents the true plant parameters [75].

An experimental system identification applies known input, pseudorandom binary sequence (PRBS) pressure value, at channel inlets. The position of an interface in a channel of interest, the system output, is measured in response to these inputs. The process is repeated for each channel of interest (COI).

Experimental Setup

A microfluidic chip was prepared in a standard manner. Refer to Chapter 2 for full details. For each COI, a droplet was manually positioned in the channel midpoint FOV.

Offset Pressue Identification

First, the pressure offset value for the channel of interest must be found. While all other pressures are zero, the pressure in the COI is adjusted until the channel interface is ap-

proximately stationary at the midpoint. A feedforward pressure, using the determined magnitude, is applied to the water channels throughout the identification pressure.

Collection

A PBRS input signal is designed by the procedure described by [100]. The procedure was adapted slightly as the amplitude was manually adjusted to ensure droplets remain within the COI. The resulting PRBS had a 3 [s] clock rate and 0 to 20 [mBar] amplitude. The PRBS pressure signal is applied to the system. Interface position is recorded with the lensless system.

Parameter Identification

Prior to identification, output data was made zero mean to mitigate the influence of arbitrary data offsets. Additionally, if present, outlier position measurements caused by imaging processing faults were removed [75].

Following prepossessing, a standard system identification algorithm, N4SID, is applied to find the system parameters [75] [101]. This procedure was carried out with System Identification Toolbox (Matlab, MathWorks). This particular approach was selected as it is a standard technique that is applied without difficulty [102].

Validation

The methodology section has detailed an approach for the model development. Given a model, it is important to validate the model. Validation ensures the model will sufficiently approximate the system to be useful for control [75]. To validate the model the system identification process, outlined in Section 4.2.4, is repeated to generate a data set only used for validation.

4.3 Results

4.3.1 Validation

Residual Error Analysis

Inspecting the residuals between the model and the validation data set can be used to assess model correctness [75]. A standard residual analysis of the simplified model approach yields satisfactory results .

First, a satisfactory model has residuals, errors between the model and the validation data set, that are small and uncorrelated. Examination of Figure 4.5a shows the auto-corrletion between the residuals and is small (< 0.1) and within 95 % confidence interval bounds, shown as a broken horizontal line in the Figure.

Secondly, residuals should be uncorrelated with past inputs. Plots B through F assess the cross-correlation between the residuals and past inputs from each active channel inlet. Only the five nearest inputs are analyzed as other channels inlets are have negligible contribution to the system dynamics. Again, any correlation between the inputs and residuals stays within acceptable bounds. Note the 95 % confidence bounds, horizontal lines, are at the 0.1 level which is adequate. One should note that Plot D, corresponding to input 3 and the controlled channel, shows some correlation between with five past inputs. This correlation is slight. Given the inherently large variations in microfluidics and the simplified nature of the model, it is deemed acceptable.

Time Domain

Examination of model and validation data set in the time domains further validates the simplified approach. Figure 4.6a compares the measured data set to what is predicted by the model with the same applied inputs. Overall the model follows the predicted data closely which is indicative of a good model. Numerically the model goodness can be expressed by normalized root mean square error (NRMSE, Equation 4.11) which has a value of 69.2 [75].

To further assess model accuracy consider an explicit examination of model error, Figure 4.6b. The peak error never exceeded ± 50 $[\mu m]$ and for most of the experimental period is the error below ± 25 $[\mu m]$. Such a low error demonstrates that the model is accurate for control purposes. Overall, time-domain model testing shows that the modeling approach yields good control models.

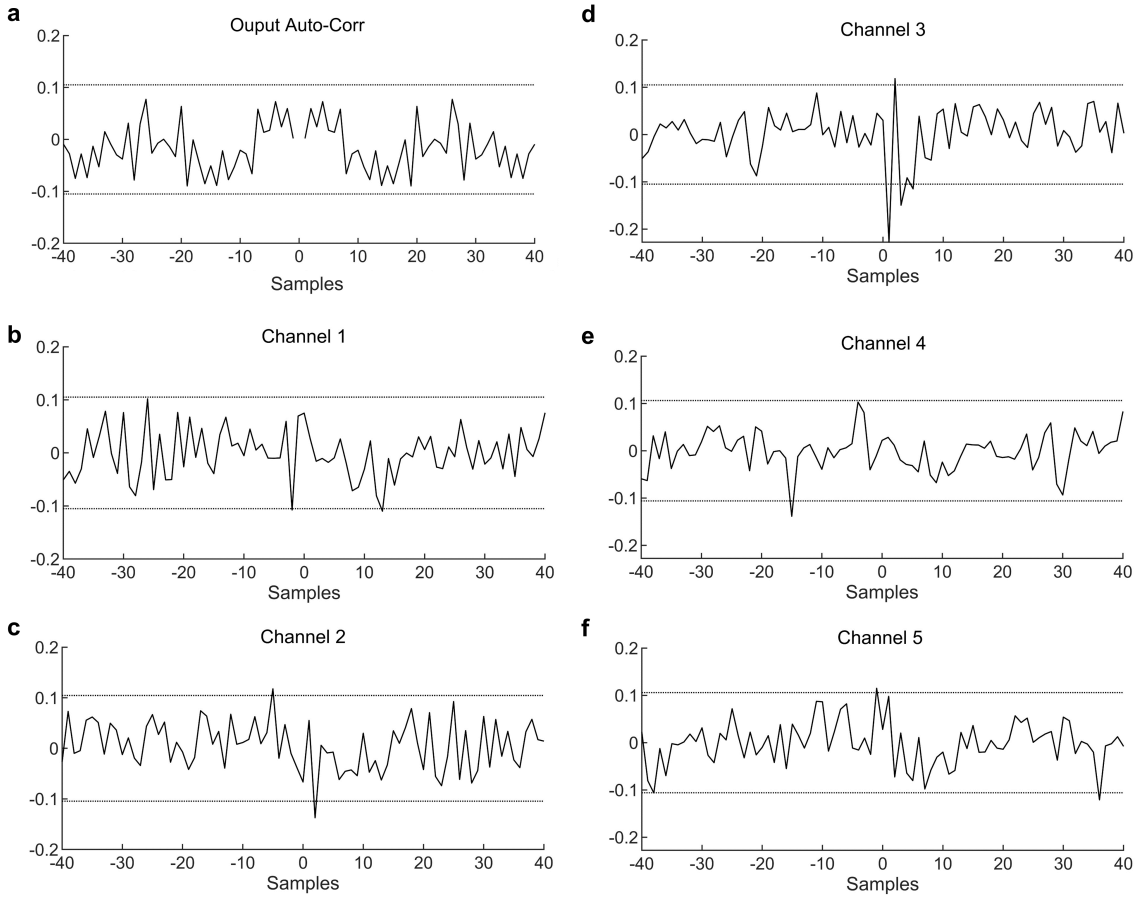

Figure 4.5: Typical Model Residuals

$$NRMSE = 100\left(1 - \frac{||y - \hat{y}||}{||y - mean(y)||}\right) \tag{4.11}$$

4.3.2 Frequency Domain

Investigating the RCL modeling approach in the frequency domain will further strengthen the validity of disregarding high-frequency poles. Consider the microfluidic plant model

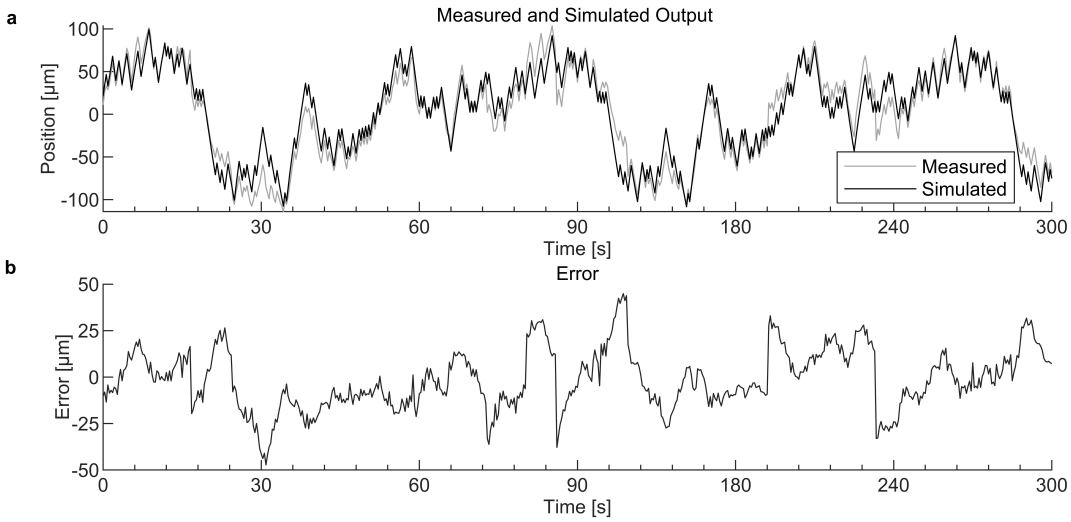

Figure 4.6: Typical Prediction Error

with one controlled channel as a prototypical example. Model parameters are found analytically. Figure 4.7 shows the pole-zero plot of this model.

Note that there appear to be two groups of poles, one near the origin and another further away at $s = -20$. Examining the plot, it is clear the separation between the two groups is large, approximately 100 times, thus it is sufficient for decomposition to an approximate system.

Substitution shows capacitive and inductive elements create the pole grouping furthest from the origin. This pole grouping's effects decay much faster than the dominant poles justifying neglecting the capacitive and inductive elements [103] [104]. Studying the RCL plant model in the frequency domain supports the application of the simplified approach.

4.3.3 Plant Step Response

Step response analysis further confirms the soundness of ignoring the RCL method's high frequency components. Consider the following examination of a standard microfluidic chip. The chip is filled with 50 Cst Silicone Oil, except channel four which is filled with DI water. All channels have pressure zeroed excluding channel four. Channel four has 35 [mBar] pressure applied to compensate for the offset pressure (Described in Section 4.2.4) . From this initial state pressure in steps of 15 [mBar], 30 [mBar] and 80 [mBar] are

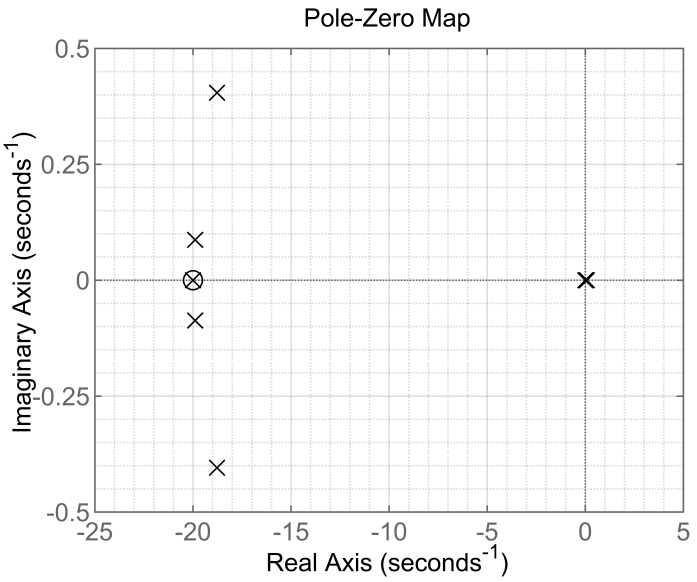

Figure 4.7: Pole Zero Plot of System Chip using RCL modeling

applied to channel four. With the lensless setup, droplet interface position is found with normalized cross-correlation template matching (Chapter 3).

The system's time response to these step inputs is shown in Figure 4.8. The response of the systems is that of a gain and integrator. Any effects from capacitive or inductive elements appear negligible. This supports the simplification of the plant model.

However, in the initial 0.5 [s] there is slight damping effect. This is likely due to pump dynamics [26], tubing and chip compliance [27]. Nevertheless, it decays quickly, as predicted by the frequency domain analysis, and thus does not affect plant dynamics greatly.

The system does not appear to have significant nonlinearities as a function of step size. The lack of nonlinearities is apparent as the system response does not change with the magnitude of the step.

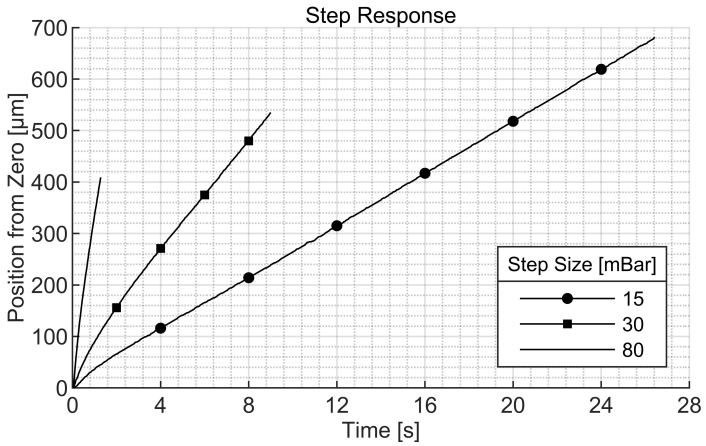

Figure 4.8: System Response to 15, 30 and 80 [mBar] Step

4.3.4 Plant Model Properties

Model Order

The RCL modeling approach yields higher order models.For T-Junction type geometry, Equation 4.12 describes the relationship between the number of controlled channels n_c, number of inputs p, number of uncontrolled channels, n_{uc} and model order s_o. Compare this to Equation 4.13 for the simplified approach. The simplified approach will lead to lower-order models.

$$s_o = 3n_c + 5p - 2n_{uc} \tag{4.12}$$

$$s_o = n_c \tag{4.13}$$

Numerical Condition

In general, the simplified modeling approach provides better-conditioned models than the RCL method. The magnitude of the difference is depended on the specific system being modeled.

The condition number, the ratio between the largest and smallest singular value of the system, indicates how sensitive the system is to small perturbations [105]. Systems with large condition numbers can give significantly different results based on small changes. Thus, from the control system perspective, ill-conditioned models are undesirable. An example can illustrate the difference in numerical conditioning between approaches. The

system considered is an analytical model of a standard chip (Chapter 2) with two controlled channels (two outputs). Figures 4.9 a and b show the numerical condition numbers as a function of frequency for the RCL and simplified approach for the example system, respectively. From the figures, it is clear that the RCL model is ill-conditioned whereas the simplified model is not.

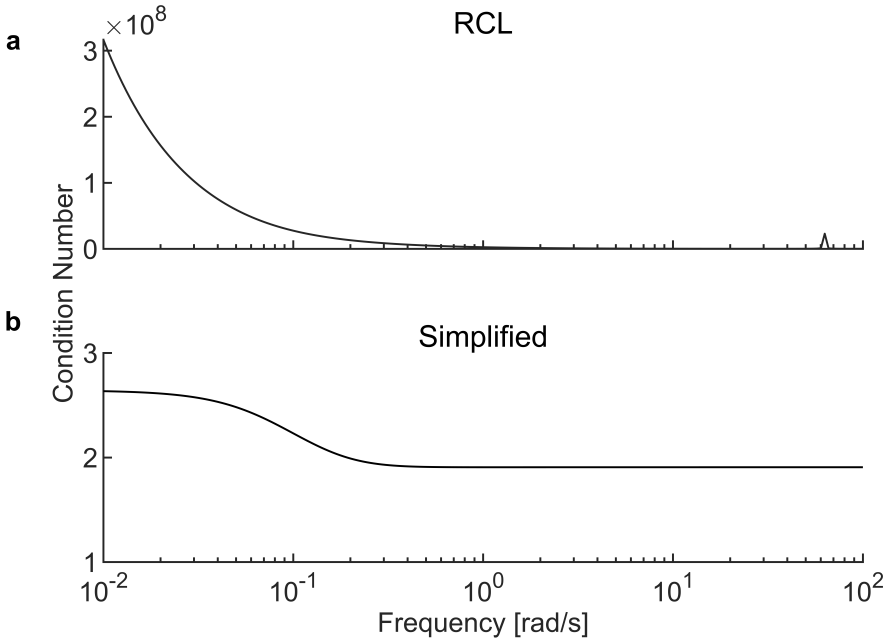

Figure 4.9: Numerical Conditioning by Modeling Method

4.4 Discussion

The key finding shows that the simplified modeling approach yields valid, low order, numerically well-conditioned models. Models with such properties are advantageous for control design.

By examining an example system our findings show that this approach can yield valid models. Consider that our model for the example system had residuals with good whiteness and limited correlation with past inputs. The prediction error is within sufficient bounds for the model to be useful for control. These properties indicate that the model is viable for use in control. Now consider that even for a simple chip, such as a T junction, the RCL

will yield 22^{nd} order model [25]. For a T-junction the simplified method will result in at worst a 2^{nd} order system. The difference in model order for more complicated chip designs becomes even greater. Clearly, the simplified approach results in lower-order models.

Again by example, the results indicate that the simplified approach yields numerically well-conditioned systems. This is important as ill-conditioned systems require non-standard analysis techniques, complicating control design [26]. Secondly, poor conditioning can lead to discrepancies between the system and model. For example, an ill condition system can lead to the existence of a right-hand pole (RHP) within a model, whereas the true system may have not had an RHP. This again causes challenges for control design. This effect is particularly large when the variation of channel lengths on a single chip is large.

Compared to the RCL approach the models created are significantly lower order, better numerically conditioned, and require no tuning values. This simplifies the creation and use of feedback controllers in the microfluidic context.

Furthermore, modeling the system as first-order means, the minimum realization, has full state feedback. Thus, no estimator is needed by the control law. This again further simplifies the control system design.

Finally, the use of a simplified model allows other control strategies to be used. For example, Model Predictive Control needs to solve a optimization problem each time step [78]. This optimization is computationally expensive and may be sensitive to poor numerical conditioning [86]. High order and numerically ill conditioned models would challenge the optimization step. Therefore, a simple model may allow more complex control strategies, like MPC, to be used.

Despite the benefits of this approach, a major limitation is the assumption of time invariance. This is not the case as the plant over multi-hour periods varies. It is postulated that the physical causes of the time variance are the changes in surface wetting, dust, and buildup of fluid interfaces.

Changes in surface wetting are likely a significant source of time variance. Droplet microfluidic chips undergo surface treatment to ensure channel surfaces are hydrophobic. This ensures good surface wetting for droplet formation. Over time this treatment degrades leading to poor surface wetting. Two images showing examples of poor surface wetting are shown in Figure 4.10.

Changes in this surface wetting in effect change the channel resistance significantly. Consider the left image in Figure 4.10. As a result of poor surface wetting the effective channel width is decreased, which changes the resistance of the channel.

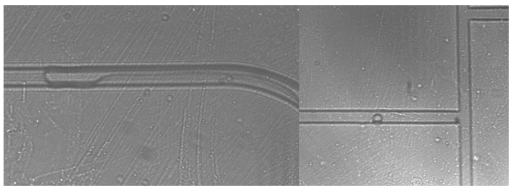

Figure 4.10: Examples of Poor Surface Wetting

Large dust particles within microchannels are another significant source of variance. Large dust particles cause increases in channel resistance. If the dust particle is continuously mobile it can move within the microchannel network leading to time-variant behaviour. Additionally, as the dust particles move from one channel to another it can cause rapid changes in resistance. The speed of such changes limits the applicability to adaptive control techniques. During chip operation new droplet interfaces can form. These interfaces, due to Laplace pressure, can lead to large changes in channel resistance. Again this leads to the time-variant behaviour of the plant.

The presence of time-variant behaviour limits the long-term performance of the feedback control system. Compensation requires either an extremely conservative controller design or periodic re-calibration. Further study of the cause of plant time variance and correction measures would be useful in this regard.

Despite this limitation, these results suggest that this method is much easier to use while being comparable to the existing RCL method in the control sense. For this reason, there is a significant benefit to using this method.

4.5 Summary

For control purposes, existing methods model droplet microfluidic dynamics with resistive, capacitive, and inductive elements. However, the RCL approach yields high order, numerically ill-conditioned models that require further tuning. This chapter presented a simplified method where the model structure is composed of resistive gain and integrator. A system identification procedure finds gain values. In contrast to RCL, this simplified technique produces low order, numerically well-conditioned, model with no tuning. The simplified models sufficiently describe system dynamics for control. The resulting models are simpler to use, are valid for more complex chip topologies, and make feedback control more accessible.

Chapter 5

Model Predictive Control

5.1 Introduction

The application of control theory has promising benefits for the robustness and usability of microfluidic systems. Feedback laws compensate for chip variations and disturbances while providing users a simple alternative to directly specifying actuator actions.

Recently work by Wong and Hebert has demonstrated successful pressure-driven visual feedback microfluidic control systems [25][27]. These systems use Linear Quadratic Regulator (LQR) type controllers to manipulate input pressures to microfluidic chips.

However, pressure-driven LQR controllers have a practical challenge. Commercial microfluidic pressure pumps are usually unidirectional [90]. Yet, in microfluidic applications, LQR controllers command bidirectional flows. The discrepancy between requested and available actuation leads to actuator saturation and controller windup. Consequently, especially for complex chip topologies, control problems may arise.

This chapter formulates a Model Predictive Controllers (MPC) for microfluidic systems. Unlike LQR, MPC, through explicit consideration of actuator limits, lacks issues resulting from actuator saturation. Here, we show adequate MPC stability and performance through simulation and experimental results. The findings present a successful method to extend feedback control strategies to chips with complex topologies and unidirectional pumps.

5.2 Control Design

5.2.1 Overview

Figure 5.1 show block diagram of the control system. The control algorithm sets channel flows for the plant to carry out prescribed actions. MPC is the core part of the algorithm as it calculates optimal pressure given the system state and desired trajectory. Complementing MPC, the trajectory generation function creates the desired control trajectory. A gain scheduling block selects the MPC controller model and tuning values. Finally, a feedforward term accounts for biased channel pressurization.

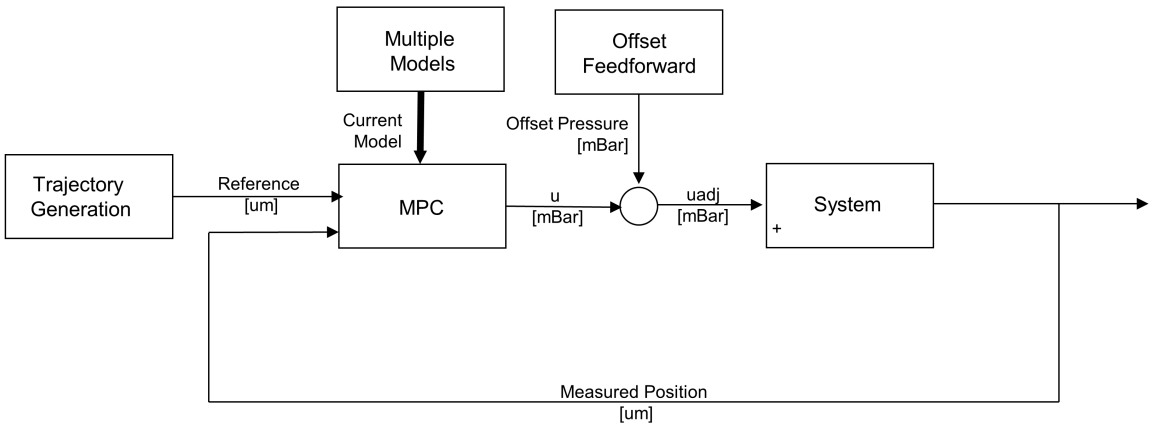

Figure 5.1: Controller Architecture

5.2.2 Multiple Model

As discussed in Chapter 3, a full model of the microfluidic system is highly nonlinear. Quite clearly droplet movement between channels or any behavior at channel intersections will be nonlinear. Fortunately, if one assumes the relevant droplets will not move between channels, a linear model can be used. However, this linear model is only valid for that particular set of channels. If droplets move from one to another channel, the model and controller would no longer work.

Yet, practical device application requires droplets to move between channels. To allow such required behavior, multiple models are added. Essentially, the controller gain, model,

and tuning are taken from a set generated at compile time. A supervisor controller, discussed in Chapter 6, selects which model, gains, and tuning values the controller will use at a specific time.

5.2.3 Pressure Offset Feedforwad

The presence of a pressure offset within channels was described in Chapter 4. In certain circumstances, the pressure offset can cause performance degradation or even instability in the controller. To compensate for this a feedforward offset term is added to the control algorithm. The value of this feedforward offset is found by the system identification procedure of Chapter 4.

5.2.4 Trajectory Generation

Unlike the previous modeling methods, the approach used in this work does not consider pump dynamics, which greatly reduces model order. However, neglected pump dynamics and the integral plant model can lead to infeasibly high slew rate demands on input pressures. A Trajectory Generation scheme is used to ensure that pressure commands will never exceed the maximum slew rate [76]. This is done by scaling a reference trajectory to the commanded change in pressure, as shown in Figure 5.2. This trajectory is effective for step sizes of 20 to 300 [μm]. For smaller or larger step sizes, the reference duration is adjusted to limit the increase response time or prevent slew rate saturation. The MPC controller then follows the scaled trajectory.

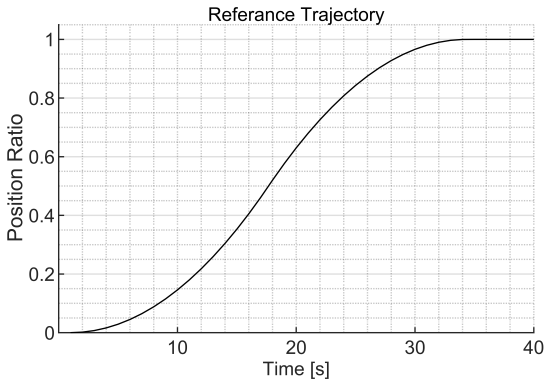

Figure 5.2: Nominal Reference Trajectory

5.2.5 Model Predictive Control Details

Model

Internal models are generated using the procedure of Chapter 3. Multiple configurations require multiple models to be created. These models are selected by the gain scheduling scheme.

Additionally, the MPC internal models include a disturbance component. The microfluidic plant can vary due to surface wetting, dust, and time variance in the offset pressure. These factors can lead to the MPC controller having instability or large steady state errors. These variations are modeled as step input disturbances.

Optimizer

A KWIK based active set solver algorithm, MPC Toolbox Implementation (Matlab 2020a, Mathworks), was used as the MPC optimizer [86] [78][106]. The solver was selected as it is fast and robust while having commercial implementations readily accessible [86]. The commercial implementations provide greater accessibility while having sufficient performance.

Cost Function

The overall cost function, Equation 5.1, is the standard cost function in the Matlab MPC library [86]. The cost function minimizes tracking error, J_y, applied input J_u and penalizes large changes in inputs, $J_{\Delta u}$.

$$J = J_y + J_u + J_{\Delta u} \tag{5.1}$$

The tracking error, J_y is the sum of individual cost functions for all controlled variables, cv (Equation 5.2). For n periods of the control horizon, the individual cost function is based on the weighting for the controlled variable, w_{cv}, and the error between the reference, r, and current measurement, y at the current time step, k [86].

$$J_{y,cv} = \sum_{i=1}^{n} w_{cv}^2 (r_k - y_k)^2 \tag{5.2}$$

The actuation error, J_u is the sum of individual cost functions for all inputs, u (Equation 5.3). The actuation error terms allows the optimization to track preferred values of actuator

inputs. The actuation error is the current pressure input versus the target pressure, $\bar{u}$, scaled by a tuning value, w_u [86].

This cost function formulation differs from standard cost functions which simply try to minimize actuator effort. For most chip configurations almost all actuation targets are zero. However, it was found that performance could be increased by removing the actuation target if the controlled channel directly connects to pressure input. Secondly, for the droplet generation unit operation, having a nominal target (typ. 30 [mBar]) on an adjacent input can increase the robustness of this operation. These tuning rules can be implemented algorithmically in combination with the standard language, Chapter 6.

$$J_u = \sum_{i=1}^{n_k} w_u^2 (u_k - \bar{u}_k)^2 \tag{5.3}$$

For each input, the optimization function minimizes the change between consecutive inputs (Equation 5.4). Large shifts in actuator input are not ideal and can lead to saturation of pump hardware. The cost function for each input is scaled by a tuning value, $w_{\Delta u}$, and is based on the difference between the current and previous time step inputs [86].

$$J_{\Delta u} = \sum_{i=1}^{n} w_{\Delta u}^2 (u_k - u_{k-1})^2 \tag{5.4}$$

Additionally, this cost function is subject to constraints the limit actuation levels for each input, i, with Equation 5.5. This constraint prevents actuator saturation that challenged LQR control strategies. Typically, U_{max} is set to 100 [mBar].

$$0 \leq u_i \leq U_{max} \tag{5.5}$$

MPC Tuning

MPC is tuned to a 0.25 [s] sample time, a prediction horizon of 20, and a one-period control horizon. This rather conservative tuning was useful for experimental work with significant uncertainty. It is likely that the controller can be tuned to be more aggressive.

5.3 Methods

5.3.1 Experimental Validation

For experimental MPC validation, the microfluidic chip was prepared according to Chapter 2. The testbed used the lensless method, outlined in Chapter 3, for feedback. The MPC internal plant model was developed with the system identification procedure from Chapter 4. Matlab (MathWorks) generated an MPC given the plant model and standard tuning parameters.

To validate control, the MPC was tasked with having two droplets, in separate channels (Numbers 4 and 5) of a single T-Junction, track a square wave position reference (300 [μm] Amplitude, 150 [s] Period, 50 Percent Duty Cycle). The dual-channel configuration was used as it was challenging given high coupling between channels 4 and 5 and showed MIMO functionality. Other configurations have lower coupling between channels would be easier to control.

5.3.2 Simulation Validation

Simulation Model

For simulation, the base model from Chapter 4 was augmented with a nonlinear actuator and sensor dynamics. Figure 5.3 shows the full simulation model. The nonlinear actuator model has rate limitations (10 [mBar/s]), saturation (0 to 100 [mBar]), quantization (2.5 [μm]) and a band limited additive noise (0.1 [mBar]). The plant's output added quantization (2 [μm]) and band limited additive noise (0.1 noise power) to account for sensor characteristics. Additionally, a pressure offset, 15 mBar, was added to channel four.

The plant input matrix parameters were individually scaled by random values in the range of 0.1 to 10. This scaling was meant to model plant channel resistance variation due to surface wetting, dust, and other effects. The values were chosen as they reflected worst case variations observed over system operation.

Simulation

To supplement experimental investigation, MPC was validated with additional simulations with the modified plant. Unlike the experimental plant, which has unmanageable

variations, simulations allowed controller testing with precisely modified and repeatable plants. Although, less rigorous than formal mathematical stability analysis, this method, in context with experimental results, further supports MPC effectiveness.

With the non-linear plant, the controller was tasked with tracking the two step references (300 and 150 [μm]) using a set (n=10) of simulated plant models. Plant models differ based on the scaling of the input matrix. Simulink (MathWorks) was used for simulations.

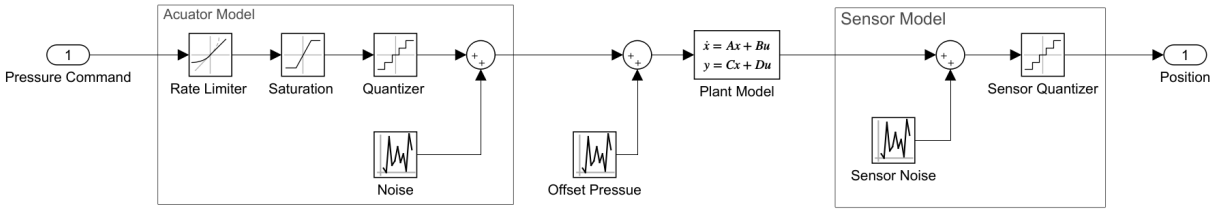

Figure 5.3: Simulation Model

5.4 Results

5.4.1 Experimental

To demonstrate MPC effectiveness, droplets in separate channels of a T-junction followed a square wave position reference confirming stability and satisfactory performance (Figure 5.4a). MPC stability for this plant is apparent in the results. Comparing reference and measured positions shows the MPC can follow references. The steady-state error and overshoot are negligible. Minimizing overshoot is desirable as it prevents droplets from undesired 'jumping' to uncontrolled channels. Assessing the commanded pressures shows the MPC controller does require bidirectional flow (Figure 5.4b). Overall, these results indicate that MPC can be successfully applied in microfluidic systems with unidirectional pumps.

5.4.2 Simulation

Simulated results further support MPC effectiveness by assessing simulated performance tracking a step position reference. Figure 5.5 shows a typical result with one of the augmented plants. However, all modified plants had a similar stable response. The shown

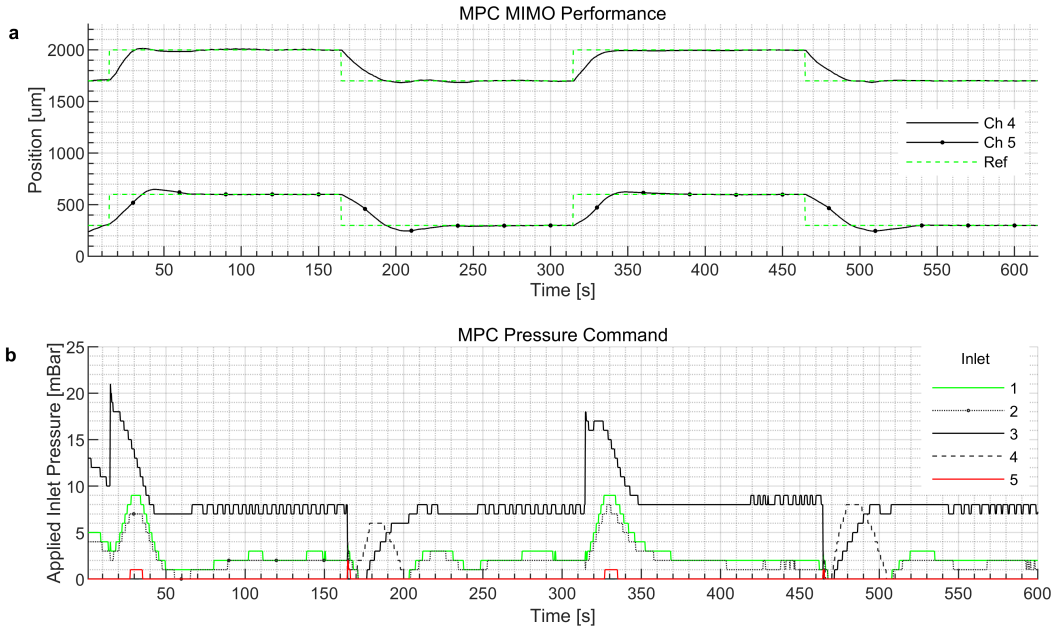

Figure 5.4: MPC Experimental Effectiveness

performance occurs with a very incorrect internal model. Yet despite this simulated plant variation, any steady-state error or overshoot is minimal. Similar to the experimental results, the MPC is stable and can track the position reference. The MPC controller does saturate the actuator. These results suggest that MPC is effective in spite of possible plant variation.

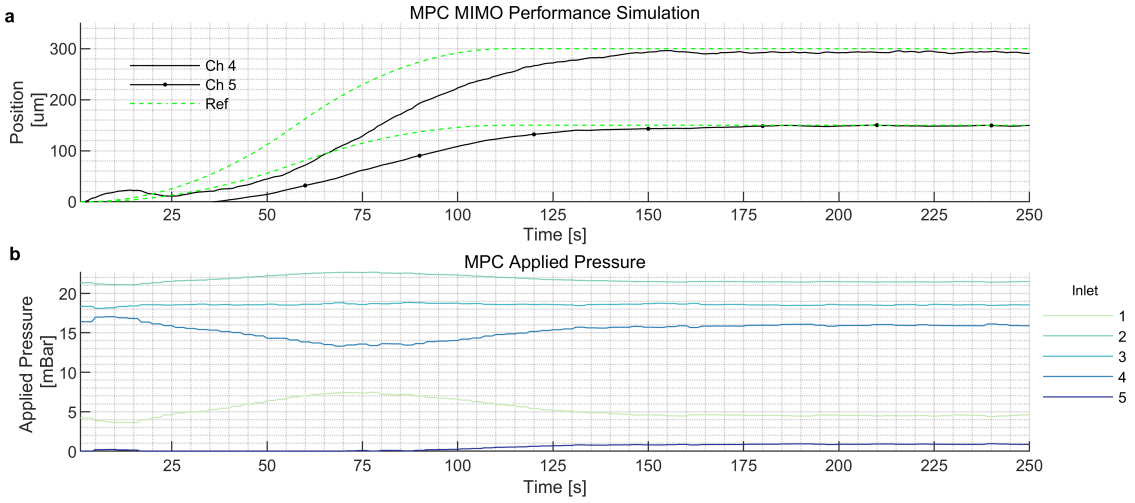

Figure 5.5: MPC Simulation Effectiveness

5.5 Discussion

These results show that the MPC can effectively control a complex microfluidics chip using unidirectional pumps. MPC is stable, can track references, limit overshoot, minimize steady-state error, and does not saturate pumps.

MPC based control differs from earlier LQR methods as actuator bounds are explicitly considered in the control law. Thus, unlike LQR, MPC will not command bidirectional flows that commercial microfluidic pumps cannot provide. Consequently, MPC control can be used for more complex chip topologies where actuator saturation and controller windup could affect controller performance or stability.

The MPC is important in the context of the proposed microfluidic platform. LQR control had poor performance and limited stability for the system chip. Yet, the lensless system and degree of freedom constraints restrict the chip layout. Thus, MPC facilitated the development of this system. These findings should not be generalized for all chip designs as LQR control works quite well for single, double, or even triple T-Junctions.

However, MPC has limitations. Firstly, MPC requires intensive computations. For real-time systems, this can elevate hardware cost and limit performance. Secondly, MPC design and analysis are more complicated than for LQR methods. Especially, analysis of constrained MPC necessitates challenging non-linear analysis.

Despite these challenges, MPC can act as an important tool in some situations. It allows complex microfluidic chips to be regulated where other methods may face challenges. In particular, for the system shown in Chapter 2, MPC becomes a critical building block.

5.6 Summary

Commercially available microfluidics pumps are often unidirectional. Yet, feedback control implementations in droplet microfluidics, often LQR-type controllers, assume bidirectional flows are available. For complex chip topologies, this situation can lead to control system instability. This study shows that an MPC can be successfully applied as it accounts for the unidirectional flow limitations of pumps.

Chapter 6

Supervisor

6.1 Introduction

Despite the inherent advantages, microfluidics has received less use than the potential advantages would suggest. The complexity of successfully operating devices by non-experts appears to be a significant cause of this gap [4]. Alternate approaches based on Digital Microfluidics or MLSI have other downsides.

Wong suggested that feedback control could help address this issue. Through a user interface, Wong's system allowed droplet position to be manually controlled [25]. Hebert later extended this approach by adding fundamental unit operations that are carried out semi-automatically [9]. However, neither of these approaches is fully automated. Both approaches required direct operator interaction with the system and do not completely abstract device operation. Neither is sufficient to allow the device operation to be completely abstracted. Therefore, a new approach is needed.

In this chapter, a new approach is presented. The basis of the idea is that any arbitrary droplet behavior can be decomposed into a sequence of reference operations that a feedback controller can track. To facilitate this, a standard method of describing references is devised. Additionally, a method implementing the standard description is created. These methods are then successfully applied in carrying out automatically the fundamental droplet operations; droplet generation, splitting, merging, sorting, and movement.

6.2 Working Principle

6.2.1 Decomposition

This automatic control method is based on the idea that any arbitrary droplet behaviour is decomposable into a sequence of simple forward or backward fluid motions in systematically selected fluid channels. A feedback controller then readily carries out the simple motions by manipulating input pressures. Through this decomposition, complex actions, for example, droplet splitting, are broken into a simple sequence of motions that through feedback are easily achievable.

An example of equally splitting a droplet can illustrate this method. Consider the droplet initially positioned symmetrically at the T-Junction in Figure 6.1 (a). A feedback controller (of the type used by Wong or described in Chapter 5) can not be told directly told to split the droplet. But it is possible to have the controller move the interfaces in two of the channels slightly away (waypoints in Figure 6.1) from the T-Junction (b). If this process is repeated sufficient times (c), eventually the two interfaces will move far enough apart that the droplet will split (d). This is the idea of decomposing. A complex action, droplet splitting, can be carried out by a feedback controller receiving a sequence of simple motion references.

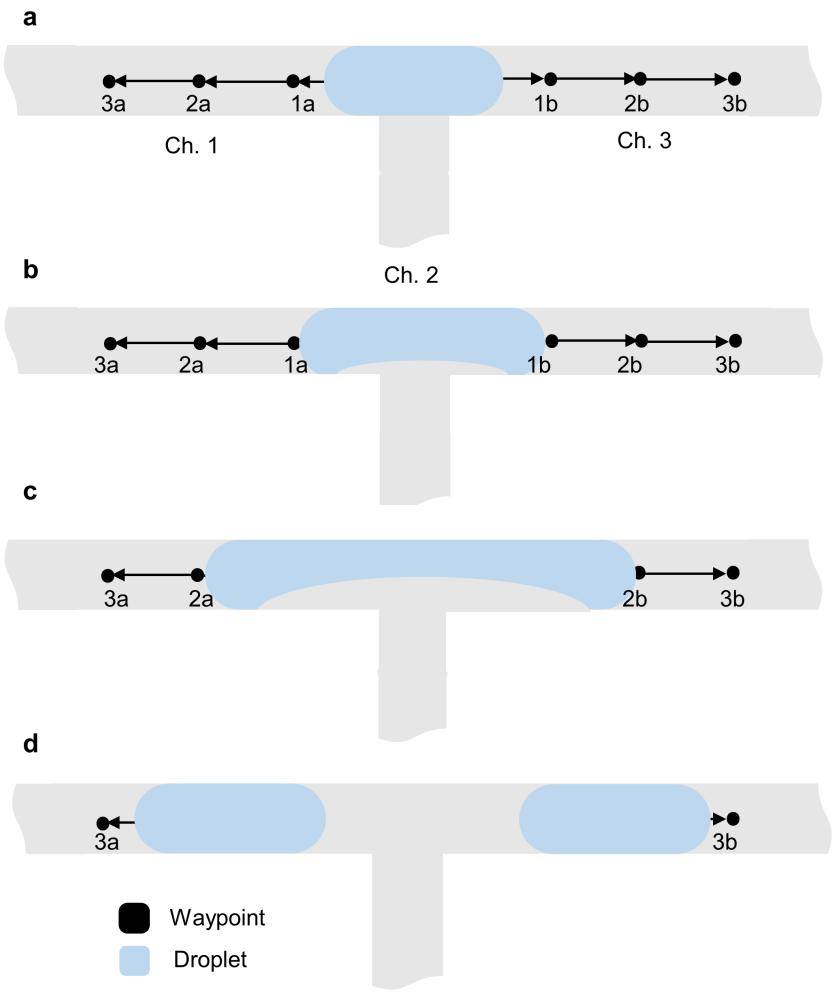

Figure 6.1: Droplet Splitting by Decomposition

6.3 Automation Approach

6.3.1 Automation Approach Overview

Based on the decomposition approach a method of automated droplet manipulation is created. The system consists of a Supervisory Controller, a Program (an instruction sequence), and a set of feedback controllers as shown in Figure 6.2.

Briefly, the program and instructions describe what the system is to do and the feedback controller set can carry out the desired actions. The supervisor based on the state of the system selects which feedback controller and instruction is to run at the current time.

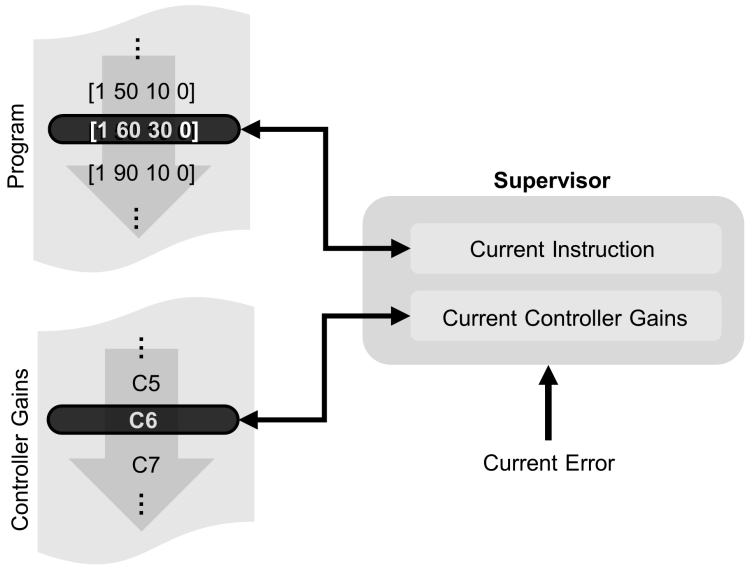

Figure 6.2: Overview of Automation Approach

6.3.2 Standard Language

For the decomposition idea to be applied effectively, a standard way of expressing the required individual motions is needed. In the following section, a standard way of describing required control actions is devised.

Instruction

The fundamental building block of the standard language is called an instruction and is simply a set of four numbers as illustrated in callout 6.1. The convention is that the first number, termed Channel Command, specifies the channel in which the control action will occur. The second number, termed Initial Position, is the assumed position of the droplet interface at the start of the command. Note the assumed initial position and true initial

position do not need to be the same. In fact, a difference between the stated and true start position can be exploited to carry out more complex operations. Examples using such a scheme are shown in results sections 6.5.1, 6.5.4, and 6.5.5.

The third number, Movement Command, represents the desired distance (in μm) to move the droplet interface from the initial position. For example, if a droplet interface is located 500 [μm] away from a reference point, and it is desired to move the interface to a point 600 [μm] away, this Movement Command would be set to 100. The convention used is that a positive number means that if multiple interfaces are detected within the channel the interface closest to the channel origin is controlled, while if this number is negative, the interface furthest away from the channel origin is controlled.

Finally, the fourth number termed special command is for situations where feedback control can not be used or a modified feedback control law is needed. For example, in certain desired operations an interface may appear, disappear, or no interface exists during an instruction. Thus, if the special command is anything other than zero, a custom controller specified by the user will be run in place of the standard controller. It should be noted that the use of such a special controller will be sparse. None of the fundamental unit operations require the use of this special command.

$$\left[Channel, InitialPosition, Movement, Special\right] \tag{6.1}$$

6.3.3 Program

Individual instructions are often of little practical use. However, multiple instructions carried out in sequence can be used to carry out useful actions. A program is a term used to describe a sequence of instructions. Section 6.5 shows example programs for droplet generation, splitting, merging, sorting, and movement. Note that the presented programs are not the only or even ideal way of carrying out the actions.

Program Example

An example of a standard program to illustrate this concept is as follows. Instruction set 6.2 defines the channels that will be controlled. During the first instruction (row 1) channels one and two are controlled. During the second instruction (row 2) channels 1 and 9 will be controlled. These are defined by the standard nomenclature shown in Figure 2.3 (Chapter 2).

$$Channel = \begin{bmatrix} 1 & 2 \\ 1 & 9 \end{bmatrix} \tag{6.2}$$

Next in instruction set 6.3, the initial position of the leading droplet and lagging droplet interface is described for channels 1 and 2 (Row 1). Units are assumed to be in microns. The value is given along the length of the channel. By convention, the zero position is defined as the left or bottom-most point in the channel. The positions during the second instruction are shown in row two.

$$InitialPosition = \begin{bmatrix} 100 & 200 \\ 200 & 200 \end{bmatrix} \tag{6.3}$$

Next, in instruction set 6.4, we describe the movement in the channel. In the example, the first instruction (row 1) will move channels one and two 100 microns right and 50 microns down, respectively. By convention, left to right and down to up is defined as the positive direction. Row 2 shows the movement in the second instruction.

$$Movement = \begin{bmatrix} 100 & -50 \\ -100 & 50 \end{bmatrix} \tag{6.4}$$

Finally, in instruction set 6.5 we introduce the Special Command. Although the lensless system increases the FOV, not all of the chip has visual feedback. If a channel has no feedback or a unit operation is to take place in which an interface disappears (for example, in some implementations of droplet merging) the special command is set to 1. This informs the controller that a special controller is to be used for this program instruction. Thus, in the first instruction (Row 1) no special controller is used. In the second instruction (Row 2) a special controller is used.

$$Special = \begin{bmatrix} 0 \\ 1 \end{bmatrix} \tag{6.5}$$

6.3.4 Unit Operation Templates

Templates add a further level of abstraction to the standard language which simplifies the process of creating programs. When developing programs one will notice that there are similarities in the structure of different programs. For example, a program for the droplet

Table 6.1: Droplet Sort Template

Instruction	Channel	Position	Initial	Special
1	S	500	2500	0
2	S	500	2500	0
3	S	0	3000	0
4	E	500	0	0

generation unit operation will be very similar regardless of which channel contains the dispersed phase.

This structural similarity can be used to simplify program creation for unit or even other more complex operations to a standard form. These standard forms are referred to as templates. With templates, the form of the program remains the same, only template parameters are changed. The use of templates allows a greater level of abstraction and reuse. System users can simply select and parameterize existing templates rather than create entire programs. Templates for droplet generation, splitting, merging, sorting and movement have been created.

As an example, a droplet sorting template is shown in Table 6.1. This program allows droplet interfaces to move either left or right in the channel. The users do not need to create the program in its entirety. Instead, the user replaces the S parameter with the channel number where the droplet is first found. For example, channel four on the standard chip. The users then replace E with channel the droplet ought to move to, for example, channel three. If in the future it is desired to move to droplet to channel five instead of three, the template can be reused. Only the E parameter in the template is replaced.

6.3.5 Supervisor

To implement the program specified in the standard language a higher-level controller, called the supervisor, is needed. The supervisor manages the individual control actions. The supervisor carries out the automated nature of the system. It takes a program and then carries out the control actions needed to achieve full automation.

Algorithm 1: Supervisory Controller

input : Current Error, C_e,
Error Threshold, E_t
Wait Period, W_p
Controller Set, $C = \{C_1, C_2, ..., C_n\}$.
output: Current Controller, C_{curr}
for *each controller,* $i \in C$ **do**
  if $C_e < E_t$ **then**
    wait for W_p;
    $C_{curr} \leftarrow C_{i+1}$;
  end
end

The supervisor controller algorithm is shown in Algorithm 1. Before run time the user provides the supervisor controller a set of controllers and a program. The supervisor controller selects the initial controller and initial instruction from the program. The initial controller manipulates pressures as required by the initial instruction.

When the supervisor controller detects that the error is below a threshold it begins a waiting period. The waiting period ensures that the error threshold was not achieved only transiently. If the error is below the threshold after the waiting period, the next controller and instruction set is selected. The new controller then also manipulates pressures as needed. The process repeats until all instructions in the program have been carried out.

6.4 Methods and Materials

All work was carried on the microfluidic chip detailed in Chapter 2. The continuous and dispersed phase consisted of 50 [cSt] silicon oil (Sigma) and water respectively. A Model Predictive Controller (MPC), previously described in Chapter 5, sets pressures on two pumps (MFCS-EZ, Flugient) connected to the microfluidic chip. Visual feedback was provided by the lensless technique (Chapter 3). The microfluidic chip position was adjusted to the appropriate zero position.

To study the automated property, the system was configured to execute fundamental unit operations. Automatic Droplet generation, splitting, merging, sorting, and movement were examined. Analyzing these operations allows systematic and generalized assessment of the automatic system. Droplet generation and splitting performance are quantified by

comparing desired to achieved droplet size and split ratio, respectively. Unit operations are recorded with the lensless technique.

6.5 Results

6.5.1 Automatic Droplet Generation

Droplet generation is a fundamental and required unit operation. Thus in the following section, Automatic Droplet Generation (ADG) is demonstrated and performance quantified.

Figure 6.4 shows a successful ADG process as specified by the program in Table 6.2. Frame 1 and 2 show the dispersed phase interface moving from its initial to the secondary position. Frame 3 captures the movement of the dispersed phase to the continuous phase channel. Frame 4 shows the generated droplet in the continuous phase channel.

X_p in Table 6.2 is the adjusted position reference in the continuous phase channel. The X_p value determines droplet size. The value of X_p is taken from an experimentally generated calibration curve. An example calibration curve is shown in Figure 6.4b.

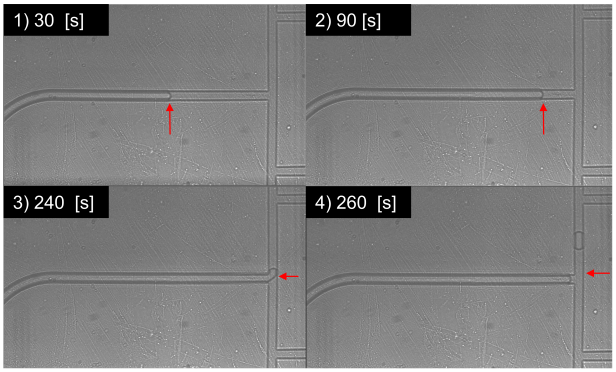

Figure 6.3: Automatic Droplet Generation

The quantified performance of ADG is shown in Figure 6.4. Figure 6.4a shows the measured length of the generated droplet in the continuous phase channel as a function the specified reference length. Note the relatively small variation in droplet size between trials. Figure 6.4b shows the relationship between the reference and mean droplet length. This relationship is used as a calibration curve and may vary between chips. Figure 6.4c

Table 6.2: Droplet Generation Program

Instruction	Channel	Position	Initial	Special
1	4	500	2000	0
2	4	500	2500	0
3	4	0	3000	0
4	5	X_p	0	0

shows the performance of the ADG with the adjusted reference, from which it is apparent that the ADG performance is acceptable.

Interestingly, it was observed that ADG was successful even with significant surface wetting after recalibration. Figure 6.5 shows heavy surface wetting, yet despite these conditions, ADG operated successfully.

In summary, these results show that automatic droplet generation is achievable and has acceptable droplet size accuracy. Furthermore, the ADG process appears to have some level of robustness as it can compensate for heavy surface wetting.

6.5.2 Automatic Droplet Spitting

A secondary but equally necessary unit operation is automatic droplet splitting (ADS). To show the fully automatic capability of the system, a successful ADS procedure is demonstrated and performance quantified.

A successfully ADS, described in Table 6.3, is presented in Figure 6.6a to f. The 480 [μm] long droplet moves past the first waypoint in frame A. Frame B shows the formation of the second leading interface. Frame C and D present the two leading interfaces moving towards further waypoints. The splitting process occurs in frame E as the interfaces keep tracking ever-separated waypoints. The final result, two split droplets, is seen in frame F.

Figures 6.7a and b characterize the accuracy of ADS. Figure 6.7a compares the set droplet ratio to the resulting measured value. Note that because of offset in the raw data the set droplet ratio is adjusted by a calibration factor. It is suspected that the selection of the channel boundaries influences this offset.

From Figure 6.7b it is clear the droplet split ratio can be adequately controlled through ADS. Calibration can improve performance by adjusting for setup issues. Overall, these results indicate that the ADS process is successful. The ADS can split droplets as specified

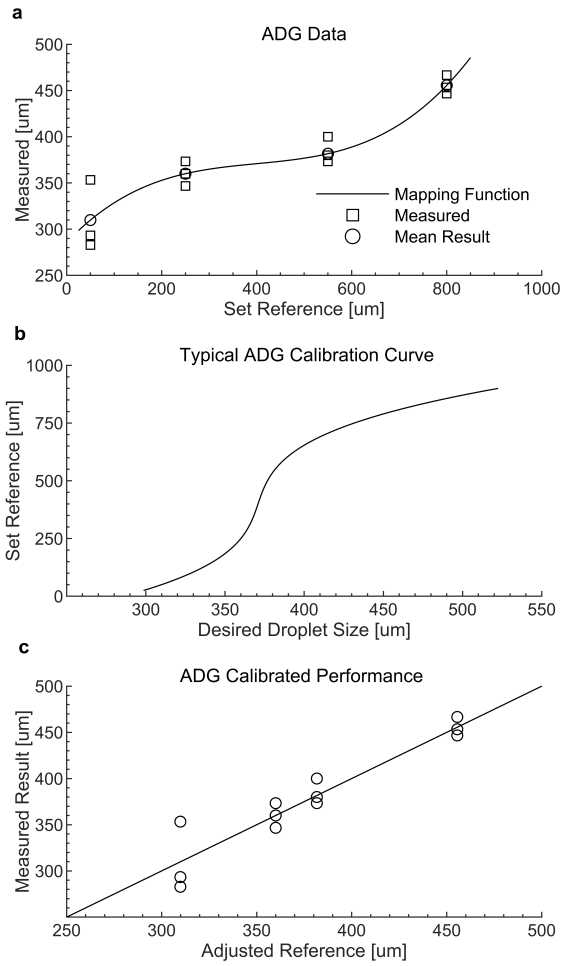

Figure 6.4: Automatic Droplet Generation Characterization

with sufficient accuracy. However, some droplet splits appear to have a large variance. The cause is unknown, but differences between channel flow velocities near the splitting point, for example in frame 5, likely play a role.

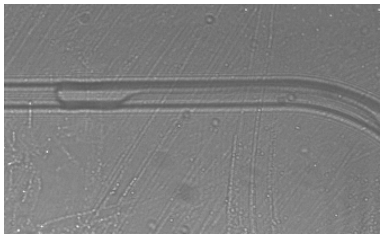

Figure 6.5: Automatic Generation Sorting with Surface Wetting

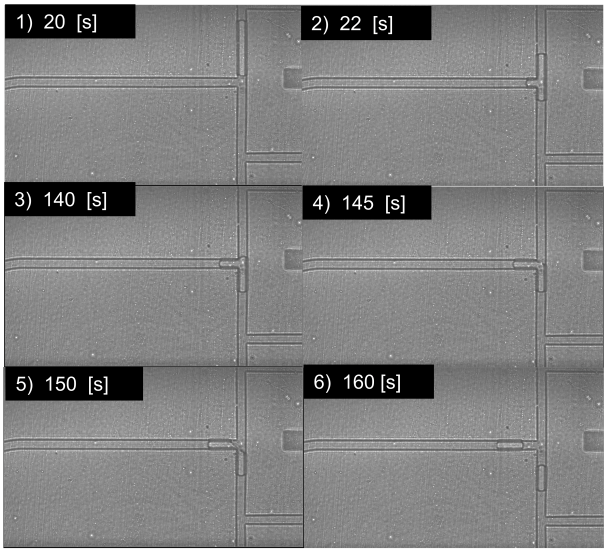

Figure 6.6: Automatic Droplet Splitting

6.5.3 Automatic Droplet Merging

A further fundamental unit operation, droplet merging, is also achievable. Figure 6.8 shows a successfully droplet merge process as specified by Table 6.4.

In Figure 6.8, frame a shows two droplets in a movement towards the T-junction. Frame b and c show the movement of droplets to the second waypoint where merging occurs. Finally, fame d shows the completed merge process. During this process, two droplets have been merged into one, and it is clear the automatic merge process is successful.

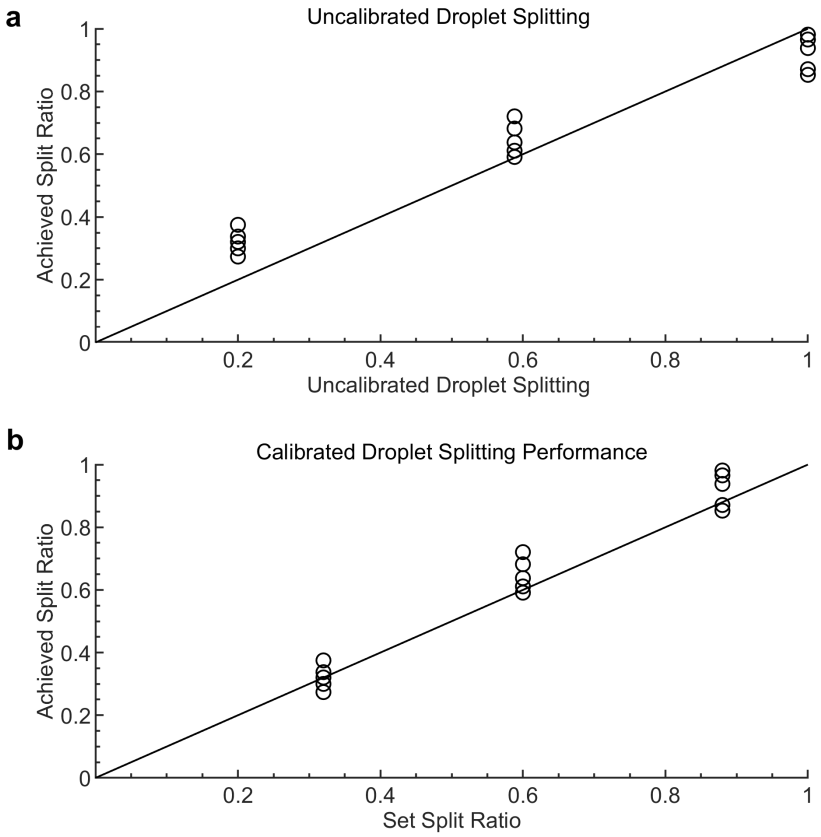

Figure 6.7: Automatic Droplet Splitting Characterization

6.5.4 Automatic Droplet Sorting

Droplet sorting is another fundamental unit operation that is required for a fully automatic system. This is illustrated in Figure 6.9 and Table 6.5. InFigure 6.91A to 4A the droplet is sent to the left channel at the T-junction. The droplet moves past the first way-point (Frame 1A), towards the second (Frame 2A), where it switches channels (Frame 3A), and moves in the designated direction (Frame 4A). Frames 1B to 4B show the same process for a sort to the right channel at the T-junction. It is clear that minor changes to the template enable the droplets to be sorted correctly and automatically to either side.

Interestingly, the droplets sorted are of different sizes, yet the same programs can carry

Table 6.3: Droplet Split Program

Instruction	Channel	Position	Initial	Special
1	3 4	-150 -1	850 3000	0
2	3 4	-150 -150	700 2850	0
3	3 4	-150 -150	550 2700	0
4	3 4	-150 -150	400 2550	0
5	3 4	-150 -150	250 2400	0

Table 6.4: Droplet Merge Program

Instruction	Channel	Position	Initial	Special
1	3 4	150 150	700 2850	0
2	3 4	-150 -50	1000 3150	0

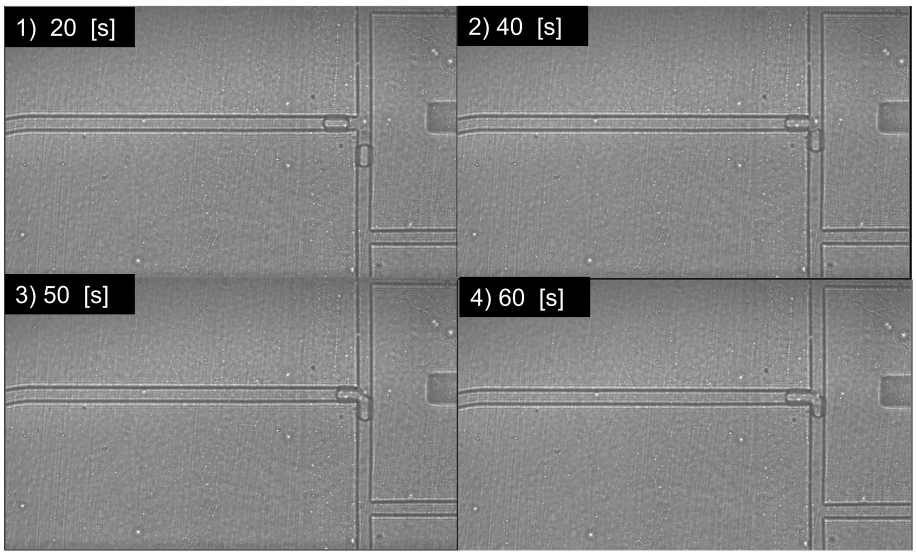

Figure 6.8: Automatic Droplet Merge

out this unit operation. This indicates that this unit operation is at least partiality robust to variations in droplet length.

Overall, these results how have presented successful droplet sorting indicating that the

Table 6.5: Droplet Sort Left Program

Instruction	Channel	Position	Initial	Special
1	4	500	2000	0
2	4	500	2500	0
3	4	0	3000	0
4	5	500	0	0

Table 6.6: Droplet Cross-Channel Movement Program

Instruction	Channel	Position	Initial	Special
1	3	-50	50	0
2	3	-500	550	0

unit operation is possible. Additionally, the results have shown that the unit operation can withstand variations in droplet length.

6.5.5 Automatic Droplet Movement

The final unit operation that is required is droplet movement. For droplets to be of use, it must be possible to move them within the device. Figure 6.10 and Table 6.6 shows an example of a droplet crossing a T Junction. The droplet reaches the initial waypoint in frame 1, moves across the intersection region in frame 2, and reaches the final waypoint in the opposing channel in frame 3. From this result, it is clear that droplet movement across the T-Junction is achievable.

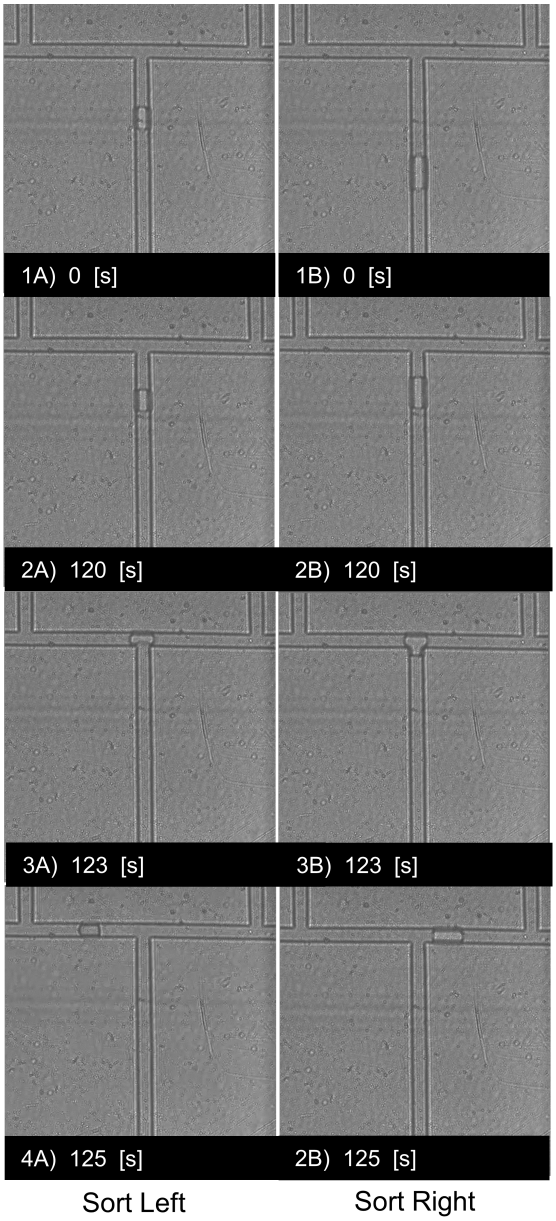

Figure 6.9: Automatic Droplet Sorting

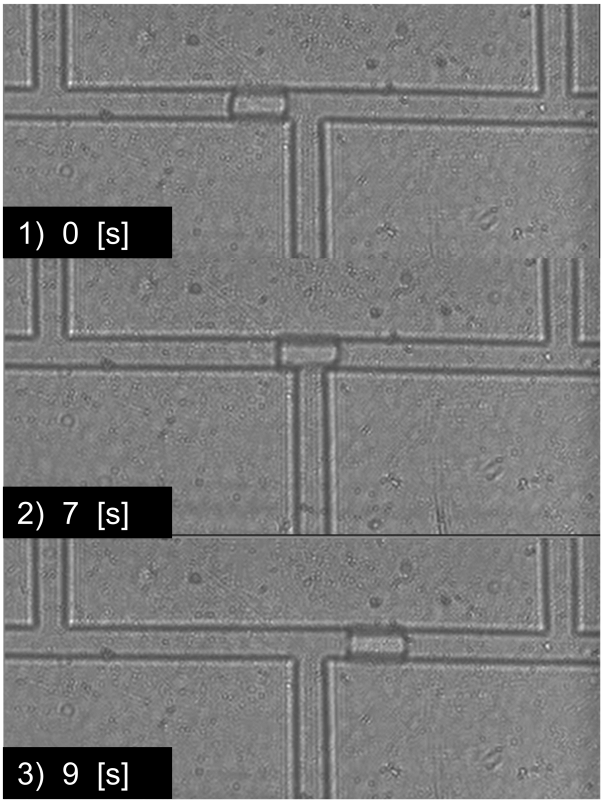

Figure 6.10: Automatic Droplet Cross-Channel Movement

6.6 Discussion

These results show it is possible to automate droplet microfluidic devices. The findings have demonstrated that the fundamental unit operations, droplet generation, splitting, merging, sorting, and movement, are achievable. In this sense, this method allows full automation as no human operator is needed after initializing the system and specifying the program.

This method contrasts with previous visual feedback pressure-driven approaches that require a human operator. Wong's approach requires any action to be directly managed by a user. Hebert has some aspects of automation, but still requires an operator's input to initialize droplet position within the chip and select relevant droplet interfaces. Unlike these methods, with this approach during the operation of the system no operator is needed

for all unit operations.

The fully automated nature of the system allows a great deal of abstraction in the system's use. Although only some unit operations have been shown, any droplet manipulations with one-directional channel flow can be created with this method. In this sense, only human creativity limits what desired actions are achievable as this method is very generalizable. It adds a layer of abstraction between specifying the desired action and carrying it out. An analogy may be drawn between computer programming and this method. A computer programmer does not need aware of how computer hardware works beyond the general level to write software. Similarly, a user of the device does not need to consider detailed microfluidic fluid physics of the device to use it.

The findings also offer benefits over alternative approaches that are not based on visual feedback pressure-driven control. For instance, this method does not require any direct actuation mechanisms that active microfluidics or digital microfluidics need. This makes the approach more congruent to a wider set of applications where interaction between the sample and actuation method or residue are undesirable. Compared to active and MLSI methods, the design of the system is significantly simpler and less costly, thus more widely adaptable. Finally, compared to passive methods the operation of this system is significantly simpler. Unlike the purely passive approach, no significant experience in microfluidic chip design or operation is needed.

This finding has important implications for the expansion of the microfluidic community and the advancement of these very advantageous techniques. Despite the many apparent benefits of droplet microfluidics, these techniques have been poorly adopted. As this method is widely applicable, has minimal equipment needs, and yet is simple for the end-user to use, it provides a new powerful tool to address the big challenges in biology, chemistry, material science, and medicine.

Unfortunately, there are limitations in the current implementation of this approach. Firstly, not all unit operations are robust to calibration errors, variations in droplet size, and transients in plant response. In particular, droplet merging is very sensitive to variations in droplet length. Furthermore, the design of programs requires experimental fine-tuning. Secondly, partly due to significant plant time variance the controller is tuned to be conservative. As a result, the plant can experience large error transients when switching between some waypoints. Large transients can cause unwanted droplet movement between channels leading to instability. Finally, interaction with a program is not inviting. The development of a user interface could aid this approach. Figure 6.11 shows a mock-up of such a user interface. To use the user-interface, the operator selects from a set of unit operation templates (Set 1) and arranges them sequentially (Step 2). The users then parameterize

the unit operations (Step 3). The program is validated (Step 4) and outputted (Step 5).

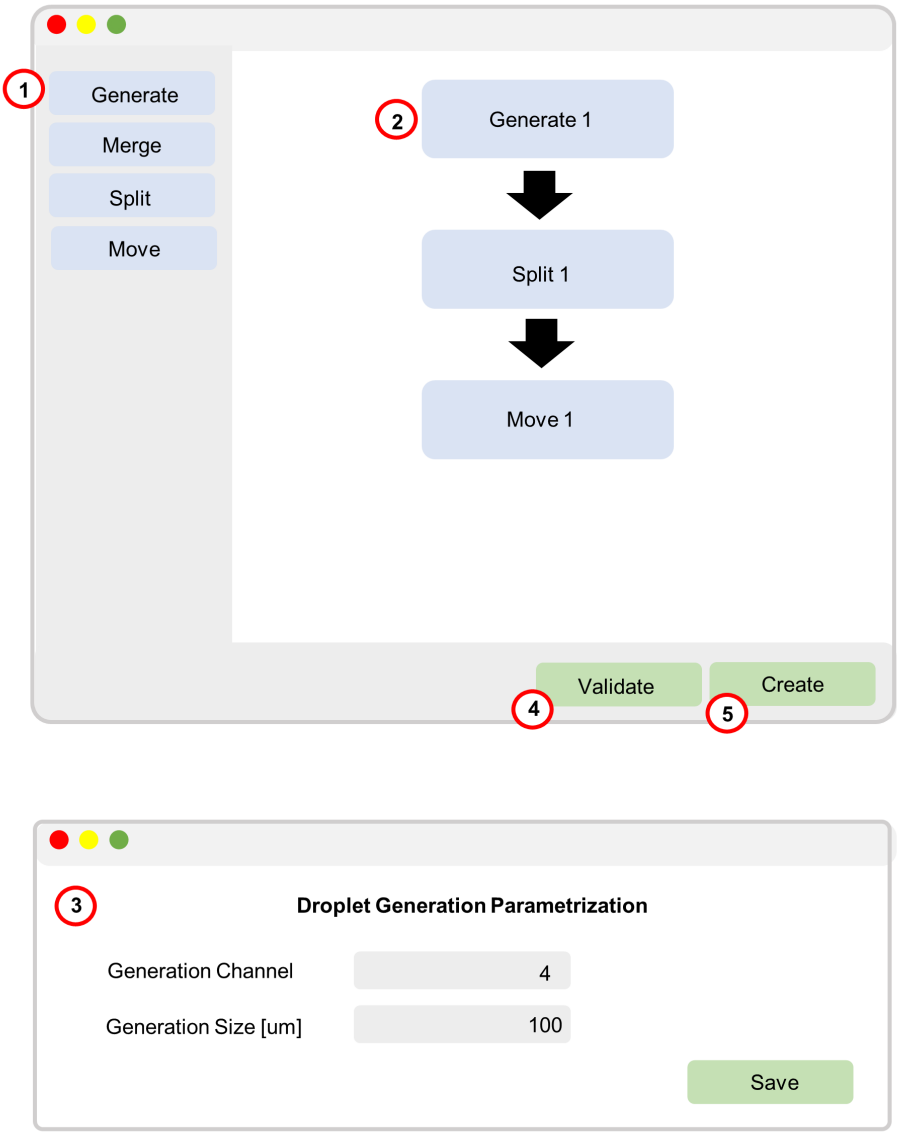

Figure 6.11: Proposed User Interface Mock Up

These limitations are not fundamental problems but rather solvable practical challenges. Further development in this direction can lead to even greater accessibility of microfluidics

and the associated benefits. Doing so would give researchers in biology, chemistry, material science, and medicine easily accessible but powerful new capabilities in addressing the challenges of the future.

6.7 Summary

For wide-scale adoption, feedback-controlled droplet microfluidic platforms require high abstraction to make use simple. This chapter presents a method of describing droplet manipulations and a controller scheme to carry out described actions automatically. Successful automatic droplet generation, splitting, merging, and moving are demonstrated. Through this technique operator interaction is removed, building towards to goal of wide-scale adoption of microfluidics.

Chapter 7

Conclusion

7.1 Summary

Despite many hopes, microfluidics has failed to live up to its potential as a widely used tool. Although the fundamental benefits of working at the microscale are well demonstrated, the widespread use of microfluidic techniques is too challenging in practice. Unlike well-known methods, recent methods based on Feedback Control Microfluidics do not have the same fundamental or practical challenges. However, current methods in FCM have some challenges with chip design, feedback, modeling, control, and automation. In response, a new chip topology with greater capability is presented. This new chip topology is only usable due to a novel feedback system based on lensless techniques. This system is developed and validated in this work. Furthermore, a new simplified method of modeling is created and verified. The new model is used with a Model Predictive Controller to compensate for pump limitations. Leveraging these advantages a method of specifying and automatically manipulating droplets is demonstrated. The combinations of these systems and methods create a new type of FCM system. Further development of the FCM systems will lead to even greater accessibility of microfluidics. A future FCM system gives researchers in biology, chemistry, material science, and medicine access to a new and powerful tool, microfluidics, to pursue the challenges of the future.

7.2 Future Work

7.2.1 Chip Fabrication

PDMS based microfluidic chips are the cause of significant control system and usability challenges. Variability between different chips and over the operating life of the chip is significant. To compensate for this variability, calibration procedures and conservative controllers are used. However, these countermeasures do not solve the problems but only minimize the effects. For the system to be used universally, a more stable and consistent microfluidic fabrication method is needed.

7.2.2 Lensless System Improvements

Microscopy based techniques are very well developed and are often leveraged in microfluidic devices. An example is the use of fluorescent microscopy. For widespread uses, extending these techniques to lensless systems would be valued. Within the literature, such modifications exist [96] [97], but none within the control system context.

7.2.3 Pumps

The current system leverages commercial pumps. However, microfluidic pumps are designed and optimal for passive systems thus limiting for feedback systems. Firstly, being meant for passive systems the dynamic response of most pumps is slow from the control system perspective. Secondly, the unidirectional nature of most pumps, as stated in Chapters 1 and 5, can cause problems. From a more practical perspective, most pumps are costly, require an external air source, and are often large. None of these characteristics are conducive to widely accessible systems.

7.2.4 Improved System Identification

Current methods of system identification are cumbersome, error prone, and time consuming requiring much operator effort. The experimental procedure of system identification is difficult. A method of more easily gathering this data would improve usability.

7.2.5 User Interface

Currently, the automated method relies on user created programs to specify desired droplet manipulations. For novice users, such a method is unwelcoming and difficult. Creating a user interface, an example user interface is suggested in Chapter 6, will make use of the system easier.

7.2.6 Waypoint Generation

Controller waypoints are generated through a combination of manual specifications and templates. However, system performance could likely be improved if waypoints are generated with a deeper understanding of device physics, especially for highly non-linear operations. But for system use to remain abstracted such generation would have to be automated. Thus, an automated waypoint generation scheme that includes a deeper understanding of device physics is needed.

References

[1] G. M. Whitesides, "The origins and the future of microfluidics," *Nature*, vol. 442, July 2006.

[2] H. Song, D. L. Chen, and R. F. Ismagilov, "Reactions in Droplets in Microfluidic Channels," *Angewandte Chemie International Edition*, vol. 45, no. 44, pp. 7336–7356, 2006.

[3] X. C. i. Solvas and A. deMello, "Droplet microfluidics: recent developments and future applications," *Chemical Communications*, vol. 47, pp. 1936–1942, Feb. 2011.

[4] C. Ren and A. Lee, eds., *Droplet Microfluidics*. Soft Matter Series, The Royal Society of Chemistry, 2021.

[5] Y.-C. Tan, J. S. Fisher, A. I. Lee, V. Cristini, and A. P. Lee, "Design of microfluidic channel geometries for the control of droplet volume, chemical concentration, and sorting," *Lab on a Chip*, vol. 4, pp. 292–298, July 2004.

[6] P. Zhu and L. Wang, "Passive and active droplet generation with microfluidics: a review," *Lab on a Chip*, vol. 17, pp. 34–75, Dec. 2016.

[7] T. Thorsen, S. J. Maerkl, and S. R. Quake, "Microfluidic Large-Scale Integration," *Science*, vol. 298, pp. 580–584, Oct. 2002.

[8] K. Choi, A. H. Ng, R. Fobel, and A. R. Wheeler, "Digital Microfluidics," *Annual Review of Analytical Chemistry*, vol. 5, no. 1, pp. 413–440, 2012.

[9] M. Hébert, M. Courtney, and C. L. Ren, "Semi-automated on-demand control of individual droplets with a sample application to a drug screening assay," *Lab on a Chip*, vol. 19, pp. 1490–1501, Apr. 2019.

[10] T. Thorsen, R. W. Roberts, F. H. Arnold, and S. R. Quake, "Dynamic Pattern Formation in a Vesicle-Generating Microfluidic Device," *Physical Review Letters*, vol. 86, pp. 4163–4166, Apr. 2001.

[11] J. Melin and S. R. Quake, "Microfluidic large-scale integration: the evolution of design rules for biological automation," *Annual Review of Biophysics and Biomolecular Structure*, vol. 36, pp. 213–231, 2007.

[12] I. E. Araci and P. Brisk, "Recent developments in microfluidic large scale integration," *Current Opinion in Biotechnology*, vol. 25, pp. 60–68, Feb. 2014.

[13] M.-P. Chang and M. M. Maharbiz, "Electrostatically-driven elastomer components for user-reconfigurable high density microfluidics," *Lab on a Chip*, vol. 9, pp. 1274–1281, May 2009.

[14] S. Ghosh, C. Yang, T. Cai, Z. Hu, and A. Neogi, "Oscillating magnetic field-actuated microvalves for micro- and nanofluidics," vol. 42, p. 135501, June 2009.

[15] C. Neumann, A. Voigt, L. Pires, and B. E. Rapp, "Design and characterization of a platform for thermal actuation of up to 588 microfluidic valves," *Microfluidics and Nanofluidics*, vol. 14, pp. 177–186, Jan. 2013.

[16] S. Vyawahare, S. Sitaula, S. Martin, D. Adalian, and A. Scherer, "Electronic control of elastomeric microfluidic circuits with shape memory actuators," *Lab on a Chip*, vol. 8, pp. 1530–1535, Sept. 2008.

[17] X. Xu, L. Sun, L. Chen, Z. Zhou, J. Xiao, and Y. Zhang, "Electrowetting on dielectric device with crescent electrodes for reliable and low-voltage droplet manipulation," *Biomicrofluidics*, vol. 8, p. 064107, Nov. 2014.

[18] L. Davoust and J. Theisen, "Evaporation rate of drop arrays within a digital microfluidic system," *Sensors and Actuators B: Chemical*, vol. 189, pp. 157–164.

[19] M. J. Jebrail, R. F. Renzi, A. Sinha, J. Van De Vreugde, C. Gondhalekar, C. Ambriz, R. J. Meagher, and S. S. Branda, "A solvent replenishment solution for managing evaporation of biochemical reactions in air-matrix digital microfluidics devices," *Lab Chip*, vol. 15, pp. 151–158, 2015.

[20] R. B. Fair, A. Khlystov, T. D. Tailor, V. Ivanov, R. D. Evans, V. Srinivasan, V. K. Pamula, M. G. Pollack, P. B. Griffin, and J. Zhou, "Chemical and biological applications of digital-microfluidic devices," *IEEE Design Test of Computers*, vol. 24, no. 1, pp. 10–24.

[21] T. J. Hutama and R. D. Oleschuk, "Magnetically manipulated droplet splitting on a 3d-printed device to carry out a complexometric assay," *Lab on a Chip*, vol. 17, no. 15, pp. 2640–2649, 2017.

[22] S. K. Fan, C. Hashi, and C. J. Kim, "Manipulation of multiple droplets on nxm grid by cross-reference ewod driving scheme and pressure-contact packaging," *Proceedings of the IEEE Micro Electro Mechanical Systems (MEMS)*, pp. 694–697, 2003.

[23] J. Park, J. H. Jung, K. Park, G. Destgeer, H. Ahmed, R. Ahmad, and H. J. Sung, "On-demand acoustic droplet splitting and steering in a disposable microfluidic chip," *Lab on a Chip*, vol. 18, no. 3, pp. 422–432, 2018.

[24] G. Whitesides, "Microfluidics in late adolescence," *arXiv:1802.05595 [physics, q-bio]*.

[25] D. Wong and C. L. Ren, "Microfluidic droplet trapping, splitting and merging with feedback controls and state space modelling," *Lab on a Chip*, vol. 16, no. 17, pp. 3317–3329.

[26] Y. H. Wong, "Feedback controls in droplet microfluidics," Master's thesis, The school of the thesis, University of Waterloo, 12 2016.

[27] M. Hebert, *Expanding the droplet microfluidic community – towards a modular active platform*. PhD thesis, University of Waterloo, 12 2020.

[28] G. F. Franklin, J. D. Powell, and A. Emami-Naeini, *Feedback control of Dynamic Systems*. Pearson, 209.

[29] B. Kuczenski, P. R. LeDuc, and W. C. Messner, "Pressure-driven spatiotemporal control of the laminar flow interface in a microfluidic network," *Lab on a Chip*, vol. 7, no. 5, pp. 647–649.

[30] Y. Kim, P. LeDuc, and W. Messner, "Modeling and control of a nonlinear mechanism for high performance microfluidic systems," *IEEE Transactions on Control Systems Technology*, vol. 21, no. 1, pp. 203–211.

[31] E. Miller, M. Rotea, and J. P. Rothstein, "Microfluidic device incorporating closed loop feedback control for uniform and tunable production of micro-droplets," *Lab on a Chip*, vol. 10, no. 10, pp. 1293–1301.

[32] W. Zeng, S. Li, and Z. Wang, "Closed-loop feedback control of droplet formation in a t-junction microdroplet generator," *Sensors and Actuators A: Physical*, vol. 233, pp. 542–547.

[33] M. Armani, S. Chaudhary, R. Probst, and B. Shapiro, "Using feedback control of microflows to independently steer multiple particles," *Journal of Microelectromechanical Systems*, vol. 15, no. 4, pp. 945–956.

[34] D. Wong, K. Erkorkmaz, and C. L. Ren, "RoboDrop: A multi-input multi-output control system for on-demand manipulation of microfluidic droplets based on computer vision feedback," *IEEE/ASME Transactions on Mechatronics*, vol. 25, no. 2, pp. 1129–1137.

[35] A. B. D. O. and J. B. Moore, *Optimal control: Linear quadratic methods*. Dover Publications, 2007.

[36] K. W. Oh and C. H. Ahn, "A review of microvalves," vol. 16, no. 5, pp. R13–R39.

[37] J. Wu, G. Zheng, and L. M. Lee, "Optical imaging techniques in microfluidics and their applications," *Lab on a Chip*, vol. 12, no. 19, pp. 3566–3575, 2012.

[38] Robert E. Fischer and Biljana Tadic-Galeb, *Optical System Design*. SPIE Press Book, 2000.

[39] W. J. Smith., *Modern Optical Engineering*. McGraw-Hill, New York, 2000.

[40] J. Rietdorf, *Microscopy techniques*. Springer-Verlag GmbH., 2005.

[41] N. Ruijuan, "Overview of the microscope objective," Master's thesis, University of Arizona, The address of the publisher, 4 2017.

[42] J. T. Collins, J. Knapper, J. Stirling, J. Mduda, C. Mkindi, V. Mayagaya, G. A. Mwakajinga, P. T. Nyakyi, V. L. Sanga, D. Carbery, L. White, S. Dale, Z. J. Lim, J. J. Baumberg, P. Cicuta, S. McDermott, B. Vodenicharski, and R. Bowman, "Robotic microscopy for everyone: the OpenFlexure microscope." Company: Cold Spring Harbor Laboratory Distributor: Cold Spring Harbor Laboratory Label: Cold Spring Harbor Laboratory Section: New Results Type: article.

[43] A. Rodríguez-Pena, J. Uranga-Solchaga, C. Ortiz-de Solórzano, and I. Cortés-Domínguez, "Spheroscope: A custom-made miniaturized microscope for tracking tumour spheroids in microfluidic devices," *Scientific Reports*, vol. 10, no. 1, p. 2779.

[44] K. K. Ghosh, L. D. Burns, E. D. Cocker, A. Nimmerjahn, Y. Ziv, A. E. Gamal, and M. J. Schnitzer, "Miniaturized integration of a fluorescence microscope," *Nature Methods*, vol. 8, no. 10, pp. 871–878.

[45] Y. Lee, B. Kim, I. Oh, and S. Choi, "Optofluidic modular blocks for on-demand and open-source prototyping of microfluidic systems," *Small (Weinheim an Der Bergstrasse, Germany)*, vol. 14, no. 52, p. e1802769.

[46] W. A. Liberti, L. N. Perkins, D. P. Leman, and T. J. Gardner, "An open source, wireless capable miniature microscope system," vol. 14, no. 4, p. 045001.

[47] D. Aharoni and T. M. Hoogland, "Circuit investigations with open-source miniaturized microscopes: Past, present and future," *Frontiers in Cellular Neuroscience*, vol. 13, p. 141.

[48] A. D. Jacob, A. I. Ramsaran, A. J. Mocle, L. M. Tran, C. Yan, P. W. Frankland, and S. A. Josselyn, "A compact head-mounted endoscope for in vivo calcium imaging in freely behaving mice," *Current Protocols in Neuroscience*, vol. 84, no. 1, p. e51.

[49] S. B. Tristan-Landin, A. M. Gonzalez-Suarez, R. J. Jimenez-Valdes, and J. L. Garcia-Cordero, "Facile assembly of an affordable miniature multicolor fluorescence microscope made of 3d-printed parts enables detection of single cells," *PLOS ONE*, vol. 14, no. 10, p. e0215114.

[50] K. Sakai, F. Charlot, T. Le Saux, S. Bonhomme, F. Nogué, J.-C. Palauqui, and J. Fattaccioli, "Design of a comprehensive microfluidic and microscopic toolbox for the ultra-wide spatio-temporal study of plant protoplasts development and physiology," *Plant Methods*, vol. 15, no. 1, p. 79.

[51] J. Wu, L. Ouyang, N. Wadhawan, J. Li, M. Zhang, S. Liao, D. Levin, and F. Lin, "A compact microfluidic system for cell migration studies," *Biomedical Microdevices*, vol. 16, no. 4, pp. 521–528.

[52] J. R. Krogmeier, I. Schaefer, G. Seward, G. R. Yantz, and J. W. Larson, "An integrated optics microfluidic device for detecting single DNA molecules," *Lab on a Chip*, vol. 7, no. 12, pp. 1767–1774. Publisher: The Royal Society of Chemistry.

[53] S. Camou, H. Fujita, and T. Fujii, "PDMS 2d optical lens integrated with microfluidic channels: principle and characterization," *Lab on a Chip*, vol. 3, no. 1, pp. 40–45. Publisher: The Royal Society of Chemistry.

[54] S.-K. Hoi, Z.-B. Hu, Y. Yan, C.-H. Sow, and A. A. Bettiol, "A microfluidic device with integrated optics for microparticle switching," *Applied Physics Letters*, vol. 97, no. 18, p. 183501.

[55] K. E. Bates and H. Lu, "Optics-integrated microfluidic platforms for biomolecular analyses," *Biophysical Journal*, vol. 110, no. 8, pp. 1684–1697.

[56] Y. Liu, A. M. Rollins, R. M. Levenson, F. Fereidouni, and M. W. Jenkins, "Pocket MUSE: an affordable, versatile and high-performance fluorescence microscope using a smartphone," *Communications Biology*, vol. 4, no. 1, pp. 1–14.

[57] D. J. You, T. S. Park, and J.-Y. Yoon, "Cell-phone-based measurement of TSH using mie scatter optimized lateral flow assays," *Biosensors and Bioelectronics*, vol. 40, no. 1, pp. 180–185.

[58] H. Zhu, U. Sikora, and A. Ozcan, "Quantum dot enabled detection of escherichia coli using a cell-phone," *The Analyst*, vol. 137, no. 11, pp. 2541–2544.

[59] K. Yang, H. Peretz-Soroka, Y. Liu, and F. Lin, "Novel developments in mobile sensing based on the integration of microfluidic devices and smartphones," *Lab on a Chip*, vol. 16, no. 6, pp. 943–958.

[60] Dolomite Microfluidics, *Digital Microscope Part No. 3200293*, 2020. v1.4.

[61] X. Niu, M. Zhang, S. Peng, W. Wen, and P. Sheng, "Real-time detection, control, and sorting of microfluidic droplets," *Biomicrofluidics*, vol. 1, no. 4, p. 44101.

[62] M. Kelleci, H. Aydogmus, L. Aslanbas, S. O. Erbil, and M. S. Hanay, "Towards microwave imaging of cells," *Lab on a Chip*, vol. 18, no. 3, pp. 463–472.

[63] M. H. Zarifi, H. Sadabadi, S. H. Hejazi, M. Daneshmand, and A. Sanati-Nezhad, "Noncontact and nonintrusive microwave-microfluidic flow sensor for energy and biomedical engineering," *Scientific Reports*, vol. 8, no. 1, p. 139.

[64] C. Elbuken, T. Glawdel, D. Chan, and C. L. Ren, "Detection of microdroplet size and speed using capacitive sensors," *Sensors and Actuators A: Physical*, vol. 171, no. 2, pp. 55–62.

[65] Z. Göröcs and A. Ozcan, "On-Chip Biomedical Imaging," *IEEE Reviews in Biomedical Engineering*, vol. 6, pp. 29 – 46, 2013.

[66] M. Roy, D. Seo, S. Oh, J.-W. Yang, and S. Seo, "A review of recent progress in lens-free imaging and sensing," *Biosensors and Bioelectronics*, vol. 88, pp. 130–143, 2017. Special Issue Selected papers from the 26th Anniversary World Congress on Biosensors (Part I).

[67] A. Ozcan and E. McLeod, "Lensless imaging and sensing," *Annual Review of Biomedical Engineering*, vol. 18, no. 1, pp. 77–102, 2016.

[68] D. Lange, C. W. Storment, C. A. Conley, and G. T. Kovacs, "A microfluidic shadow imaging system for the study of the nematode caenorhabditis elegans in space," *Sensors and Actuators, B: Chemical*, vol. 107, no. 2, pp. 904–914, 2005.

[69] S. Seo, T.-W. Su, A. Erlinger, and A. Ozcan, "Multi-color lucas: Lensfree on-chip cytometry using tunable monochromatic illumination and digital noise reduction," *Cellular and Molecular Bioengineering*, vol. 1, no. 2-3, pp. 146–156, 2008.

[70] A. Ozcan and U. Demirci, "Ultra wide-field lens-free monitoring of cells on-chip," *Lab on a Chip*, vol. 8, no. 1, pp. 98–106, 2007.

[71] X. Cui, L. M. Lee, X. Heng, W. Zhong, P. W. Sternberg, D. Psaltis, C. Yang, M. Lee, X. Heng, W. Zhong, P. W. Sternberg, D. Psaltis, and C. Yang, "Lensless high-resolution on-chip optofluidic microscopes for caenorhabditis elegans and cell imaging," 2008.

[72] G. Zheng, S. A. Lee, Y. Antebi, M. B. Elowitz, and C. Yang, "The epetri dish, an on-chip cell imaging platform based on subpixel perspective sweeping microscopy (spsm)," *Proceedings of the National Academy of Sciences of the United States of America*, vol. 108, no. 41, pp. 16889–16894, 2011.

[73] S. B. Kim, H. Bae, J. M. Cha, S. J. Moon, M. R. Dokmeci, D. M. Cropek, and A. Khademhosseini, "A cell-based biosensor for real-time detection of cardiotoxicity using lensfree imaging," *Lab on a Chip*, vol. 11, no. 10, pp. 1801–1807, 2011.

[74] U. A. Gurkan, S. Moon, H. Geckil, F. Xu, S. Wang, T. J. Lu, and U. Demirci, "Miniaturized lensless imaging systems for cell and microorganism visualization in point-of-care testing," *Biotechnology Journal*, vol. 6, no. 2, pp. 138–149, 2011.

[75] L. Ljung, *System identification: Theory for the user*. Prentice-Hall, 2009.

[76] P. Hippe, *Windup in control its effects and their prevention*. Springer London, 2006.

[77] C. Gokcek, P. Kabamba, and S. Meerkov, "An LQR/LQG theory for systems with saturating actuators," *IEEE Transactions on Automatic Control*, vol. 46, no. 10, pp. 1529–1542.

[78] J. M. Maciejowski, *Predictive control: With constraints*. Prentice Hall, 2008.

[79] W. S. Levine, *Control System Advanced Methods*. CRC, 2011.

[80] W. S. Levine, "The essentials of model predictive control," in *Handbook of Model Predictive Control* (S. V. Raković and W. S. Levine, eds.), Control Engineering, pp. 3–27, Springer International Publishing.

[81] E. F. Camacho, *Model predictive control*. Springer, 2007.

[82] A. Bemporad, "Model predictive control quadratic programming and explicit mpc."

[83] M. J. Best, *Quadratic Programming with Computer Programs*. Chapman and Hall/CRC.

[84] P. E. Gill and E. Wong, "Sequential quadratic programming methods," in *Mixed Integer Nonlinear Programming* (J. Lee and S. Leyffer, eds.), The IMA Volumes in Mathematics and its Applications, pp. 147–224, Springer.

[85] M. Hovd, "A brief introduction to model predictive control," 3 2004.

[86] A. Bemporad, R. N. Lawrence, and M. Morari, *Model Predictive Control Toolbox Reference*. Matlab Inc, 9 2020.

[87] T. Glawdel and C. L. Ren, "Global network design for robust operation of microfluidic droplet generators with pressure-driven flow," *Microfluidics and Nanofluidics*, vol. 13, no. 3, pp. 469–480.

[88] A. K. Johan and W. Bjorn, *Adaptative control*. Addison Wesley, 1995.

[89] D. Qin, Y. Xia, and G. M. Whitesides, "Soft lithography for micro- and nanoscale patterning," *Nature Protocols*, vol. 5, no. 3, pp. 491–502, 2010.

[90] Fluigent, *TMfcs-ez microfluidic flow control system user manual*, 2016.

[91] G. Bradski, "The OpenCV Library," *Dr. Dobb's Journal of Software Tools*, 2000.

[92] A. Oliva, A. Torralba, and P. G. Schyns, "Hybrid images," *ACM Trans. Graph.*, vol. 25, p. 527–532, July 2006.

[93] D. M. W. Powers, "Evaluation: from precision, recall and f-measure to roc, informedness,markedness and correlation," *CoRR*, vol. abs/2010.16061, 2020.

[94] Y. Benjamini and Y. Hochberg, "Controlling the false discovery rate: A practical and powerful approach to multiple testing," *Journal of the Royal Statistical Society. Series (Methodological)*, vol. 57, no. 1, pp. 289–300, 1995.

[95] Basler AG, *daA2500-14um*, 2 2021.

[96] A. F. Coskun, T.-W. Su, I. Sencan, and A. Ozcan, "Lensless fluorescent microscopy on a chip," *Journal of Visualized Experiments: JoVE*, no. 54, p. 3181.

[97] A. F. Coskun, T. W. Su, and A. Ozcan, "Wide field-of-view lens-free fluorescent imaging on a chip," *Lab on a Chip*, vol. 10, no. 7, pp. 824–827, 2010.

[98] T. Kailath, *Linear Systems*. Prentice-Hall, 1980.

[99] L. C. Westphal, *Handbook of Control Systems Engineering*. Springer US, 2001.

[100] W. Garcia-Gabin and M. Lundh, "Input prbs design for identification of multivariable systems,"

[101] P. Van Overschee and B. De Moor, "N4sid: Subspace algorithms for the identification of combined deterministic-stochastic systems," *Automatica*, vol. 30, no. 1, pp. 75–93.

[102] L. Ljung, "Practical issues of system identification," Tech. Rep. LiTH-ISY-R-2810, University of Linköpings, June 2007.

[103] E. Davison, "A method for simplifying linear dynamic systems," *IEEE Transactions on Automatic Control*, vol. 11, no. 1, pp. 93–101.

[104] Z. Elrazaz and N. K. Sinha, "A review of some model reduction techniques," *Canadian Electrical Engineering Journal*, vol. 6, no. 1, pp. 34–40.

[105] C. S. Chin, *Computer-aided control systems design: Practical applications using MATLAB and simulink*. CRC Press, 2017.

[106] C. Schmid and L. T. Biegler, "Quadratic programming methods for reduced hessian SQP," *Computers & Chemical Engineering*, vol. 18, no. 9, pp. 817–832.

APPENDICES

Appendix A

Droplet Tracking

This appendix is a video file, titled “droplettracking.mp4”.

Appendix B

Droplet Generation

This appendix is a video file, titled “dropletgen.mp4”.

Appendix C

Droplet Split

This appendix is a video file, titled “dropletsplit.mp4”.